

AD-751 982

THE INFLUENCE OF AERODYNAMIC DECELERATORS ON SUPERSONIC WAKES: WITH AN APPLICATION OF THE GAS HYDRAULIC ANALOGY

Charles A. Babish, III

Air Force Flight Dynamics Laboratory
Wright-Patterson Air Force Base, Ohio

August 1972

DISTRIBUTED BY:

NTIS

National Technical Information Service
U. S. DEPARTMENT OF COMMERCE
5285 Port Royal Road, Springfield Va. 22151

AD751982

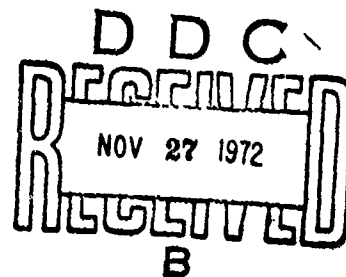
AFFDL-TR-72-54

**THE INFLUENCE OF AERODYNAMIC DECELERATORS
ON SUPERSONIC WAKES: WITH AN APPLICATION
OF THE GAS HYDRAULIC ANALOGY**

CHARLES A. BABISH III

TECHNICAL REPORT AFFDL-TR-72-54

AUGUST 1972



Approved for public release; distribution unlimited.

Reproduced by
NATIONAL TECHNICAL
INFORMATION SERVICE
U S Department of Commerce
Springfield VA 22151

**AIR FORCE FLIGHT DYNAMICS LABORATORY
AIR FORCE SYSTEMS COMMAND
WRIGHT-PATTERSON AIR FORCE BASE, OHIO**

R
100

NOTICE

When Government drawings, specifications, or other data are used for any purpose other than in connection with a definitely related Government procurement operation, the United States Government thereby incurs no responsibility nor any obligation whatsoever; and the fact that the government may have formulated, furnished, or in any way supplied the said drawings, specifications, or other data, is not to be regarded by implication or otherwise as in any manner licensing the holder or any other person or corporation, or conveying any rights or permission to manufacture, use, or sell any patented invention that may in any way be related thereto.

ACCESSION FOR	
NTIS	White Section <input checked="" type="checkbox"/>
DOC	Buff Section <input type="checkbox"/>
UNANNOUNCED	<input type="checkbox"/>
JUSTIFICATION.....	<input type="checkbox"/>
BY	
DISTRIBUTION/AVAILABILITY CODES	
Dist.	AVAIL. and/or SPECIAL
A	

Copies of this report should not be returned unless return is required by security considerations, contractual obligations, or notice on a specific document.

UNCLASSIFIED

Security Classification

DOCUMENT CONTROL DATA - R & D

(Security classification of title, body of abstract and indexing annotation must be entered when the overall report is classified)

1. ORIGINATING ACTIVITY (Corporate author) Air Force Flight Dynamics Laboratory AFFDL/FER Wright-Patterson AFB, Ohio 45433		2a. REPORT SECURITY CLASSIFICATION Unclassified	
		2b. GROUP	
3. REPORT TITLE THE INFLUENCE OF AERODYNAMIC DECELERATORS ON SUPERSONIC WAKES: WITH AN APPLICATION OF THE GAS HYDRAULIC ANALOGY			
4. DESCRIPTIVE NOTES (Type of report and inclusive dates) Final Report, April 1965 to December 1969			
5. AUTHOR(S) (First name, middle initial, last name) Charles A. Babish III			
6. REPORT DATE August 1972	7a. TOTAL NO. OF PAGES 90-104	7b. NO. OF REFS 53	
8a. CONTRACT OR GRANT NO.		9a. ORIGINATOR'S REPORT NUMBER(S) AFFDL-TR-72-54	
b. PROJECT NO. 6065	9b. OTHER REPORT NO(S) (Any other numbers that may be assigned this report)		
c. Task 606505			
d.			
10. DISTRIBUTION STATEMENT Approved for Public Release; Distribution Unlimited.			
11. SUPPLEMENTARY NOTES		12. SPONSORING MILITARY ACTIVITY Air Force Dynamics Laboratory (FER) Wright-Patterson AFB, Ohio 45433	
13. ABSTRACT Two-body performance characteristics can be predicted with a reasonable degree of accuracy for deployable aerodynamic decelerators operating in conventional supersonic wakes. However, under certain geometric and flight conditions, the decelerator can modify the base flow region of the forebody, thus invalidating the performance prediction techniques. A literature review, supplementary wind tunnel tests, and a large number of shallow water tow table tests were performed to obtain a description of the process of wake modification and identify those parameters that influence the process. Wake modification was found to begin when the bow shock wave of the trailing decelerator became located at the wake sonic point. At this critical trailing distance, supersonic wake centerline velocities are eliminated and gas flows upstream into the forebody base region from the higher pressure region ahead of the decelerator. The critical trailing distance was shown to increase with (1) increasing base bleed, (2) increasing trailing body size and bluntness, (3) decreasing trailing body porosity, (4) decreasing forebody bluntness, and (5) the addition of forebody supports and forebody-decelerator connectors. The critical trailing distance first increases, then decreases, and finally levels off as Reynolds number increases over three orders of magnitude. No definite relationship between Mach number and critical trailing distance has been established. Additional wind tunnel investigations should be conducted to obtain explicit quantitative relationships between critical trailing distance and the influencing parameters. Existing analytical performance prediction techniques should be extended to include decelerators in modified wakes.			

DD FORM 1 NOV 66 1473

UNCLASSIFIED
Security Classification

UNCLASSIFIED

Security Classification

14. KEY WORDS	LINK A		LINK B		LINK C	
	ROLE	WT	ROLE	WT	ROLE	WT
Supersonic Wake Modification						
Critical Trailing Distance						
Supersonic Aerodynamic Decelerators						
Gas-Hydraulic Analogy						
Shallow Water Tow Table Tests						
Wind Tunnel Tests						
Flow Field Interactions						
Supersonic Parachutes						
Hydrostatics						
Aerodynamics						
Wake						

-ii-

UNCLASSIFIED

Security Classification

**THE INFLUENCE OF AERODYNAMIC DECELERATORS
ON SUPERSONIC WAKES: WITH AN APPLICATION
OF THE GAS HYDRAULIC ANALOGY**

CHARLES A. BABISH III

Approved for public release; distribution unlimited.

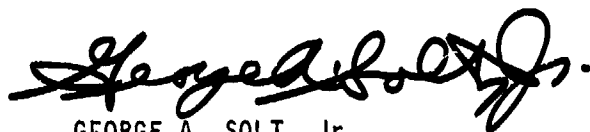
FOREWORD

This report was prepared by the Recovery and Crew Station Branch of the Air Force Flight Dynamics Laboratory (AFFDL/FER) under Project 6065, "Parachute Design and Performance for Tactical Air Drop and Military Vehicle Recovery", Task 606505, "Parachutes for Supersonic/Hypersonic Drag and Stability Augmentation of Weapon Systems". The work covered in this report was initiated in April, 1965 and completed in December, 1969. The report was submitted in May, 1972.

All efforts were accomplished in-house by or under the direction of Project Engineer Charles A. Babish III. Experimental testing was performed at the Arnold Engineering Development Center (AEDC) von Karman Gasdynamics Facility (VKF) and at the Air Force Flight Dynamics Laboratory Shallow Water Tow Test Facility.

The author wishes to express his appreciation to Mr. James H. DeWeese of the Recovery and Crew Station Branch for his participation in the preparation of the report and in the performance of the experimental investigations. Special acknowledgement is made to Mr. Laurence Gleason and Miss Sharon Black for their assistance during the shallow water tow tests and to the personnel at the AEDC-VKF Facility for their assistance and cooperation during the wind tunnel tests.

This technical report has been reviewed and is approved.



GEORGE A. SOLT, Jr.
Chief, Recovery & Crew Station Branch
Vehicle Equipment Division
Air Force Flight Dynamics Laboratory

TABLE OF CONTENTS

SECTION	PAGE
I INTRODUCTION	1
II REVIEW OF THE LITERATURE AND SUPPLEMENTARY WIND TUNNEL TESTS	3
1. Overall Considerations	3
a. General and Definitions	3
b. Decelerator Trailing Distance	6
2. Influencing Parameters	8
a. Mach Number	8
b. Reynolds Number	9
c. Flow Field Interferences	15
d. Forebody Shape	22
e. Trailing Body Shape	23
f. Trailing Body Size	23
g. Trailing Body Porosity	25
3. Indicated Trends and General Conclusions	25
III SHALLOW WATER TOW TABLE TEST PROGRAM	27
1. Test Objective and Approach	27
2. Theory of the Gas-Hydraulic Analogy	28
3. Description of the Test Facility	31
4. Description of the Test Models	33
5. Test Instrumentation	39
6. Precision of the Data	40
7. Test Program	42
a. Test Run Summary	42
b. Test Procedure	44
c. Data Gathered	45

TABLE OF CONTENTS-CONTINUED

SECTION	PAGE
IV DISCUSSION OF TEST PROGRAM RESULTS	46
1. Preliminary Tests	46
a. Applicability of Water Table Tests to the Study of Wake Modification	46
b. Experimental Considerations	48
2. Flow Field Interference Studies	57
a. Shock Impingement	57
b. Flow Splitter	61
c. Disturbing Body	61
d. Base Bleed	63
3. Influencing Parameter Investigations	64
a. Froude Number and Trailing Body Size	64
b. Trailing Body Size and Shape	67
c. Forebody Shape	70
V MECHANISM FOR WAKE MODIFICATION	75
1. Shallow Water Flow	75
2. Compressible Gas Flow	79
3. Relationships Between Critical Trailing Distance and the Influencing Parameters	81
VI CONCLUSIONS AND RECOMMENDATIONS	83
1. Conclusions	83
2. Recommendations	84
REFERENCES	86

LIST OF ILLUSTRATIONS

FIGURE	PAGE
1. Nomenclature Applicable to Wake Modification for High Speed Gas Flow Fields	4
2. Types of Leading Body-Trailing Body Flow Field Interactions	5
3. Wake Conditions Behind a Cone Cylinder with a Trailing Hyperflo Type Parachute for Various Free-Stream Reynolds Numbers at $M_{\infty} = 3.0$	11
4. Effect of Reynolds Number on the Critical Sting Length; Replotted from References 19 and 22	13
5. Variation of Minimum Disturbance Length (Expressed in Base Heights) with Reynolds Number at $M_{nom} = 2.92$; Replotted from Reference 20	13
6. Schlieren Photographs of the Flow Fields About a Hyperflo Type Parachute With and Without Base Bleed Through the Forebody at $M_{\infty} = 3.0$	16
7. Schlieren Photographs of the Flow Fields About a Hyperflo Type Parachute With and Without Forebody Supports at $M_{\infty} = 4.0$	21
8. Photographs of the Shallow Water Tow Table Facility at the Air Force Flight Dynamics Laboratory, Wright-Patterson Air Force Base, Ohio	34
9. Test Models	37
10. Photograph of Selected Test Models	38
11. Slotted Acrylic Plastic Mounting Sheet for Test Models	38
12. Shallow Water Tow Table Carriage and Lighting Arrangement	41
13. Comparison of the Flow Fields About Leading and Trailing Bodies Tested in the Wind Tunnel and on the Shallow Water Tow Table	47
14. Variation of Critical Trailing Distance with Trailing Body Size for a Plate Trailing a Thin Wedge	48
15. Variation of Hydraulic Jump Angle with Free-Stream Froude Number for Various Water Depths and Two Wedge Deflection Angles	52

LIST OF ILLUSTRATIONS (CONT'D)

FIGURE		PAGE
16.	Variation of Wake Trailing Hydraulic Jumps Convergence Point Location with Water Depth	53
17.	Variation of Critical Trailing Distance and Wake Trailing Hydraulic Jumps Convergence Point Location with Water Depth	53
18.	Variation of Hydraulic Jump Detachment Distance with Free-Stream Froude Number for Various Cylinder Diameters	55
19.	Variation of Hydraulic Jump Detachment Distance with the Inverse Square of the Depth Ratio Across a Normal Hydraulic Jump for Various Cylinder Diameters	55
20.	Comparison of the Shallow Water Flow Fields About Three Wedge Models	56
21.	Shock Impingement Interference Study Test Arrangement and Flow Field Patterns	58
22.	Shadowgraphs from Selected Tests Showing the Effect of Impingement of Oblique Hydraulic Jumps on the Flow Field About a Sharp Wedge and a Trailing Simulated Parachute at $M_{\infty} = 3.0$	59
23.	Variation of Critical Trailing Distance With Free-Stream Froude Number for Various Strength Impinging Hydraulic Jumps and for a Flow Splitter	60
24.	Shadowgraphs From Selected Tests Showing the Effect of Flow Splitters on the Flow Field About a Sharp Wedge and a Trailing Simulated Parachute at $M_{\infty} = 3.0$	62
25.	Variation of Wake Trailing Hydraulic Jumps Convergence Point Location With Bleed Line Diameter	63
26.	Variation of Critical Trailing Distance With Free-Stream Froude Number for Various Size Simulated Parachutes Trailing a Sharp Wedge	66
27.	Variation of Critical Trailing Distance With Simulated Parachute Size for Various Free-Stream Froude Numbers	66
28.	Variation of Critical Trailing Distance With Trailing Body Size for Various Types of Trailing Bodies	69

LIST OF ILLUSTRATIONS (CONT'D)

FIGURE		PAGE
29.	Graphical Aid for the Development of an Explicit Relationship Involving Critical Trailing Distance, Hydraulic Jump Standoff Distance, and Trailing Body Size	71
30.	Comparison Between Calculated and Experimental Critical Trailing Distances	71
31.	Variation of Modified Critical Trailing Distance With Wedge Half Angle for Various Shape Wedges at $M_{\infty} = 2.5$	74
32.	Variation of Modified Critical Trailing Distance With Forebody Flare Angle at $M_{\infty} = 2.5$	74
33.	Shadowgraphs From Selected Tests Showing Two-Body Flow Patterns for Various Trailing Distances	76
34.	Sketches of Two-Body Flow Field Patterns for Closed, Modified, and Open Wakes	77

LIST OF TABLES

TABLE	PAGE
I Test Models	35
II Test Program	43
III Test Results - Hydraulic Jump Angles and X_0 Distances for Sharp Wedge Test Models	49
IV Test Results - Hydraulic Jump Standoff Distances for Circular Cylinder Test Models	50
V Test Results - Froude Number and Trailing Body Size Investigations	65
VI Test Results - Trailing Body Size and Shape Investigations	68
VII Test Results - Forebody Shape Investigations	72

LIST OF SYMBOLS

a	-	speed of sound, ft/sec
A_B	-	total area of forebody base
A_0	-	open area of forebody base
c	-	speed of an elementary surface wave, ft/sec
C_D	-	drag coefficient
d	-	trailing body diameter or width, inches
d	-	static water depth, inches
d_t	-	total water depth (at stagnation), inches
D	-	forebody base diameter or width, inches
g	-	acceleration of gravity, ft/sec ²
k	-	depth ratio across normal hydraulic jump, d_2/d_1
L	-	forebody length, inches
M	-	Mach number, V/a
M	-	Froude number, V/c
P	-	static pressure
r	-	distance from forebody base to the point of convergence of the wake recompression wave into the trailing shock, inches
r_b	-	radius of circular cylinder, inches
R	-	radius, inches
Re	-	unit Reynolds number
Re_D	-	Reynolds number based on forebody base diameter
Re_L	-	Reynolds number based on forebody length
V	-	speed of flow, ft/sec
W	-	plate trailing body width, inches
x,y	-	balloon type trailing body coordinates, inches

LIST OF SYMBOLS (CONT'D)

x	-	distance from the forebody base to the reference plane of the trailing body, inches
$(x/D)_{crit}$	-	critical trailing distance
$(x/D)^*_{crit}$	-	calculated critical trailing distance
x_0	-	distance from the forebody base to the wake convergence point, inches
β	-	hydraulic jump angle measured from upstream flow direction, degrees
γ	-	ratio of specific heats
δ	-	angle of flow deflection across an oblique shock wave or across an oblique hydraulic jump, degrees
δ	-	wedge deflection angle (wedge half angle), degrees
θ	-	shock wave angle measured from upstream flow direction, degrees
μ	-	Mach angle or Froude angle, $\left(\sin^{-1} \frac{1}{M}\right) \frac{180}{\pi}$, degrees
ν	-	Prandtl-Meyer angle (angle through which a supercritical flow is turned to expand from $M = 1$ to $M > 1$), degrees
ρ	-	static mass density
ρ_t	-	total mass density (at stagnation)
τ	-	hydraulic jump detachment (standoff) distance of body immersed in free-stream, inches
Φ	-	expression defined in Figure 29

Subscripts

1	-	conditions just upstream of a shock wave or hydraulic jump
2	-	conditions just downstream of a shock wave or hydraulic jump
∞	-	free-stream condition
nom	-	nominal free-stream condition

SECTION I
INTRODUCTION

This report deals with one aspect of the technical research area involving supersonic aerodynamic decelerators - that of the flow field interactions between leading bodies and trailing decelerators.

Deployable aerodynamic decelerators (parachutes, inflatable balloons, rigid cones, etc.) are required to decelerate and/or stabilize a variety of aerospace vehicles, payloads and weapons during supersonic flight. Prediction of the performance characteristics of a vehicle-decelerator system requires knowledge of the flow field properties surrounding the two bodies. For calculating decelerator performance, this usually means estimating the pressures, temperatures, and flow directions in the wake of the leading body. These properties can be calculated for conventional supersonic wakes to an acceptable degree of accuracy. However, significant modification of conventional wakes due to the presence of trailing decelerators invalidates these calculations. Further, the performance characteristics of most decelerators immersed in modified wake fields are generally characterized by low drag coefficients and oscillatory instabilities which are not typical of those exhibited in conventional wakes. Therefore, it becomes important to understand the flow field interactions that take place in such two-body systems and identify those parameters that influence the interactions as a first step toward establishing a decelerator performance prediction technique applicable to modified wakes.

That a trailing body can significantly alter the wake structure of a leading body has been recognized for some time. In 1948 Charters and Turetsky (Reference 1) reported that during the supersonic flight tests of cones " . . . spark photographs taken with the sabot closer than 5 calibers show that the wake does not converge, indicating that the flow behind the projectile is strongly affected. However, if the separation is greater than 5 calibers, the wake converges normally." Since 1948, a number of technical documents have been published concerning the various aspects of wake flow field interactions produced by placing a trailing

body in the wake of a leading body. In fact, Heinrich (Reference 2) has made a divergent wake behind a cone a requirement for the successful operation of his Supersonic Guide Surface parachute. However, most of the the publications are not primarily concerned with the detailed aspects of the interaction process. Nevertheless, they will be helpful for identifying influencing parameters and for establishing general relationships among the parameters.

These publications were reviewed and supplementary wind tunnel tests were accomplished to help determine the influencing parameters and relationships. As a result of these preliminary investigations it became apparent that decelerator trailing distance should be treated as a dependent variable and that the more important independent parameters were Reynolds number and trailing body geometry. A large number of shallow water tow tests were then performed to obtain a detailed description of the mechanism for the process of wake modification. After determining that the water table could be used to reasonably approximate the flow fields observed during wind tunnel tests, a governing mechanism for wake modification was postulated. This description of the interaction process was then used to substantiate the trends and relationships indicated in the literature and found during the wind tunnel tests.

The results presented are valid for models tested at zero angle of attack and at constant free-stream velocities in the Mach number range from 1.5 to 6.0. No corrections for, nor postulations concerning, scale effects are presented. However, use of the results should give a reasonable approximation of the degree of wake modification for a particular forebody-decelerator combination.

SECTION II

REVIEW OF THE LITERATURE AND SUPPLEMENTARY WIND TUNNEL TESTS

1. OVERALL CONSIDERATIONS

a. General and Definitions

A review of technical reports and other publications dealing with objects in the wakes of leading bodies immersed in supersonic free-streams was made to identify important parameters influencing wake modification. Wind tunnel investigations were performed to supplement the information found in the literature. As noted above, a trailing sabot can prevent a convergent wake from forming. The convergent supersonic wake is considered the conventional high speed wake; that is, the flow over the rear of the leading body converges toward the body centerline (expands) and at some distance downstream is compressed forming a trailing shock wave. Throughout the literature, different terminology and descriptions of the detailed aspects of this type of flow field are used. For example, the immediate vicinity of the base is called the base flow region, the separated flow region, the dead air region, the recirculation region, or the reverse flow region. Some investigators have assumed that separation only occurs smoothly from the corner of the base of a leading body (Reference 3) while others report that separation can originate on the rear face of the base (Reference 4). For the purpose of this report the nomenclature used in the literature will be altered to conform to that given in Figure 1 for the conventional high speed wake. Only those portions of the wake that proved significant to the description of wake modification are included.

Any decelerator or other object placed in the near wake region will alter the wake to some extent. The decelerator and its bow shock wave can interact with the viscous inner wake, the inviscid outer wake, the trailing shock wave, and even with the leading body bow shock wave, as shown in Figure 2a. However, for the purpose of this report, alterations that take place only in the near wake region will not be considered to

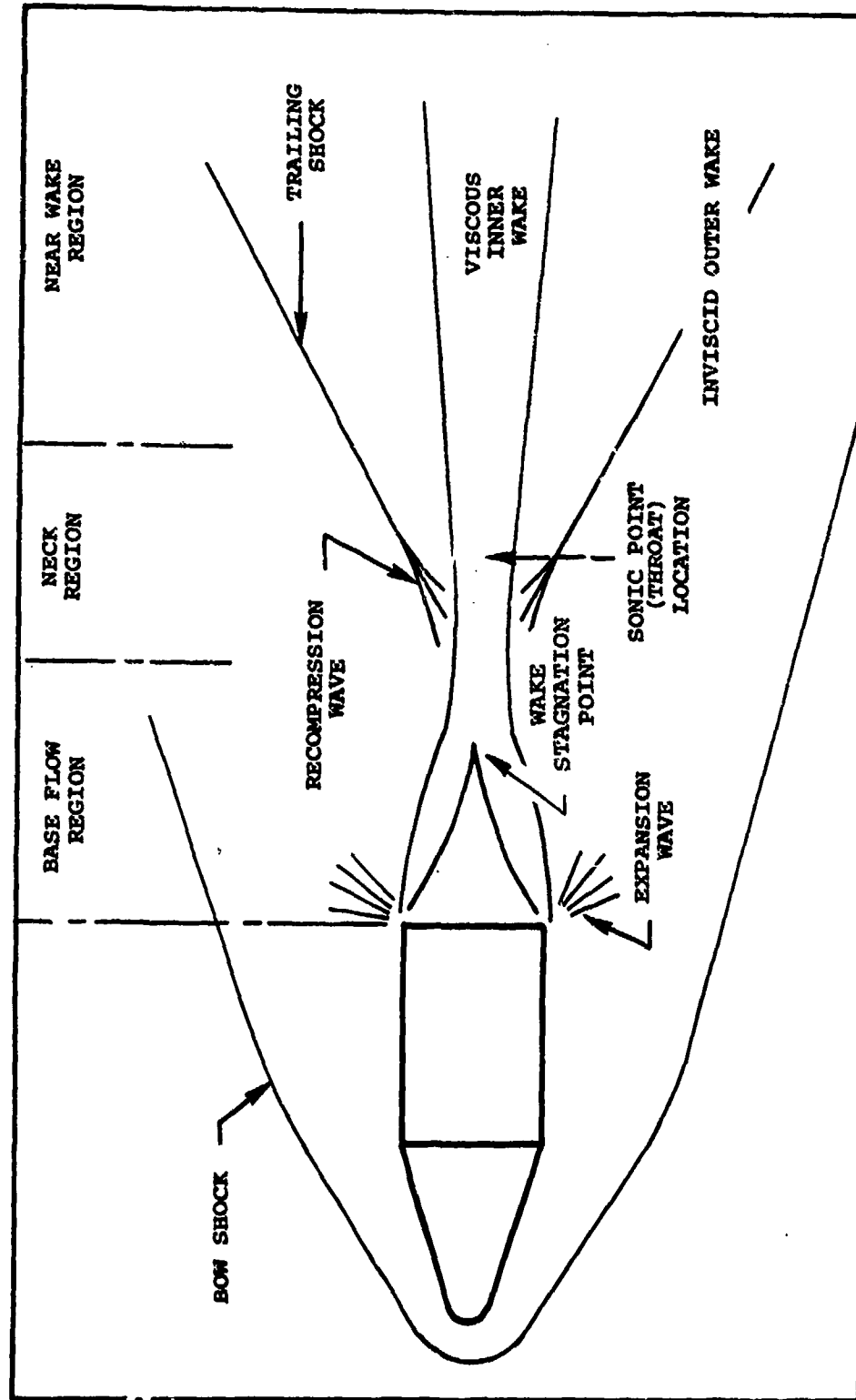
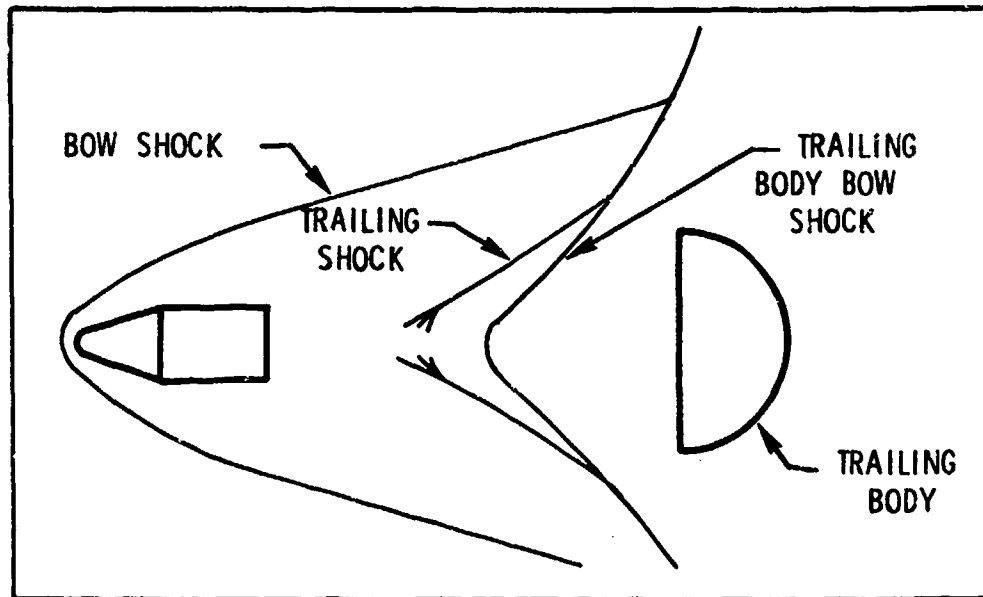
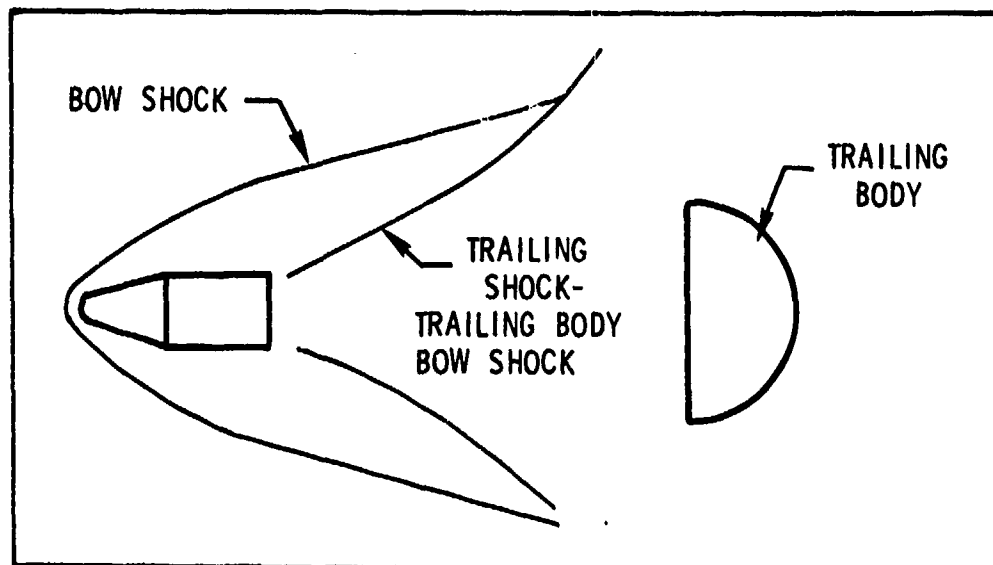


Figure 1. Nomenclature Applicable to Wake Modification for High Speed Gas Flow Fields.



a. Modification in Near Wake Region Only - Not Considered a Modified Wake



b. Modification in Base Flow Region - Considered a Modified Wake

Figure 2. Types of Leading Body-Trailing Body Flow Field Interactions

modify the leading body wake. Alterations must have taken place in the base flow region, as shown in Figure 2b, to be considered a modified wake. Modification can take the form of nonconvergence of the separated flow, increase in base pressure, or the location of the wake trailing shock wave in the base flow region.

The definition of wake modification is restricted to the above for two reasons. First, as long as flow field alterations are limited to the near wake region or downstream, wake flow field and decelerator performance prediction techniques such as presented in References 5 and 6 are valid. Second, performance characteristics of the decelerator are significantly different when the base flow region is altered as compared to when only the near wake region is altered.

References 7 through 10 report the effects of wake flow type on the performance characteristics of trailing conical type decelerators. In close proximity to the forebody (wake modified) the decelerator may be stable but has a very low drag force; at slightly longer trailing distances (wake still modified) the decelerator is unstable and the drag force is subject to abrupt changes. At large trailing distances (wake closed) the drag force is high and stability is a function only of geometry limitations.

b. Decelerator Trailing Distance

Early supersonic wind tunnel tests on aerodynamic decelerators showed that short decelerator trailing distances produced highly modified forebody wake fields as expected. Tests in the Mach number range from 1.5 to 6.0 with conical type decelerators and a variety of forebodies are documented in References 7 through 10. Coats (Reference 7) and Charczenko (References 8 and 9) reported divergent forebody wake fields at cone trailing distances less than 4 calibers. Heinrich and Hess (Reference 10) reported that the wake behind an ogive cylinder did not close until the trailing cone was located greater than 4 calibers downstream of the forebody base. References 9, 10, and 11 indicated divergent forebody wake fields for spheres trailing at less than 6 calibers. Roberts

(Reference 12) and Sims (Reference 13) reported that convergent forebody wake flow fields were obtained when model parachutes were placed at trailing distances greater than 5 calibers. The data from the above references show the obvious effect of trailing distance on wake modification; short trailing distances produce significant base flow field modifications. However, considering the large variety of test conditions and model configurations used during these investigations, the range of decelerator trailing distance where wake modification occurred was relatively small.

In 1964, during supersonic wind tunnel tests performed for the Air Force Flight Dynamics Laboratory (AFFDL) at the Arnold Engineering Development Center (AEDC), highly modified wakes were produced by decelerators at trailing distances up to 11 calibers. Bell (Reference 14) presented schlieren photographs of a balloon type decelerator in the wake of a cone-cylinder forebody that clearly showed a divergent wake at a trailing distance of 9 calibers. The free-stream Mach number was 6.0. References 15 and 16 document the results of tests performed with the same Hyperflo type parachutes and under essentially the same conditions as those in Reference 13. This time, divergent wakes were observed with parachute models as far downstream as 11 calibers in the Mach 4 to 5 range. Further evidence of wake modification at very large trailing distances was then found in a Technical Note by Slattery et al (Reference 17). A schlieren photograph of a sabot trailing a 25 degree included angle cone in normal, zero attitude flight at 5500 fps through 25 mm Hg of dry air showed a nonconvergent wake at a trailing distance of 10 to 12 calibers.

The modified wakes at large decelerator trailing distances reported in References 15 and 16 were suspected to be caused by a bleed of air through the support and out of the forebody base. This possibility and others were investigated during supplementary wind tunnel tests performed by the AFFDL and reported by Sims in Reference 16. The results of these tests indicated that decelerator trailing distances that produce wake

modification are influenced by many things and that among these are: (1) base bleed, (2) support interferences, (3) Reynolds number, (4) forebody and trailing body size and shape, and (5) Mach number. For this reason it becomes convenient to treat trailing distance as a dependent variable which is a function of the remaining wake modification influencing parameters. This variable will be non-dimensionalized and called the "critical trailing distance", $(X/D)_{crit}$. It is defined as that location of the decelerator (trailing body) in the wake of the forebody downstream of which there is no modification of the base flow region. The magnitude of the critical trailing distance is determined from the ratio of the distance from the forebody base to the reference plane of the trailing body, X , and the reference diameter of the forebody base, D . For this report, the following definitions apply unless otherwise specified: (1) the forebody and trailing body axes of symmetry are coincident, (2) X is measured along this axis, (3) the bodies are at zero angle of attack, (4) the forebody reference base diameter is the base diameter or width, and (5) the reference plane of the trailing body passes through its leading edge.

This critical trailing distance is not always constant for a given set of flow conditions and model configurations, but is also dependent upon the direction of decelerator traverse, if any. That is, the magnitude of $(X/D)_{crit}$ depends upon whether the forebody and decelerator are separated or brought closer together during a test series. References 7, 9, and 11 show an $(X/D)_{crit}$ hysteresis behavior with larger or smaller values of $(X/D)_{crit}$ for downstream or upstream decelerator traverses, respectively. The range of the hysteresis loop was as large as three calibers (Reference 11).

2. INFLUENCING PARAMETERS

a. Mach Number

The effect of Mach number on critical trailing distance is not well defined. Sims (Reference 16) indicated that $(X/D)_{crit}$ increased with increasing Mach number. Coats (Reference 7) gave $(X/D)_{crit}$ values

between 2 and 3 (including the hysteresis loop) for a 45 degree conical decelerator for all Mach numbers between 1.5 and 6.0. Alexander (Reference 11) showed a slight increase and decrease in $(X/D)_{crit}$ for increasing Mach number for the various balloon type decelerators tested between Mach 2.00 and 4.65. Charczenko (Reference 9) showed similar results for cones and spheres tested in the same Mach number range behind a variety of forebodies. Bell (Reference 14) presented data that showed a closed forebody wake for balloon type decelerator trailing distances of 6 calibers and greater for Mach numbers of 2, 3, and 5. At Mach 4 the forebody wake diverged at 6 calibers and converged at the larger separation distances. At Mach 6 the wake diverged at separation distances of 9 calibers or less.

Mach number was not the only wind tunnel flow parameter varied in the above references and no data was found to isolate the effect. Therefore, although Mach number appears to be an important parameter in the study of wake modification, no definite relationship between $(X/D)_{crit}$ and Mach number has been established.

b. Reynolds Number

During the supplementary wind tunnel tests performed by the AFFDL to investigate the parameters influencing wake modification a definite Reynolds number effect was established. A detailed description of the test set-up, instrumentation, procedure, and program for these tests can be found in References 15 and 16. The test set-up allowed for on-line monitoring of the flow field through the schlieren system. During a test of a Hyperflo type parachute, at Mach 3.0 and at a trailing distance of 6.2 calibers, a significant flow field change was observed during tunnel "shut down". To shut down the wind tunnel the total pressure (and hence Reynolds number) was decreased, holding Mach number and temperature constant. As Reynolds number decreased, the closed wake started to open, the trailing shock disappeared, and the parachute bow shock opened across the centerline. Tunnel shut down was halted and data taken at a Reynolds number per foot of 4.3×10^5 . The wake was highly modified. Reynolds number was increased until the wake closed. This occurred at Re equal

to 8.2×10^5 per foot. Reynolds number was increased to 8.7×10^5 per foot and then decreased until a modified wake was observed. Wake modification occurred at Re equal to 6.4×10^5 per foot. The changes in the condition of the wake were abrupt and readily observable on the schlieren monitor. Figure 3 graphically depicts the wake condition change with Reynolds number and shows the associated hysteresis. Schlieren photographs of the flow fields for the various Reynolds numbers are also presented. The numbers in the photographs refer to the test point numbers reported in Reference 16.

The results from these tests showed that at lower Reynolds numbers the wake could be modified at parachute trailing distances where the wake was closed at higher Reynolds numbers. It would seem then, that the critical trailing distance, $(X/D)_{crit}$, would increase with decreasing Reynolds number. That this is an accurate description of the relationship between Re and $(X/D)_{crit}$ is supported in the literature. Dayman and Kurtz, in Reference 18, discussed the wind tunnel flight tests of a sphere drogue behind a 10 degree half angle cone forebody at Mach 4. They showed that $(X/D)_{crit}$ was greater than 5 calibers for a Reynolds number based on the forebody base diameter, Re_D , of 0.85×10^5 . At Re_D of 3.40×10^5 , $(X/D)_{crit}$ was less than 5 calibers. Kavanau (Reference 19) measured the base pressure on sting mounted 60 degree apex angle right circular cones with cylindrical afterbodies 2.00 calibers long. Forebody diameters were 0.17, 0.30 and 0.60 inches, and sting to forebody diameter ratios were 0.177 and 0.233. A 60 degree apex angle disturbance cone, 0.625 inches in diameter, served as the trailing body. A summary of all of Kavanau's data is replotted in Figure 4 as the critical sting length in calibers versus Reynolds number based on the forebody length. The critical sting length is the minimum sting length possible for obtaining a base pressure within 0.5 percent of that obtained with an "infinite" sting length. A typical plot of sting length as a function of base pressure coefficient at constant Reynolds number is also included in the Figure. The critical sting length increased significantly with decreasing Reynolds number in the range of Re_L from 0.4×10^5 to 4×10^5 .

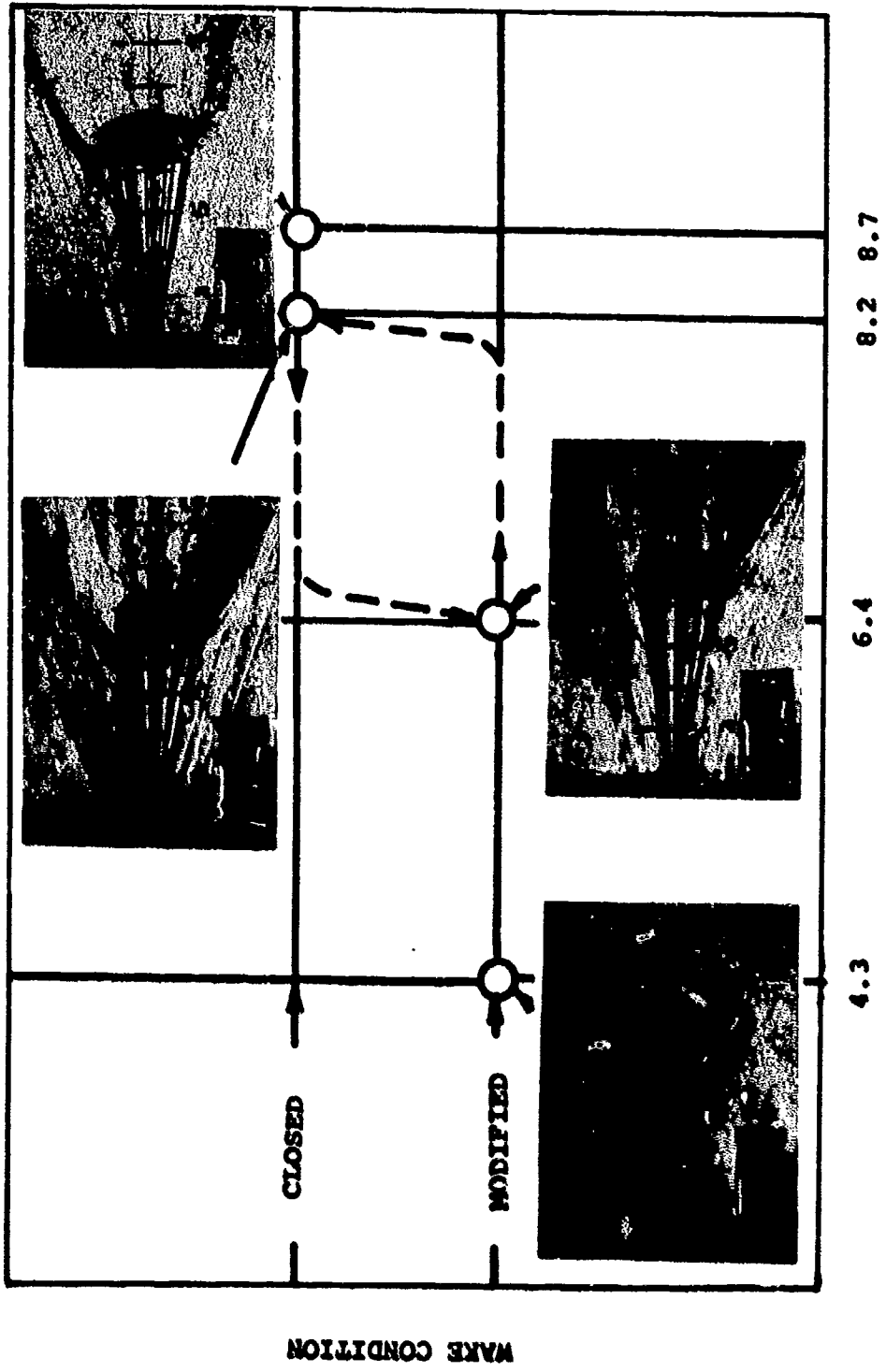


Figure 3. Wake Conditions Behind a Cone-Cylinder with a Trailing Hyperflo Type Parachute for Various Free-Stream Reynolds Numbers at $M \infty = 3.0$

The same relationship between Reynolds number and critical trailing distance was found for two-dimensional bodies. Van Hise (Reference 20) showed the variation of minimum disturbance length with Reynolds number for probes in the wake of ogival forebodies at Mach 2.92. Van Hise's results, presented in Figure 5, show the increase in critical trailing distance with decreasing Reynolds number. Critical trailing distance, again, is that distance downstream of which the base pressure is not affected by the probe. One probe was so small compared to the forebody that Van Hise felt that the location of the probe tip at the minimum disturbance length was the critical point referred to by Crocco and Lees in Reference 21. According to Crocco and Lees, a singularity in their basic equations indicated a critical point in the wake flow which acts like a throat of a nozzle in determining the base pressure; that is, disturbances introduced into the wake at positions downstream of the critical point are not able to affect base pressure.

Also plotted in Figure 5 is Van Hise's curve for r/D versus Re_L . This ratio was obtained from schlieren photographs from his tests where r was measured from the forebody base to the point of convergence of the wake recompression wave into the trailing shock. Van Hise commented that, because of the good agreement between the r/D values and the minimum disturbance lengths for the small probes, the location of the convergence point of the trailing recompression wave is a good indication of the location of the critical point or wake throat.

Later experimental tests performed by Kavanau in rarefied supersonic flow (Reference 22) showed an increase in critical trailing distance with increasing Reynolds number. These tests employed the same models he used for the tests reported in Reference 19, but were in the range of Re_L from 4×10^2 to 7×10^3 and at Mach numbers of 2.1 and 4.0. His interpolation of the data for a Mach number of 2.84 is presented in Figure 4. Interpretation of all his data indicates that, while $(X/D)_{crit}$ was strongly influenced by Reynolds number, the relationship between $(X/D)_{crit}$ and Re was dependent upon Reynolds number range.

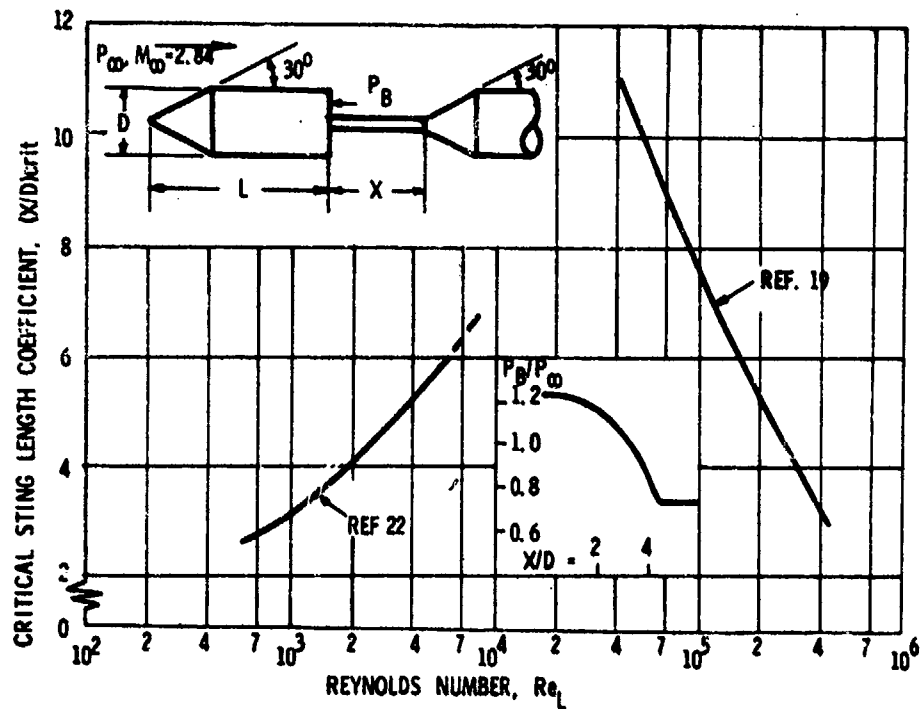


Figure 4. Effect of Reynolds Number on the Critical Sting Length; Replotted from References 19 and 22

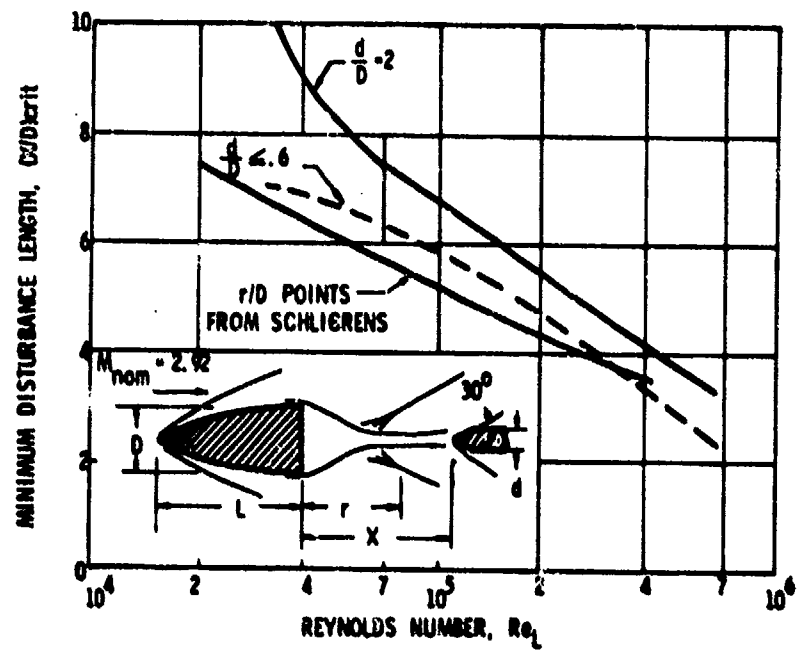
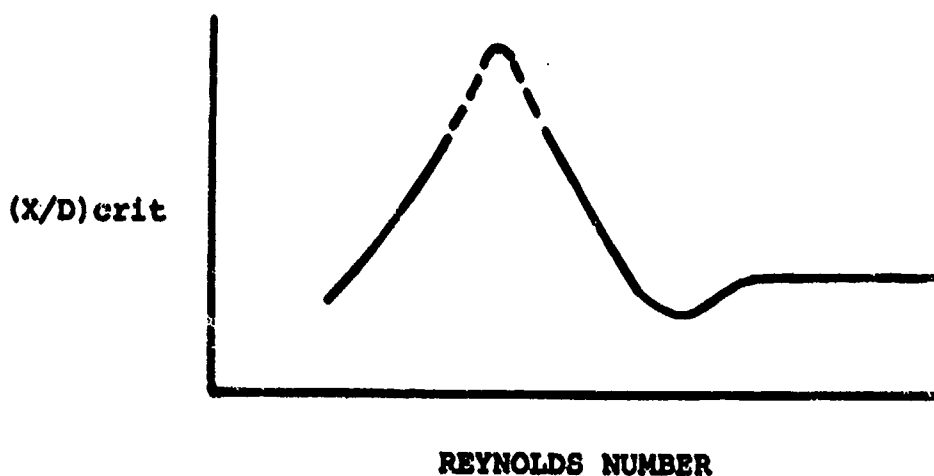


Figure 5. Variation of Minimum Disturbance Length (Expressed in Base Heights) with Reynolds Number at $M_{nom} = 2.92$; Replotted from Reference 20

Whitfield (Reference 23) discussed this increase then decrease of $(X/D)_{crit}$ with increasing Reynolds number, Re_L , but he presented strong arguments that $(X/D)_{crit}$ is a function of both the length and transition Reynolds numbers at a given Mach number. In other words, in the Re_L range of decreasing $(X/D)_{crit}$, a reduced length Reynolds number gives a greater critical sting length for a given relative transition location, and a greater relative location of transition gives a greater critical sting length for a given length Reynolds number. Whitfield's tests were similar to Kavanau's and performed in the Reynolds number range from 10^5 to 10^6 per inch and at Mach numbers of 3.00 and 3.98.

In addition to the influence of transition Reynolds number, Whitfield and Potter (Reference 24) and Miller (Reference 25) cautioned that critical sting length values can be misleading when blunt forebodies are involved and the results are referenced to a Reynolds number based on free-stream properties. Both authors obtained better correlation among all the data when the Reynolds number was based on flow conditions at the outer edge of the boundary layer immediately ahead of the model base.

In any event, Reynolds number has been shown to be an important parameter influencing wake modification. The typical variation of critical trailing distance with Reynolds number is shown in the sketch below. (Critical sting length has been found to be relatively insensitive to Reynolds number at Re_L above 2×10^6 for slender bodies; see, for example, Reference 26).



c. Flow Field Interferences

(1) Base Bleed

From the results of the wind tunnel tests reported in Reference 16, Sims concluded that air flowing through the forebody base into the base flow region could significantly affect wake modification. The test set-up for his experiments allowed for the remote positioning of the trailing parachute by means of a cable routed in a sealed channel through the forebody, a strut, and tunnel wall to externally mounted control hardware. When the hole in the tunnel wall was not sealed, air could flow through the cable routing channel into the base flow region. Sims performed tests with the hole alternately sealed and open to the atmosphere for comparative evaluations. Highly modified wakes were obtained with a parachute model at trailing distances of 7, 9, and 11 calibers at Mach 5 with the hole open. The same parachute model under identical tunnel conditions produced closed wakes at trailing distances greater than 7 calibers when the hole was sealed.

Additional data on a model decelerator in the wake of a forebody with and without base bleed were obtained by the AFFDL. These tests were performed at the conclusion of the tests reported by Myers and Hahn in Reference 27 and in the same test facility with the same test set-up, instrumentation, support system, and forebody (Configuration 2 from Reference 27). The trailing decelerator was a model Hyperflo type parachute (Configuration 1 from Reference 15). Free-stream tunnel conditions were as follows: Mach number 2.98, stagnation pressure 3.0 psia, dynamic pressure 0.52 psia, and stilling chamber temperature 579R. The vacuum tank housing the externally mounted control hardware was alternately opened and closed to the atmosphere. Schlieren photographs of the resulting flow fields about the parachute at various trailing distances aft of the forebody are presented in Figure 6. Examination of the photographs reveals that the forebody wake flow field was modified when the vacuum tank was opened to the atmosphere. While the modification is not as pronounced as that reported by Sims, it can readily be seen that the wake trailing shock wave was moved away from the centerline and forward toward the forebody base by the bleed.



X/D = 4.5

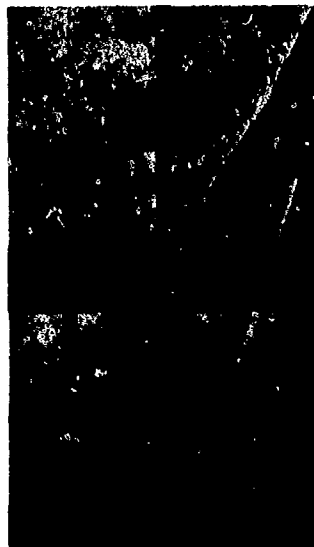


X/D = 5.0

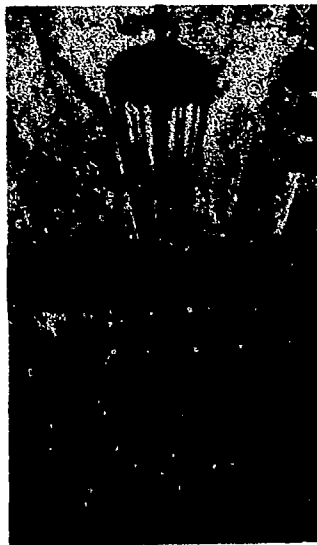


X/D = 6.0

a. - Vacuum Tank Opened to Atmosphere - Base Bleed



X/D = 4.5



X/D = 5.0



X/D = 6.0

b. - Vacuum Tank Sealed - No Base Bleed

Figure 6. Schlieren Photographs of the Flow Fields About a Hyperflo Type Parachute With and Without Base Bleed Through the Forebody at $M_\infty = 3.0$

While no other reports could be found documenting tests of a body in the wake of a leading body with base bleed, it was found that base bleed by itself could produce significant wake modifications. Bauer (Reference 28) stated that helium injected into the base flow region through the base of a cone caused the sharp pressure gradient representing the wake trailing shock wave to disappear for certain sizes and locations of the injection ports at a free-stream Mach number of 3.0. Cortright and Schroeder (Reference 29) indicated that the strength of the wake trailing shock wave decreased with base bleed for a cone-cylinder model very similar to the one Sims used. Examination of the schlieren photographs of the wake flow fields presented by Cortright and Schroeder shows the wake trailing shock wave clearly visible behind the model with no bleed. No trailing shock wave can be seen in the wake of the model with bleed.

Cortright and Schroeder's work helps to explain the more pronounced wake modification due to base bleed exhibited during Sims' test as compared to the AFFDL tests. The AFFDL model had a base exit hole 0.25 inches in diameter giving a ratio of base open to base total area, A_0/A_B , of 0.0045. For the model tested by Sims, the base exit hole was 1.5 inches in diameter and A_0/A_B was 0.5586. The diameter of the parachute positioning cable was approximately 0.125 inches in both tests. Cortright and Schroeder indicated that for a fixed bleed-air intake geometry, base flow field modification increased with increasing open area of the base.

Cassanto and Hoyt (Reference 30) showed that mass addition introduced into the base flow region through the forebody boundary layer can have a significant effect on the forebody wake. Base pressure data, obtained from full scale reentry flight tests, was plotted as a function of the rate of mass addition to the boundary layer due to the ablation of heat shield material. A near linear relationship between base pressure and mass addition rate was indicated. The authors also postulated that this mass addition decreased the flow turning angle over the base and moved the neck region downstream.

From the above, it appears that base bleed is an important parameter affecting wake modification and that $(X/C)_{crit}$ can be increased by increasing base bleed.

(2) Forebody-Trailing Body Connectors

The effects of suspected flow field interferences other than base bleed were not as pronounced. Trailing decelerators, when connected to the forebody by means of a cable or riser, take on the appearance of a disturbance cone of a wind tunnel sting mounted forebody. The geometry of the riser, then, may influence $(X/D)_{crit}$ in the same manner as sting geometry. Kavanau (Reference 22) noted that larger sting diameters gave slightly larger critical sting lengths. However, Coats' data of critical trailing distance, axial force, and forebody base pressure (Reference 7) were the same for a trailing 30 degree cone with and without a riser.

Nerem (Reference 31) postulated that, based on the no-slip condition at the surface of the riser and the assumption of negligible work due to riser skin friction, the conventional supersonic wake in the presence of a decelerator with riser will become modified to one cylindrically shaped which will not change characteristics in the axial direction. To investigate this concept some flow field surveys were performed by the AFFDL. Limited wind tunnel measurements of total pressures in the wake of a 3.22 inch diameter blunted cone-cylinder-flare (forebody Configuration 2, Reference 27) with and without a simulated riser (1/8 inch in diameter) were obtained in the Mach number range from 2 to 5. The results from these tests were documented by Henke in Reference 32. Virtually no difference was indicated between the measured pressure values for the two wakes. The centerline of the nearest pressure probe was 0.26 inches from the surface of the riser. Nerem, in a later paper (Reference 33), cautioned that at the high Reynolds numbers of these tests, the "cylindrical wake" may have been limited to a sub-layer region of the riser boundary layer which was so thin as to be almost unnoticeable experimentally. Further, in the absence of experimental data at low Reynolds numbers, Nerem felt that his concept of a cylindrical wake of appreciable diameter was still valid for laminar wakes.

In any event, the importance of the presence of connecting risers cannot be discounted in the consideration of forebody wake modifications due to trailing decelerators.

Risers are not the only forebody-decelerator connectors. For decelerators of the parachute type the parachute suspension lines join the riser at a confluence point. This juncture usually results in a mass whose effective thickness is larger than that of the riser and so can be considered as a disturbing body between the parachute and forebody base. Sims, in Reference 16, commented that at certain locations the confluence point could cause pressures to feed forward to the forebody base and result in wake modification.

The suspension lines themselves constitute a trailing body and, through their boundary layer, provide a continuous sublayer of subsonic flow through which downstream disturbances can propagate upstream to the base flow region. Roberts (Reference 12) reported a slight increase in $(X/D)_{crit}$ with increasing suspension line length for Taylor type parachutes at Mach 1.40 and 2.19.

(3) Model Supports

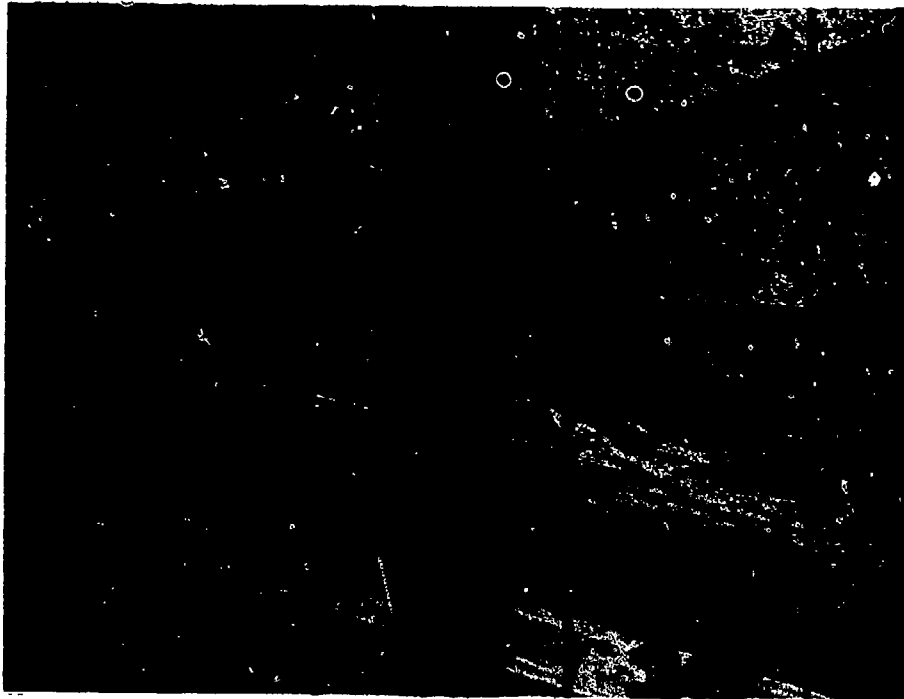
The interference effects of forebody supports on the flow fields about a forebody-decelerator system are always of great concern but are not usually known. Model tests, to obtain drag and stability data for decelerators, are usually performed in a wind tunnel with the forebody supported by lateral struts. Such was the case in References 7, 8, 9, 11, 13, 15, 16, 27 and 34. Other test arrangements include: (1) sting supports, discussed above; (2) wire supports described in Reference 12; and (3) wind tunnel free-flight tests described in References 18 and 34.

A number of diagnostic tests were performed for and by the AFFDL to evaluate the effects of forebody supports on wake modification and trailing parachute performance. These tests were documented by Sims in Reference 16. One test objective was to determine if a nonreflected oblique shock wave originating at the intersection of the strut leading

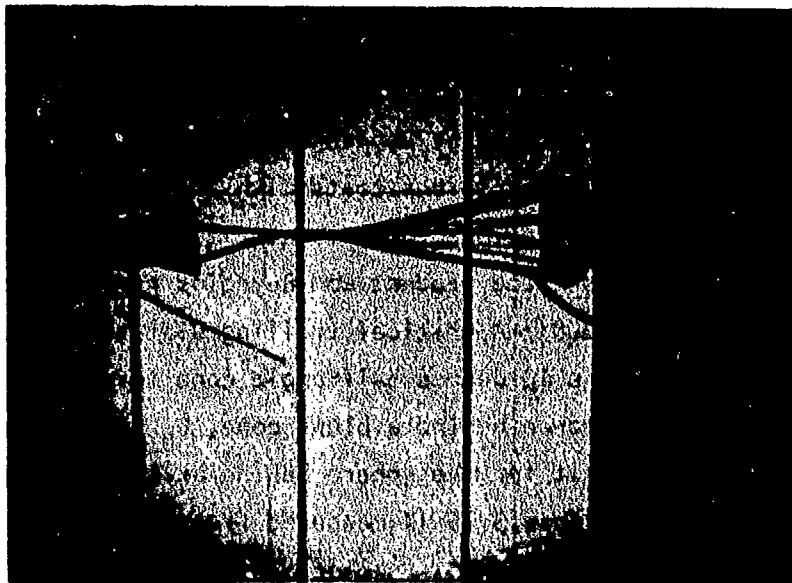
edge shock wave with the tunnel wall plate boundary layer was present. Such a shock wave was found to occur for lateral support struts tested at Mach 1.9 by Klann and Huff (Reference 35). Based on the results of the wake pressure survey portion of the diagnostic tests, the presence of such a nonreflected shock wave was highly suspect. Wake static pressure values, above those expected, were measured at X/D locations that increased with increasing Mach number. It was also noted that the location of the experimental wake centerline deviated from the geometrical forebody wake centerline.

The parachute performance portion of the diagnostic tests included tests of a 5 inch diameter Hyperflo type parachute behind a 2 inch base diameter cone-cylinder-flare-cylinder forebody. This forebody was alternately mounted on two half (tunnel) span struts of different geometry. All tests were performed at Mach 4 and at a parachute trailing distance of 7.5 calibers. For one strut the wake was modified at free-stream Reynolds numbers below 1.6×10^6 per foot and was closed at and above this Reynolds number. For the other strut the wake did not close until the Reynolds number was above 2.8×10^6 per foot. The effect of removing the strut brace rods was investigated and found negligible.

The AFFDL and AEDC later performed additional wind tunnel experiments to evaluate the effects of forebody supports on wake modification and parachute performance. In these tests, documented by Ward and Myers in Reference 34, 5 inch diameter Hyperflo type parachutes were inflated in the wake of a 3.375 inch base diameter spherical nose-cone-cylinder-flare forebody. This forebody was first mounted on a full span double wedge strut and then launched for free-flight in the wind tunnel. All tests were accomplished at Mach 4 and a Reynolds number based on the forebody diameter of 0.54×10^6 . Figure 7 presents two typical schlieren photographs obtained from these tests for a 15 percent porosity parachute trailing the forebody at 5 calibers. Analysis of photographs of these types revealed no significant flow field differences. However, as reported by Ward and Myers, the parachute drag coefficient values were lower in the free-flight tests.



a. - Full Span Double Wedge Forebody Support



b. - Free-Flight Tests - No Forebody Supports
(Photo Re-Touched to Emphasize Shock Waves)

Figure 7. Schlieren Photographs of the Flow Fields About a Hyperflo Type Parachute With and Without Forebody Supports at $M_\infty = 4.0$

Based on the results from the tests discussed above, the presence of wind tunnel forebody support struts and strut geometry can influence forebody wake structure, wake modification, and trailing parachute drag.

d. Forebody Shape

The shape of the forebody has been shown to influence the critical trailing distance. Heinrich and Hess, in Reference 10, presented schlieren photographs from wind tunnel tests of a number of trailing bodies in the wakes of a skirted hemisphere and an ogive cylinder at $M_{\infty} = 4.35$. Both the forebodies were one inch in diameter at the base. All tests were performed at the same free-stream tunnel conditions. For 1 and 2 inch diameter 45 degree half-angle cones trailing the skirted hemisphere, the critical trailing distance was between 2 and 4 calibers. For the same cones trailing the ogive cylinder, the critical trailing distance was between 4 and 6 calibers. A one inch diameter hollow hemisphere produced a highly modified wake at 3.73 calibers behind the ogive cylinder. At the same trailing distance behind the skirted hemisphere the wake was closed.

Similar results were reported by Dayman and Kurtz in Reference 18. They performed wind tunnel free-flight tests with a 1.50 inch diameter sphere trailing three different one inch diameter forebodies. The free-stream Mach number was 4 and the free-stream Reynolds number based on the forebody diameter was 85,000. A critical trailing distance between 5 and 10 calibers was found for a 10 degree half-angle cone forebody, $C_D \approx 0.16$. The critical trailing distance behind a blunt cone, $C_D \approx 0.72$, was between 3 and 5 calibers. $(X/D)_{crit}$ for the sphere behind an Apollo shape forebody, $C_D \approx 1.47$, was less than 3.75 (X measured from the Apollo shape maximum diameter).

From these test results it appears that $(X/D)_{crit}$ increases with decreasing bluntness (or drag coefficient) of the forebody.

e. Trailing Body Shape

A reverse of the above trend is indicated for critical trailing distance as a function of trailing body shape. That is, $(X/D)_{crit}$ appears to increase with increasing trailing body bluntness.

Coats (Reference 7) presented drag coefficient data for 30 and 45 degree half-angle cone probes in the wake of a Pershing reentry vehicle model in the AEDC VKF-A Wind Tunnel Facility. The forebody base diameter was 3.375 inches and the cone diameters were 2.903 inches. The data at a free-stream Mach number of 3 and a Reynolds number based on the forebody length of 3.4×10^6 are selected for comparison. Equating the range of the critical trailing distance to the range of the hysteresis loop for the sudden and large change in drag coefficient, $(X/D)_{crit}$ for the 30 degree half-angle cone was between 1.8 and 2.4. $(X/D)_{crit}$ for the 45 degree half-angle cone was between 2.0 and 3.0.

Alexander (Reference 11) presented similar data from tests performed at the NASA Langley Research Center Unitary Plan wind tunnel. He tested a 75 degree conical balloon and an 80 degree cone in the wake of a hemispherical nose-cylinder. The ratio of trailing body diameter to forebody diameter was 2.92 for both trailing bodies. At Mach 2.87, the critical trailing distance was between 0.8 and 2.8 calibers for the 75 degree conical balloon and between 3.5 and 4.5 calibers for the 80 degree cone. At Mach 2.5, $(X/D)_{crit}$ was between 1.5 and 2.5 for the conical balloon and between 4.5 and 5.5 for the 80 degree cone.

Both references showed larger critical trailing distances for the blunter trailing bodies and indicated a significant influence of trailing body shape on $(X/D)_{crit}$.

f. Trailing Body Size

Intuitively, critical trailing distance should increase with increasing size of a decelerator. That this is the case is supported in the literature.

Sims (Reference 16) showed that at free-stream Mach numbers of 5 and 5.5, an 8.2 inch diameter parachute modified the wake of a blunted cone-cylinder-flare forebody at a trailing distance of 6 calibers. The wake was closed for 5.0 and 6.8 inch diameter parachutes at the same trailing distance and Mach numbers.

Charczenko (Reference 9) presented drag coefficient data that indicated an increase in $(X/D)_{crit}$ with an increase in trailing body size at Mach numbers above 3. He tested 4, 6, and 8 inch diameter spheres in the wake of a 5.5 inch base diameter cone-cylinder-flare forebody.

Van Hise (Reference 20) reported an increase in minimum disturbance length of from 0.5 to 3.0 calibers (depending on Reynolds number) due to increasing the ratio of trailing body to forebody width from 0.6 to 2.0. His tests involved wedge tipped disturbance probes placed in the wakes of two-dimensional ogives. The free-stream Mach number was 2.92.

Pitot probes placed in the wake of a cone-cylinder magnetically suspended in a wind tunnel produced similar effects. Mirande (Reference 36) showed that the drag of the cone-cylinder was unaffected when probe trailing distances were greater than 2.1 calibers for $d/D = 0.08$ and turbulent flow. (d/D is the ratio of probe diameter to cone-cylinder diameter.) For probe diameters giving $d/D = 0.67$, the cone-cylinder drag coefficient was affected at probe trailing distances less than 3.2 calibers for turbulent flow. The free stream Mach number was 2.4.

Karpov et al (Reference 37) presented a theoretical analysis of the separated flow region between a leading conical body and a trailing spherical body that accurately predicted the relationship between $(X/D)_{crit}$ and trailing body size. For example, at Mach 2 they predicted values of $(X/D)_{crit}$ of 2.0, 3.0, and 4.1 for d/D ratios of 0.6, 1.0, and 1.4 respectively. (d/D is the ratio of trailing body diameter to leading body diameter.) Their theoretical $(X/D)_{crit}$ values were reported to be within 10 percent of experimental values obtained during "bleedings in a wind tunnel".

Based on the above test results, $(X/D)_{crit}$ has been shown to increase with increasing trailing body size.

g. Trailing Body Porosity

There are indications that the critical trailing distance is influenced by the porosity of the trailing body. Roberts (Reference 12) performed wind tunnel tests on Taylor type parachute shapes at various trailing distances behind a sharp cone-cylinder forebody. Two parachute models were used; one a solid model and the other perforated so that approximately 30 percent of the parachute surface area was removed. At Mach numbers of 1.40 and 2.19, $(X/D)_{crit}$ was decreased by 0.5 caliber by increasing the parachute porosity from 0 to 30 percent.

The results from these tests indicated that $(X/D)_{crit}$ decreased with an increase in trailing body porosity.

3. INDICATED TRENDS AND GENERAL CONCLUSIONS

A review of the literature and supplementary wind tunnel tests identified the important parameters influencing wake modification and suggested the use of critical trailing distance as a dependent parameter.

The critical trailing distance was shown to increase with (1) increasing base bleed, (2) increasing trailing body size and bluntness, (3) decreasing trailing body porosity, (4) decreasing forebody bluntness, and (5) the addition of forebody supports and forebody-decelerator connectors.

Flow field interferences such as forebody-trailing body connectors and model supports were also shown to influence forebody wake structure and trailing parachute drag.

No definite relationship between Mach number and $(X/D)_{crit}$ was established.

Reynolds number significantly affected the critical trailing distance. $(X/D)_{crit}$ was shown to first increase, then decrease, and finally level off as Reynolds number increased over three orders of magnitude.

SECTION III

SHALLOW WATER TOW TABLE TEST PROGRAM

I. TEST OBJECTIVE AND APPROACH

The objective of the shallow water tow table test program was to study the detailed flow field interactions between a leading and trailing body in order to establish a description of the mechanism for the process of wake modification.

The usefulness of studying compressible gas flow phenomena on a shallow water table has been recognized for some time. An analogy exists between the flow of shallow water with a free surface in a gravity field and the two-dimensional flow of a compressible gas. This "gas-hydraulic" analogy was postulated as early as 1911 by Isaachsen (Reference 38). Since that time the mathematical basis of the analogy has been presented and comprehensive theoretical and experimental studies have demonstrated its applicability to the study of compressible gas flow. (See for examples References 39, 40, and 41.)

The approach undertaken to meet the objective consisted of the following:

- (1) The performance of preliminary tests to establish the applicability of the gas-hydraulic analogy to the study of wake modification.
- (2) The performance of a large number of tests to evaluate the influence on wake modification of most of those parameters identified from the review of the literature and supplementary wind tunnel tests; Section II.
- (3) A detailed study of certain tests to aid in the description of the governing mechanism for wake modification.
- (4) A comparison of the postulated mechanism with the trends and relationships indicated in the literature and found during the wind tunnel and water table tests.

2. THEORY OF THE GAS-HYDRAULIC ANALOGY

The derivation of the gas-hydraulic analogy has been presented by many authors, including Preiswerk in Reference 39. Basically, it consists of writing the equations for the steady flow of shallow, inviscid, incompressible, nonheat conducting water with a free surface where the pressure on the free surface is constant, the pressure distribution forces are hydrostatic, and surface tension forces are negligible. The basic equations are continuity, momentum, and energy. The similarity between the basic equations for shallow water flow and the basic equations for the continuous flow of an inviscid nonheat conducting gas along a streamline forms the basis of the analogy. As with compressible gas flow, two useful variables are defined for shallow water flow:

- (1) The speed of an elementary surface wave

$$c \equiv \sqrt{\frac{g d}{12}} \quad , \text{ and} \quad (1)$$

- (2) Froude number,

$$M \equiv \frac{V}{C} \quad (2)$$

When these variables are introduced into the basic equations, useful dimensionless ratios can be derived - such as the total to static depth ratio:

$$d_t / d = 1 + \frac{M^2}{2} \quad (3)$$

It is noted that Equation (3) is similar to the total to static density ratio for gas flow, Equation 45 - Reference 42. That is:

$$P_t / P = \left(1 + \frac{\gamma - 1}{2} M^2\right)^{1/(\gamma - 1)} \quad (4)$$

In fact Equations 3 and 4 are identical when $\gamma = 2$, and the density and Mach number are replaced by the depth and Froude number, respectively. The similarity between these two equations leads to the often documented, but incorrect, conclusion that the flow of shallow water with a free surface is analogous to, and/or only valid for, a " $\gamma = 2$ gas".

Now, when a body is towed through shallow water or water flows past a stationary body such that the relative velocity between the body and the water exceeds the speed of an elementary surface wave, the Froude number is greater than 1. The flow is called "shooting" and is analogous to supersonic flow in gas-dynamics. (Subsonic gas flow is analogous to "streaming" water flow.) A wave in the water forms ahead of the body, raising the level of the water downstream of the wave. The phenomenon is similar to the density rise across a shock wave in supersonic gas flow. When the water flow turns away from the oncoming stream, the water level drops in a manner analogous to the density drop in expanding supersonic flow. Downstream of the body another wave is formed and the water depth rises again. This is analogous to the recompression or wake trailing shock wave and density jump in supersonic flow.

The basic equations and many useful dimensionless ratios for shooting flow with normal and oblique water waves (hydraulic jumps) and expansions are consolidated in Reference 43. Tables and charts similar to those in NACA-TR-1135 (Reference 42) are also presented. Selected ratios from References 43 and 42 are presented below to show the similarity between shallow water flow and gas flow.

Depth increase across a normal hydraulic jump:

$$\frac{d_2}{d_1} = \left(2 M_1^2 + \frac{1}{4}\right)^{\frac{1}{2}} - \frac{1}{2} \quad (5)$$

Density increase across a normal shock wave:

$$\frac{\rho_2}{\rho_1} = \frac{(\gamma+1) M_1^2}{(\gamma-1) M_1^2 + 2} \quad (6)$$

Depth increase across an oblique hydraulic jump:

$$\frac{d_2}{d_1} = \left(2 M_1^2 \sin^2 \beta + \frac{1}{4}\right)^{\frac{1}{2}} - \frac{1}{2} \quad (7)$$

Density increase across an oblique shock wave:

$$\frac{\rho_2}{\rho_1} = \frac{(\gamma+1) M_1^2 \sin^2 \theta}{(\gamma-1) M_1^2 \sin^2 \theta + 2} \quad (8)$$

Angle of flow deflection across an oblique hydraulic jump:

$$\tan \delta = \frac{\tan \beta \left[\left(1 + 8 M_1^2 \sin^2 \beta\right)^{\frac{1}{2}} - 3 \right]}{\left(2 \tan^2 \beta - 1\right) + \left(1 + 8 M_1^2 \sin^2 \beta\right)^{\frac{1}{2}}} \quad (9)$$

Angle of flow deflection across an oblique shock wave;

$$\tan \delta = \frac{2 \cot \theta \left(M_1^2 \sin^2 \theta - 1 \right)}{2 + M_1^2 \left(\gamma + 1 - 2 \sin^2 \theta \right)} \quad (10)$$

Prandtl - Meyer angle for shooting flow:

$$\nu = \frac{180}{\pi} \left[\sqrt{3} \tan^{-1} \sqrt{\frac{1}{3} (M^2 - 1)} \right] - (90^\circ - \mu) \quad (11)$$

Prandtl - Meyer angle for supersonic flow:

$$\nu = \frac{180}{\pi} \left[\sqrt{\frac{\gamma+1}{\gamma-1}} \tan^{-1} \sqrt{\frac{\gamma-1}{\gamma+1} (M^2 - 1)} \right] - (90^\circ - \mu) \quad (12)$$

From the above equations, one can readily see the similarity between Mach and Froude number, density and depth, jump and shock angle, deflection angles, Mach and Froude angles, and the Prandtl - Meyer angles. (However, only the Prandtl - Meyer angle equations are identical when $\gamma = 2$.) This discussion should serve as a review of the analogy that exists between the two types of flows but it must be remembered that analogy means "partial resemblance". The degree of agreement between gas flow and shallow water flow depends on many things and probably most important is the nature of the particular flow phenomena being studied. The validity of the analogy should be established for each test program.

3. DESCRIPTION OF THE TEST FACILITY

All shallow water tow tests were performed on the AFFDL Shallow Water Tow Table at Wright Patterson Air Force Base, Ohio. This facility is part of the AFFDL Decelerator Research Laboratory and is listed in the Air Force Technical Facility Capability Key (Reference 44).

The tow table is 45 feet long x 5 feet wide x 3 feet high and has a usable length of run for testing purposes of 38 feet. The supporting structure consists of welded structural steel. The 38 legs supporting the table are adjustable, allowing the table to be leveled to $\pm 1/8$ inch. The floor of the table consists of four pieces of high grade mirror

finish plate glass. Each is 4 feet wide x 1/2 inch thick, with the surface flatness of the glass accurate to within ± 0.001 inch. The glass is supported by 185 adjustable jack pads used for fine adjustments in leveling its surface. The glass to glass, and glass to metal joints are provided with a flexible waterproof seal.

A moving carriage, made of lightweight metal, provides for the mounting of the models, cameras, and lights. It is supported by six nylon wheels which ride on two rails, one flat and one V-groove, to reduce lateral motion of the carriage. The velocity of travel of the carriage is maintained and controlled by a variable speed-reversible-1/4 horsepower electric motor through a continuous cable-pulley arrangement. Limit switches and stops are provided.

A relay rack mounted sequence event programmer provides for the remote operation of all events and enables programming of events for automatic operation. A stereophotogrammetric data acquisition and reduction system for water depth measurements is part of the test facility.

Flow uniformity for this facility is only a function of the water depth distribution and tow carriage velocity constancy. Uniformity of the carriage velocity is presented in Section III, 6. The static water depth distribution was obtained using a micrometer depth gage; see Section III, 5. Nonuniformity in the depth within the table consists of departures from the nominal value. Spanwise depth measurements showed maximum deviations of ± 0.005 inch from the table centerline depth values for all longitudinal stations. Each station is 30 inches long.

With a centerline depth at the nominal value at the center of Station 11, the maximum longitudinal centerline depth deviations were as follows:

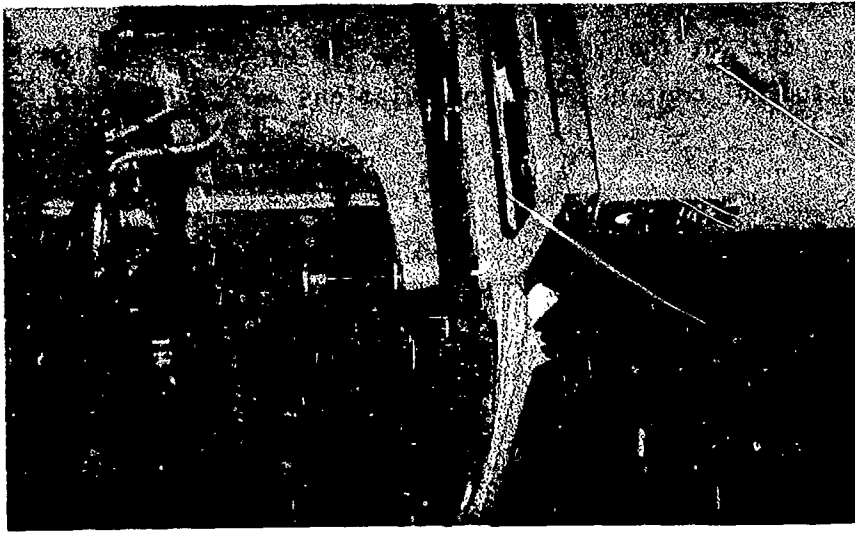
Station (s)	Depth Deviations, inch
2	-0.006
3	+0.006
4	+0.012
5	+0.016
6	+0.020
7 - 12	<u>+0.004</u>
13	+0.014
14	+0.018
15	+0.024
16	+0.026
17	-0.008
18	-0.016

The fluid medium for all tests was commercially obtained distilled water. Photographs of the shallow water tow table facility are presented in Figure 8.

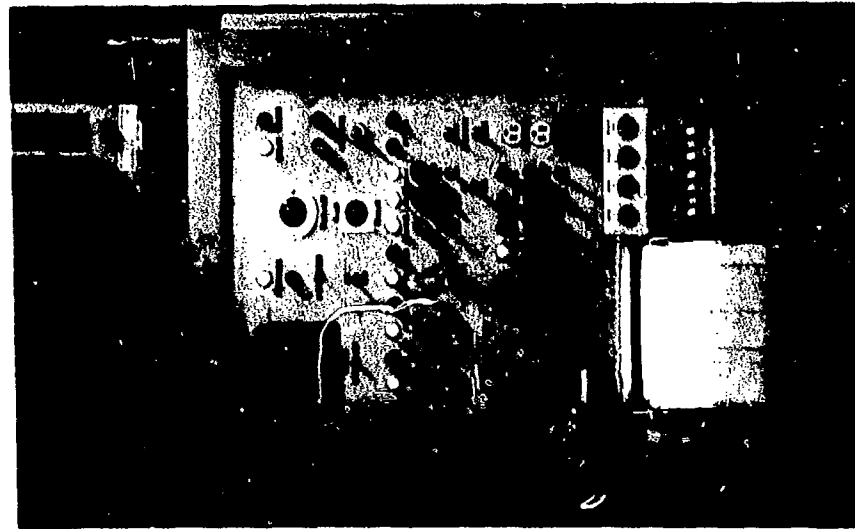
4. DESCRIPTION OF THE TEST MODELS

A listing and general description of the models used for the shallow water tow test program are presented in Table I and Figure 9. All models were made from acrylic plastic and, with the exception of the simulated parachute models, were cut from 2 inch thick "PLEXIGLAS" sheets. After polishing and drilling and tapping mounting holes, a 1/8 inch thick felt covering was glued to the bottom surface. The simulated parachute models were formed from 1/16 inch thick acrylic plastic sheets.

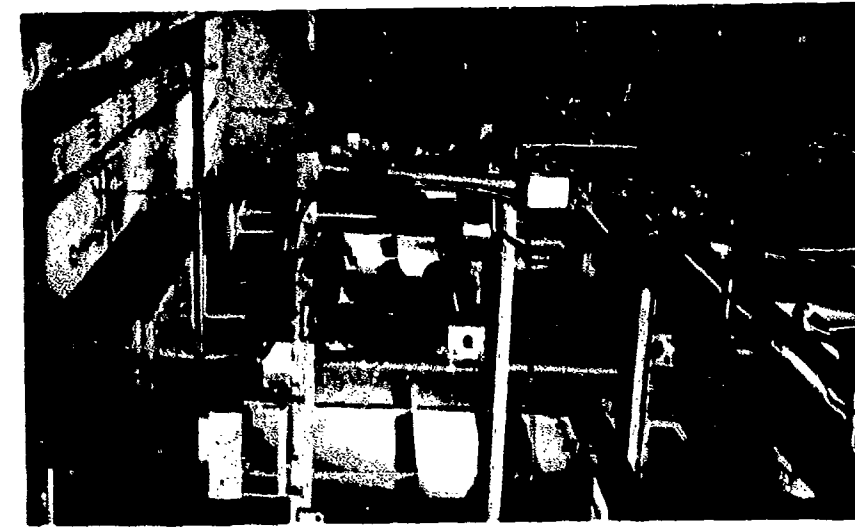
Certain models were used in combinations to form desired configurations. Photographs of selected models are presented in Figure 10.



c. Stereo-Photogrammetric Data Acquisition/Reduction System



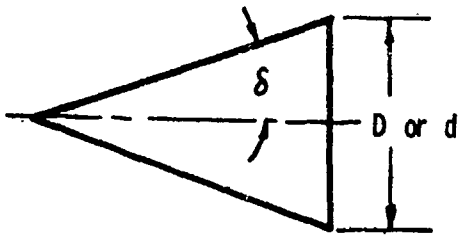
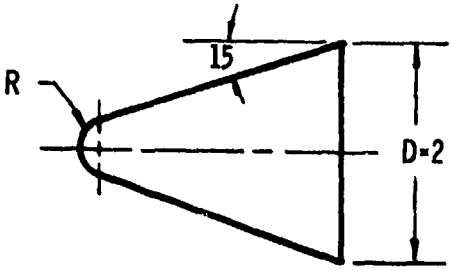
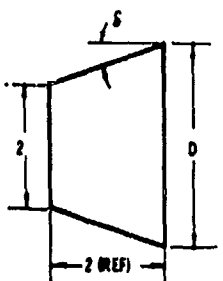
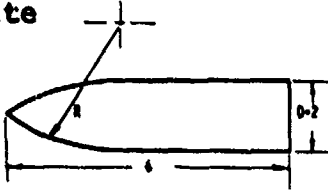
b. Relay Rack Mounted Sequence Event Programmer



a. Shallow Water Tow Table

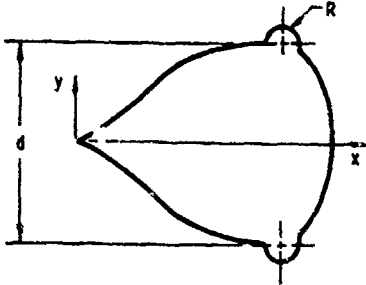
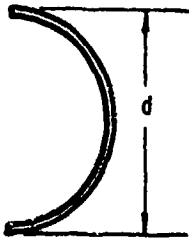
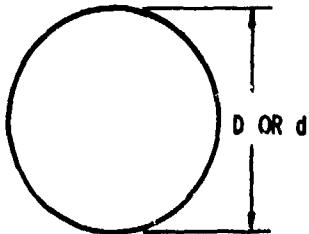
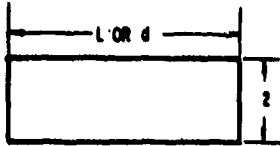
Figure 8. Photographs of the Shallow Water Tow Table Facility at the Air Force Flight Dynamics Laboratory, Wright-Patterson Air Force Base, Ohio

TABLE I
TEST MODELS

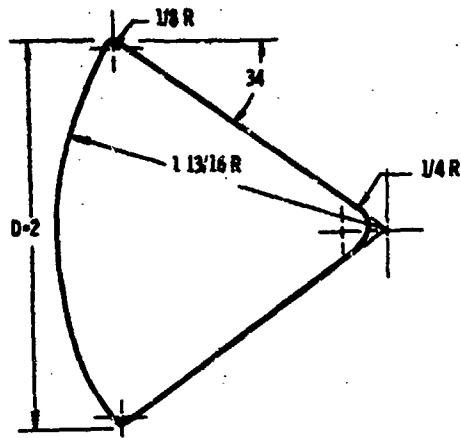
Classification	Design Variables ^a
<p>Sharp Wedge</p> 	<p> $\delta=60$; $D=2$; $d=2, 3, 4, 5, 6$ and 8 $\delta=45$; $D=2$; $d=2, 3, 4, 5, 6$ and 8 $\delta=30$; $D=2$; $d=2, 3, 4, 5, 6$ and 8 $\delta=15$; $D=2$ and 4 $\delta=10$; $D=2$ $\delta=7.5$; $D=2$ $\delta=5$; $D=2$ $\delta=3$; $D=1$ </p>
<p>Blunted Wedge</p> 	<p> $R=\frac{1}{8}, \frac{3}{8}$ and $\frac{3}{4}$ </p>
<p>Flare</p> 	<p> $\delta=5, 15$ and 25 $D=2.35, 3.07, 3.87$ </p>
<p>Ogive Plate</p> 	<p> $R=2$ and 8 </p>

^aLinear dimensions in inches; angles in degrees

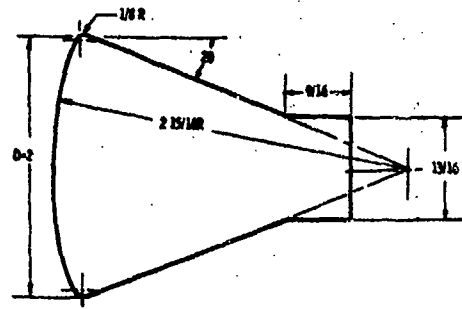
TABLE I
TEST MODELS (CONT'D)

Classification	Design Variables ^a																								
<p>Balloon Type</p> 	<p>$d=2,3,4,5,6$ and 8; $R=0.108d$</p> <p style="text-align: center;"><u>Coordinates</u></p> <table border="1" data-bbox="868 511 1455 707"> <thead> <tr> <th>x/d</th> <th>y/d</th> <th>x/d</th> <th>y/d</th> </tr> </thead> <tbody> <tr> <td>0.203</td> <td>0.000</td> <td>0.928</td> <td>0.500</td> </tr> <tr> <td>0.338</td> <td>0.149</td> <td>1.144</td> <td>0.500</td> </tr> <tr> <td>0.473</td> <td>0.269</td> <td>1.144</td> <td>0.389</td> </tr> <tr> <td>0.609</td> <td>0.440</td> <td>1.211</td> <td>0.328</td> </tr> <tr> <td>0.754</td> <td>0.487</td> <td>1.278</td> <td>0.000</td> </tr> </tbody> </table>	x/d	y/d	x/d	y/d	0.203	0.000	0.928	0.500	0.338	0.149	1.144	0.500	0.473	0.269	1.144	0.389	0.609	0.440	1.211	0.328	0.754	0.487	1.278	0.000
x/d	y/d	x/d	y/d																						
0.203	0.000	0.928	0.500																						
0.338	0.149	1.144	0.500																						
0.473	0.269	1.144	0.389																						
0.609	0.440	1.211	0.328																						
0.754	0.487	1.278	0.000																						
<p>Simulated Parachute</p> 	<p>$d=2,3,4,5,6$ and 8</p>																								
<p>Circular Cylinder</p> 	<p>$D=2$; $d=1,2,3,4,5,6$ and 8</p>																								
<p>Plate</p> 	<p>$L=1, 4$ and 8</p> <p>$d=1,2,3,4,5,6$ and 8</p>																								

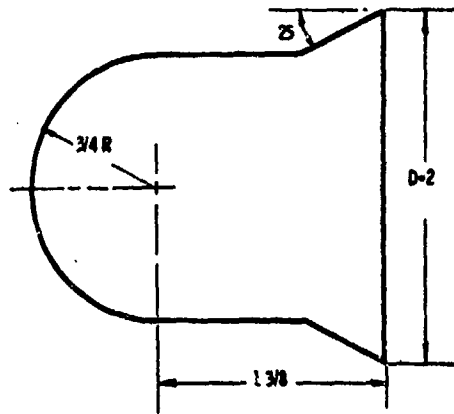
^aLinear dimensions in inches; angles in degrees



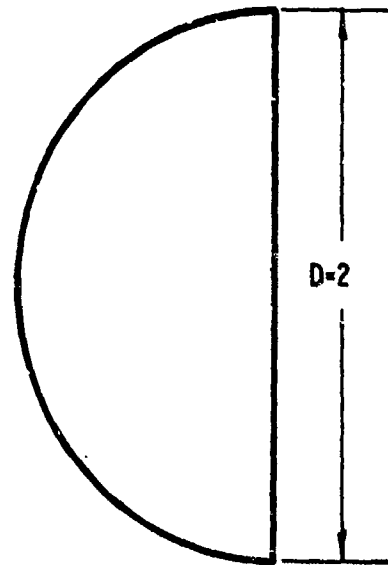
a. Apollo Type



b. Gemini Type



c. Skirted Blunt Body



d. Half Cylinder

NOTE: Linear Dimensions In Inches; Angles In Degrees

Figure 9. Test Models

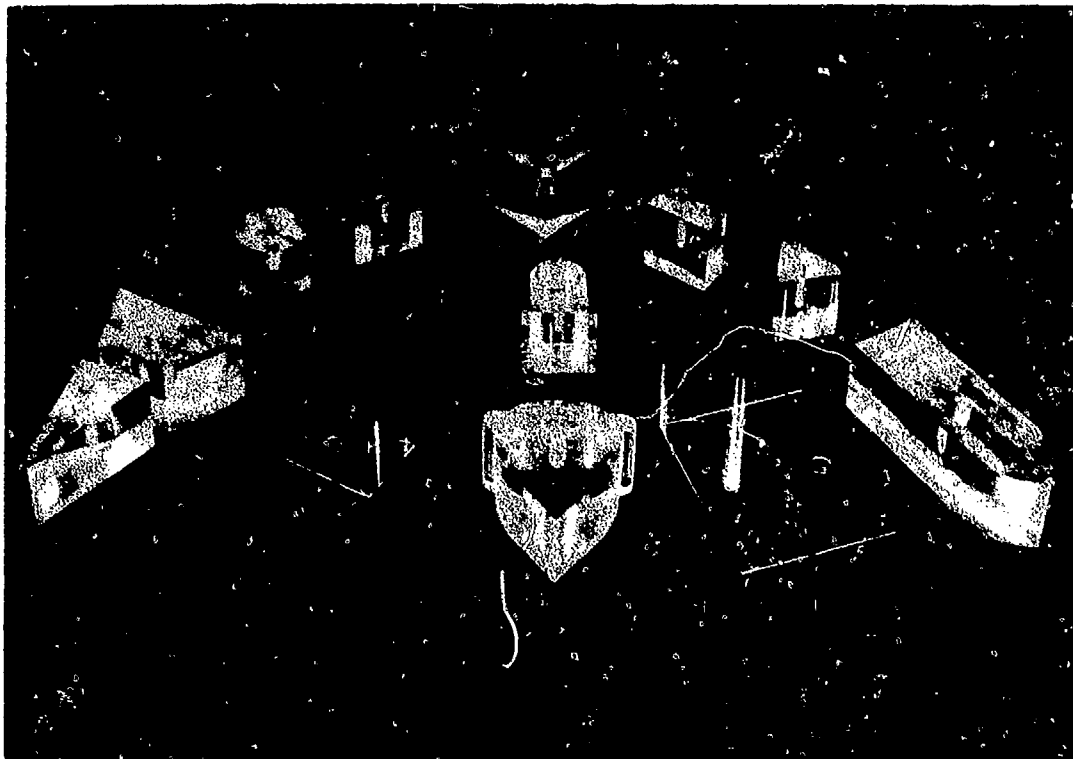


Figure 10. Photograph of Selected Test Models

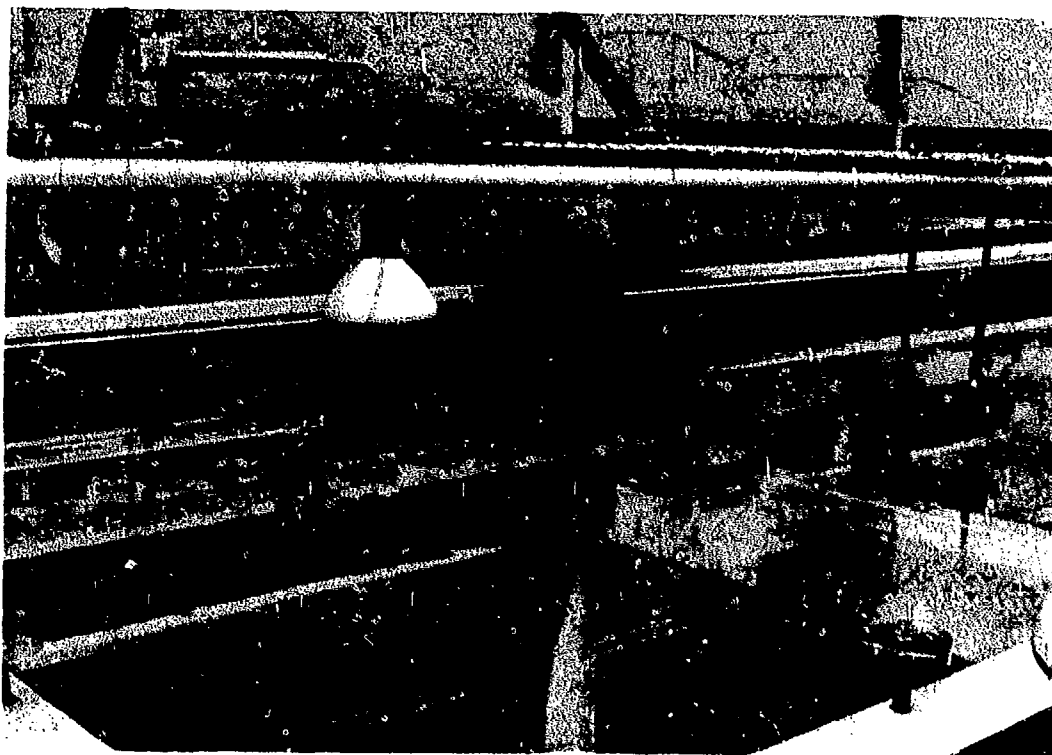


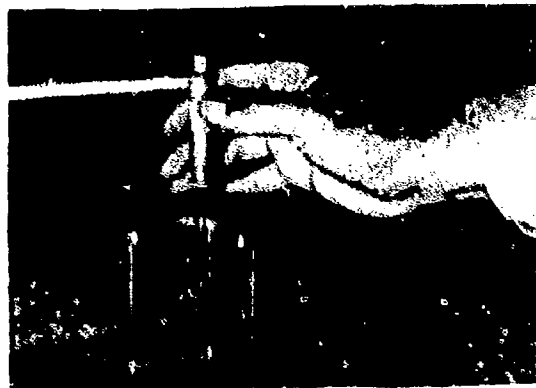
Figure 11. Slotted Acrylic Plastic Mounting Sheet for Test Models

All models were attached to slotted acrylic plastic sheets similar to the one shown in Figure 11. The mounting sheet was positioned to allow the model to ride on the table floor under its own weight. The parachute models were fastened with a wing nut and bolt and the other models were fastened with a screw threaded into the model mounting hole.

5. TEST INSTRUMENTATION

Carriage velocities were determined by differentiation of carriage displacement-time functions derived from the recordings of discrete pulses by a Honeywell 1508 Visicorder direct print oscillograph. The recorded pulses were analog voltages generated as a result of intermittent closures of a circuit loop consisting of a d-c power source, a contact strip, a wiper, a current-limiting potentiometer and a galvanometer. The contact strip was fabricated from phenolic bar stock with inlaid contacts spaced 2 inches apart and internally connected. The wiper was spring loaded and mounted to the carriage. As the carriage moved, circuit closure was accomplished as the wiper moved over an inlaid contact resulting in a pulse recorded by the oscillograph. The distance between pulses, then, represented 2 inches of carriage displacement. To determine carriage velocity, timing lines recorded by the oscillograph and generated from an internal timer were utilized. A Gerber Scientific Instrument Co. 10 Inch Variable Scale was used to check the uniformity of pulse distance and to determine the number of pulses per second.

Water depth measurements were made using the table mounted Lufkin Rule Co. Micrometer Depth Gage shown below.



Black and white sequence still photographs of the flow field in the vicinity of the towed model were obtained with a 35 mm double frame Automax motion picture camera (Model G 1-D). Quick-look photographs were provided by a Graphic 4 x 5 press still camera equipped with a Graphic Polaroid back. Lighting for both cameras was provided by two photoflood lamps (R2) mounted on the carriage as shown in Figure 12. The lamps were located on either side of the test model and aimed downward. The cameras were also aimed directly down. Twenty inches below the glass bottom a reflective surface (glossy white paint on plywood) extended the entire length of the table. Light reflected from this surface allowed for oblique back lighting of the model and water waves. Light from the two lamps absorbed by the water and traveling horizontally through the water highlighted the waves. The photographs were used for determining the degree of wake modification and for measuring displacements and angles in the flow field.

Linear dimensions were obtained from the photographs using a Benson-Lehner Corp. Continuous Trace Oscar Oscillogram Data Reducing System. Displacements from a reference zero were digitized using a Benson-Lehner Corp. Decimal Converter Model-F and tabulated using a Benson-Lehner Corp. Electrotyper, Model C (IBM Typewriter). Angles were measured from the photographs using a protractor.

6. PRECISION OF THE DATA

The precision of the velocity and water depth measurements were estimated based on repeat calibrations and are listed below.

<u>Water Depth</u>	<u>Carriage Velocity</u>	<u>Uniformity of Carriage Velocity</u>
<u>+0.0005</u> inch	<u>+0.10</u> inch/sec.	<u>+0.20</u> inch/sec.

The uncertainty in measured Froude number was estimated based on Equations (1) and (2) using the maximum uncertainties of water depth and

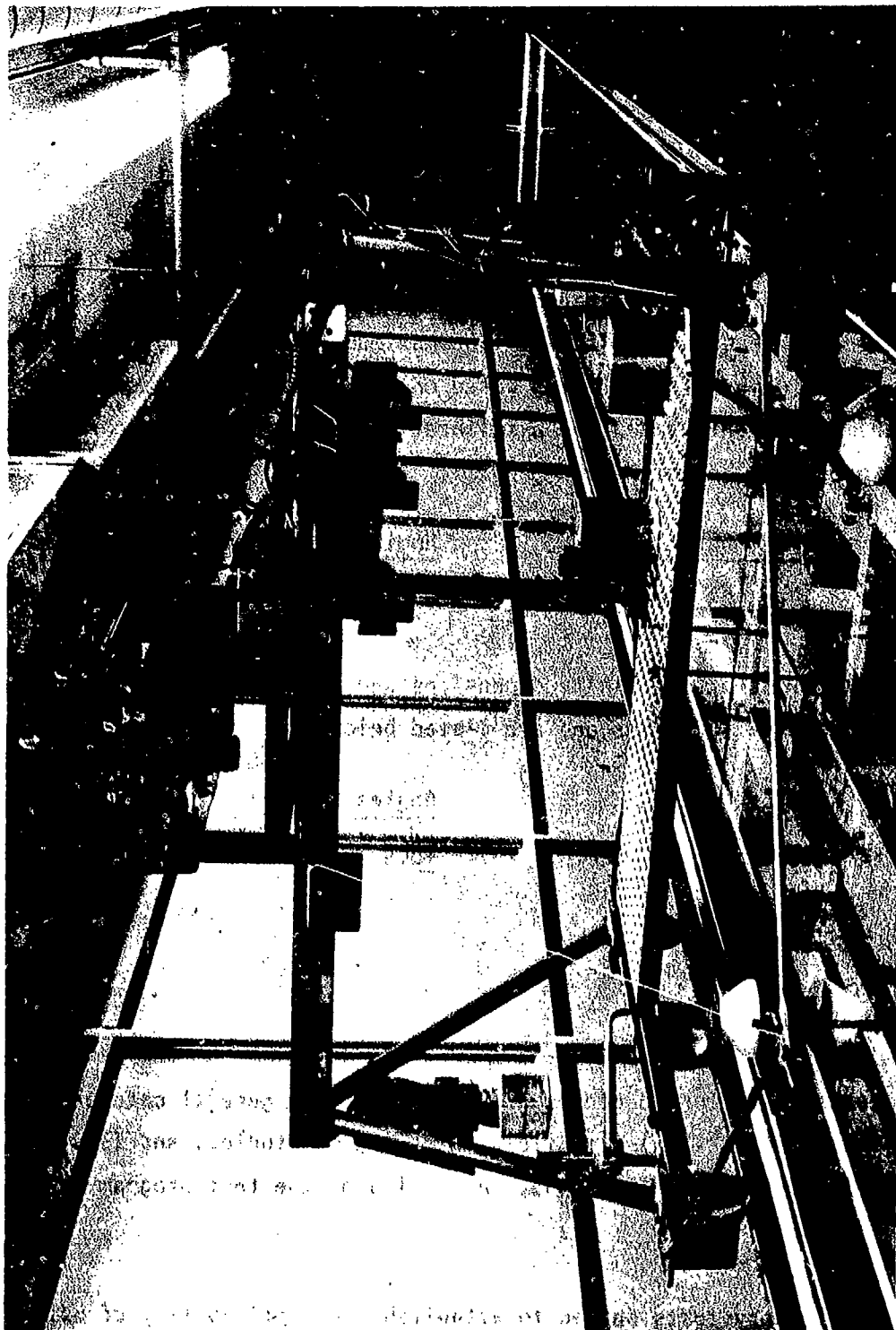


Figure 12. Shallow Water Tow Table Carriage and Lighting Arrangement

carriage velocity in combination to produce the maximum uncertainty in M for water depth of 0.1900 inches.

<u>Measured M</u>	<u>Uncertainty in M</u>
1.5	<u>+1.7%</u>
5.0	<u>+0.6%</u>

Water depth and carriage velocity measurements were not made for every run and a nominal depth and Froude number are given. The maximum uncertainty of the nominal water depth is estimated based on the pre and post test depth measurements taken. The maximum uncertainty of the nominal Froude number is estimated based on the pre and post test velocity and depth measurements taken and a calibration of uniformity of carriage velocity over a number of runs.

<u>Nominal Water Depth</u>	<u>Nominal Froude Number</u>
<u>+0.005 inch</u>	<u>+0.10</u>

The precisions of the linear dimensions and angles were estimated based on repeat calibrations and are listed below.

<u>Lengths</u>	<u>Angles</u>
<u>+0.01 inch</u>	<u>+0.5 degree</u>

7. TEST PROGRAM

a. Test Run Summary

The tests as performed can be grouped into three general categories; (1) preliminary tests, (2) flow field interference studies, and (3) influencing parameter investigations. A listing of the test program is given in Table II.

The preliminary tests served to establish the applicability of using the water table for the study of wake modification. They were also used to determine the degree of agreement between the experimental data and

TABLE II
TEST PROGRAM

Test Category	Runs	Water Depth (inch)	Froude No.	Forebodies	Trailing Bodies	Study
Preliminary Tests	C1-C36	0.190	2, 3 & 4	Wedges	Parachute	General flow field
	1-191	0.1000 to 0.4400	2, 3 & 4	5 Wedges	Parachute & Plates	Water depth, General flow field, applicability of water table for wake modification study
	DD1-DD42	0.190	1.8 to 4.0	Circular Cylinders	None	Shock wave detachment distance
Flow Field Interference Studies	AL-A80	0.190	2, 3 & 4	5 degree 2 inch Wedge	4 inch Parachute	Effect of shock impingement on wake and its modification
	AS1-A127	0.190	2, 3 & 4	5 degree 2 inch Wedge	4 inch Parachute	Effect of flow splitter
	AL28-A132	0.190	2	5 degree 2 inch Wedge	4 inch Parachute	Effect of disturbing body
	AL33-A183	0.190	4	5 degree 2 inch Wedge	4 inch Parachute	Effect of base bleed
Influencing Parameter Investigations	B1-B268	0.190	1.5 to 5.0	5 degree 2 inch Wedge	All Parachute Models	Effect of Froude number and parachute size. (Parachute alone data)
	B269-B282	0.190	2.5	Apollo & Gemini Wedges	4 inch Parachute	Effect of forebody shape
	B283-B336	"	"	Skirted Blunt Body	"	"
	B337-B344	"	"	Ogive-Plates	"	"
	B345-B356	"	"	Blunted Wedges	"	"
	B357-B375	"	"	Half Cylinder	"	"
	B376-B381	"	"	Cylinder	"	"
	B382-B398	"	"	Wedge-Plate	"	"
	B399-B422	"	"	Plates	"	"
	B423-B439	"	"	Half Cyl. - Plate	"	"
	B440-B446	"	"	Blunted Wedge - Plate	"	"
	B447-B464	"	"	Wedge - Plate - Flare	"	"
	B465-B494	"	"	Wedge - Plate - Flare	"	"
B495-B602	0.190	2.5	5 degree 2 inch Wedge	Parachutes	Effect of trailing body size and shape.	
B603-B640	"	"	"	Wedges	(Trailing body alone data)	
B641-B683	"	"	"	Balloon Types	"	
B684-B731	"	"	"	Plates	"	
				Circular Cylinders	"	

shallow water flow theory. This was helpful in selecting water depth, Froude numbers, model size and angles, and test procedures to be used for subsequent tests.

The flow field interference studies provided a visualization of the flow field interactions that take place due to the presence of those flow interferences identified during the review of the literature and supplementary wind tunnel tests discussed in Section II. Simulations on the water table of base bleed, extraneous shock waves, forebody-trailing body connectors, and disturbing bodies were accomplished.

The influencing parameter investigations established the effect of Froude number, forebody shape and trailing body size and shape on wake modification.

b. Test Procedure

Station 11 was chosen as the "test section" based on the depth distribution calibration of the facility. Starting a run at Station 2 provided 10 feet of nearly uniform water depth before reaching the test section. The test section is that station where the camera shutters were tripped and the static water depth measurements were made. A typical test proceeded as follows:

1. The model was selected and fastened to the mounting sheet. Angle of attack was adjusted to zero for all tests.
2. The water depth at the center of Station 11 was checked, adjusted, and recorded. Water depth was not always checked before a run, but was allowed to drop due to evaporation during a test series. Post test series depth checks showed water depth decreases always less than 0.005 inch.
3. The required carriage velocity was then calculated based on the actual or nominal water depth and the desired Froude number.

4. Carriage velocity control was set for the desired Froude number and carriage motion started for a trial run.
5. An oscillograph record was obtained and the velocity determined. Trial runs were repeated until the correct velocity was achieved.
6. Camera shutters were cocked and the overhead lights were turned off. The facility air conditioner was off for the tests to eliminate any water waves due to air movement.
7. The carriage was set in motion and the carriage lights were turned on.
8. The oscillograph was turned on at Station 7 and, along with the carriage lights, turned off at Station 12.
9. The carriage was returned to Station 2.
10. Quick-look Polaroid film was removed, if obtained for a particular test, and it, along with the oscillograph record, was labeled as required.
11. The model was prepared for the next run.

c. Data Gathered

Data gathered during the test program included; (1) the water depth, (2) an oscillograph record of carriage motion - with a time base, (3) sequence still photographs of each test, and (4) quick-look Polaroid photographs of some tests.

The water depth and carriage velocity (as determined from the oscillograph trace - see Section III, 5) determined the Froude number for each test. Measurements from the photographs gave; (1) model and wave angles, (2) model separation distances, (3) detachment and other distances, and (4) wave shapes. Analysis of the photographs indicated the degree of wake modification and the type or nature of flow field interactions.

SECTION IV

DISCUSSION OF TEST PROGRAM RESULTS

1. PRELIMINARY TESTS

a. Applicability of Water Table Tests to the Study of Wake Modification

As discussed previously, numerous theoretical and experimental studies have demonstrated the applicability of shallow water table tests to the study of compressible gas flow phenomena. In addition, Heinrich and Ibrahim (Reference 45) and Lau (Reference 46) have demonstrated the usefulness of such tests for the study of the flow fields surrounding two and three-dimensional primary and secondary body combinations in supersonic flow. Karpov (Reference 37) suggested that a shallow water table be used to visually evaluate the character of the flow field in the region between a leading and trailing body in supersonic flow. Because of this background, the early preliminary tests included tests with a leading body and simulated decelerators at various trailing distances.

The flow field patterns observed on the water table were certainly similar to those observed during wind tunnel tests and documented in the literature. Figure 13 is presented to show this similarity. The schlieren photographs were obtained during the wind tunnel tests reported by Myers and Hahn in Reference 27. The forebody was Configuration 2 and the trailing decelerator was a Parasonic type parachute, Configuration 1. The water table shadowgraphs were obtained for a simulated parachute model trailing a 5 degree 2 inch wedge. The wake trailing shock wave and corresponding hydraulic jump and decelerator bow shock wave and corresponding hydraulic jump are readily discernable at the larger trailing distances. At the shortest trailing distances the wakes were obviously modified.

In addition to the similarity between the wind tunnel and water table flow field patterns, the water table tests indicated the same relationship between $(X/D)_{crit}$ and trailing body size as was found during the wind



X/D = 4.5



X/D = 5.0



X/D = 6.0

- a. - Schlieren Photographs of a Parasonic Parachute Trailing an Arapaho Missile Model in a Wind Tunnel (Reference 27); Free-Stream Mach Number = 2.0



X/D = 4.25



X/D = 5.0



X/D = 6.0

- b. - Shadowgraphs of a Simulated Parachute Trailing a Sharp Wedge on the Shallow Water Tow Table; Free-Stream Froude Number = 2.0

Figure 13. Comparison of the Flow Fields About Leading and Trailing Bodies Tested in the Wind Tunnel and on the Shallow Water Tow Table

tunnel tests. It was concluded in Section II, 3 that the critical trailing distance increased with increasing trailing body size. Figure 14 shows that this same relationship was obtained during the preliminary shallow water tow tests.

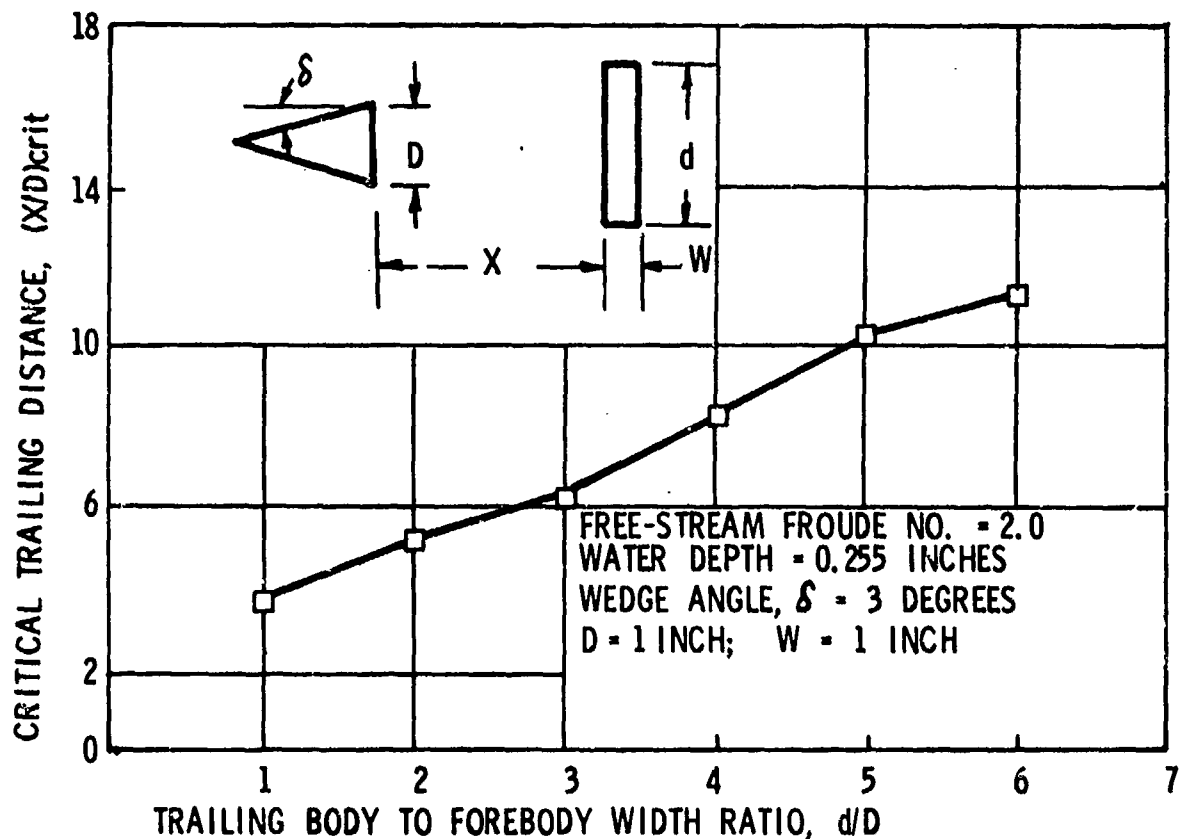


Figure 14. Variation of Critical Trailing Distance with Trailing Body Size for a Plate Trailing a Thin Wedge.

b. Experimental Considerations

Analysis of the results from the preliminary tests provided a basis for selection of test parameters and procedures for subsequent tests. Selected results obtained from these preliminary tests are tabulated in Tables III and IV.

Selection of an "optimum" water depth was aided by analytical considerations. The similarity between gas flow and shallow water flow was easily recognized when the velocity of propagation of a water wave

TABLE III

TEST RESULTS - HYDRAULIC JUMP ANGLES AND X_0
DISTANCES FOR SHARP WEDGE TEST MODELS

Nominal Water Depth	Froude Number	δ	β	X_0/D	Nominal Water Depth	Froude Number	δ	β	X_0/D
0.127	2.00	5	38.0	---	0.242	2.00	5	33.0	0.33
0.127	2.00	7.5	38.6	0.46	2.00	15	46.0	0.17	
0.127	2.00	10	---	---	1.95	15*	49.6	0.57	
0.100	2.10	15	50.7	---	2.80	5	24.4	0.33	
0.100	1.85	15*	57.2	---	2.80	15	35.5	0.37	
0.100	3.20	5	24.0	---	2.80	15*	39.3	0.62	
0.127	3.10	7.5	26.5	0.66	4.05	5	18.2	0.53	
0.127	3.10	10	29.0	0.67	4.10	15	29.0	0.90	
0.100	3.20	15	35.3	---	4.10	15*	29.0	0.97	
0.100	3.20	15*	35.0	---	0.300	2.00	5	32.2	0.20
0.100	4.15	5	19.6	---	2.00	15	44.5	0.43	
0.127	4.30	7.5	20.5	---	2.00	15*	48.2	0.48	
0.127	4.00	10	26.1	0.85	3.00	5	22.4	0.37	
0.100	4.15	15	29.2	---	3.00	15	32.2	0.53	
0.100	4.10	15*	30.1	---	3.00	15*	33.0	0.66	
0.150	2.00	5	37.2	0.43	4.10	5	17.9	0.50	
2.00	15	48.5	0.53		4.10	15	26.5	1.00	
1.95	15*	51.1	0.60		4.10	15*	28.0	1.10	
2.95	5	24.4	0.45		0.372	1.95	5	31.3	0.15
3.00	15	35.1	0.70		2.00	15	42.7	0.30	
2.95	15*	35.8	0.59		1.95	15*	44.1	0.38	
3.90	5	19.1	0.30		3.05	5	21.8	0.43	
3.90	15	27.9	0.66		3.05	15	31.5	0.73	
3.90	15*	30.4	---		3.05	15*	32.5	0.71	
4.40	5	16.9	0.53		4.00	5	17.6	0.73	
4.35	15	25.8	0.73		4.05	15	25.1	1.63	
4.40	15*	30.0	---		4.05	15*	27.5	1.14	
0.200	2.00	5	34.7	0.26	0.440	1.95	5	28.7	0.17
1.90	7.5	37.3	0.18		1.95	15	43.6	0.41	
1.90	10	41.5	0.24		1.95	15*	43.5	0.33	
1.95	15	44.9	0.48		3.00	5	20.4	0.50	
2.00	15*	49.0	0.66		3.00	15	31.2	0.83	
3.05	5	22.9	0.33		3.00	15*	31.5	0.67	
2.90	7.5	25.3	0.24		4.00	5	16.8	0.83	
2.90	10	30.1	0.47		4.00	15	24.4	1.93	
3.05	15	34.8	0.33		4.00	15*	27.2	1.14	
3.05	15*	35.9	0.66						
3.95	5	18.7	0.57						
4.00	7.5	21.8	---						
4.00	10	25.2	0.49						
3.90	15	30.4	0.70						
3.95	15*	30.4	0.94						

Notes:
(1) D = 2 inches except for $\delta = 15^*$ which has D = 4 inches.
(2) Depth in inches; angles in degrees

TABLE IV
 TEST RESULTS - HYDRAULIC JUMP STANDOFF DISTANCES
 FOR CIRCULAR CYLINDER TEST MODELS

D (Inches)	Froude Number	τ/D	D (Inches)	Froude Number	τ/D
1	1.80	1.71	4	1.70	---
	1.90	1.57		1.80	1.12
	2.60	0.50		2.60	0.78
	3.00	0.39		3.00	0.75
	3.55	0.26		3.50	0.43
	4.20	---		4.10	0.43
2	1.80	1.45	5	1.75	1.22
	1.90	---		1.75	1.08
	2.65	0.76		2.55	0.54
	3.00	---		2.85	0.57
	3.55	0.50		3.50	0.46
	4.10	0.24		4.05	0.46
3	1.75	1.23	6	1.75	1.11
	1.90	---		1.90	1.02
	2.60	0.73		2.55	0.59
	2.90	0.45		2.85	0.50
	3.50	0.34		3.45	0.46
	4.15	0.41		4.00	0.39

(Equation 1, Section III, 1) was introduced into the basic equations for shallow water flow. This wave velocity, c , was defined as:

$$c \equiv \left(g \frac{d}{12} \right)^{\frac{1}{2}} \quad (1)$$

and is analogous to the speed of sound or disturbance propagation velocity through a compressible gas. That is:

$$a \equiv \left(\frac{\gamma}{\rho} p \right)^{\frac{1}{2}} \quad (13)$$

In accordance with Lamb (Reference 47) the above velocities are not constant functions of the independent parameters; especially when waves of finite amplitude are considered. For finite amplitude water waves Lamb showed that the wave velocity, c , is a function of water and air density, surface tension, water depth, and wave length even when vertical accelerations can be neglected. However, Laitone (Reference 48) and Gupta (Reference 49) showed that Equation 1 is accurate within 1 percent for waves of wave length greater than 1 inch at a water depth of 0.19 inches. Waves of wave length less than 1 inch are capillary ripples not accounted for in the analogy.

The effects of water depth on (1) hydraulic jump angle, (2) wake convergence point location, and (3) critical trailing distance are shown in Figures 15, 16, and 17. The wake convergence point is that juncture at the wake centerline of two readily observable water waves immediately downstream of the forebody. This point does not necessarily coincide with the wake stagnation point nor the wake sonic point which are much more difficult to locate. Figure 15 indicates that the shallow water flow theory agrees best with the experimental hydraulic jump angle data obtained at a water depth of 0.20 inches. While wake convergence point location changes with water depth as shown in Figures 16 and 17, no definite relationship is indicated. Figure 17 shows that the critical trailing distance also changes slightly with changing water depth.

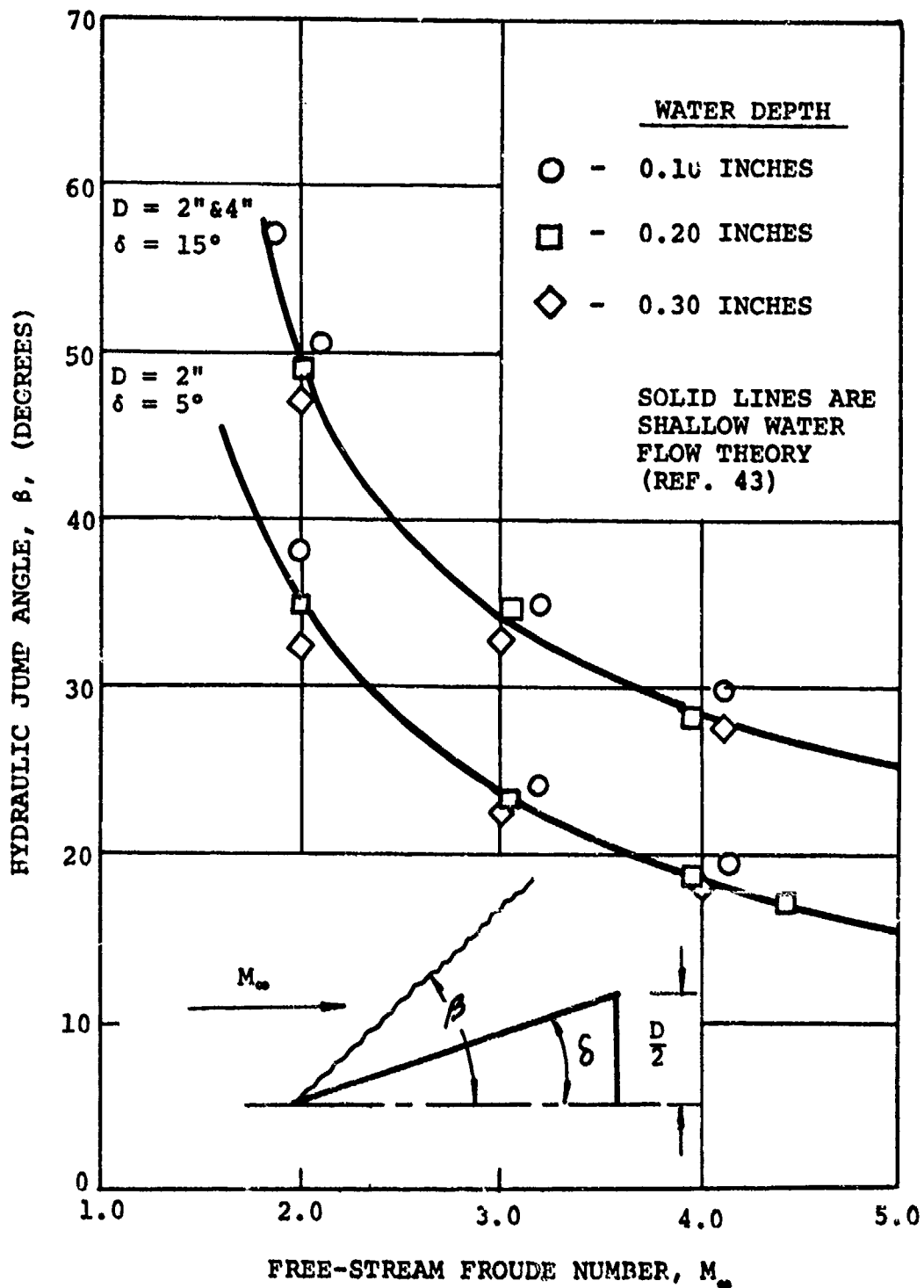


Figure 15. Variation of Hydraulic Jump Angle with Free-Stream Froude Number for Various Water Depths and Two Wedge Deflection Angles

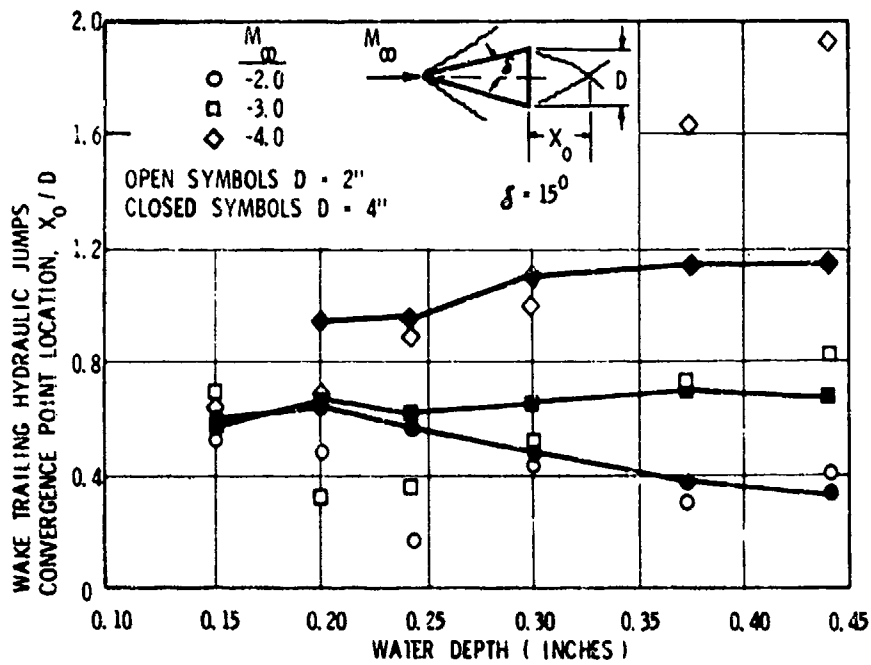


Figure 16. Variation of Wake Trailing Hydraulic Jumps Convergence Point Location with Water Depth

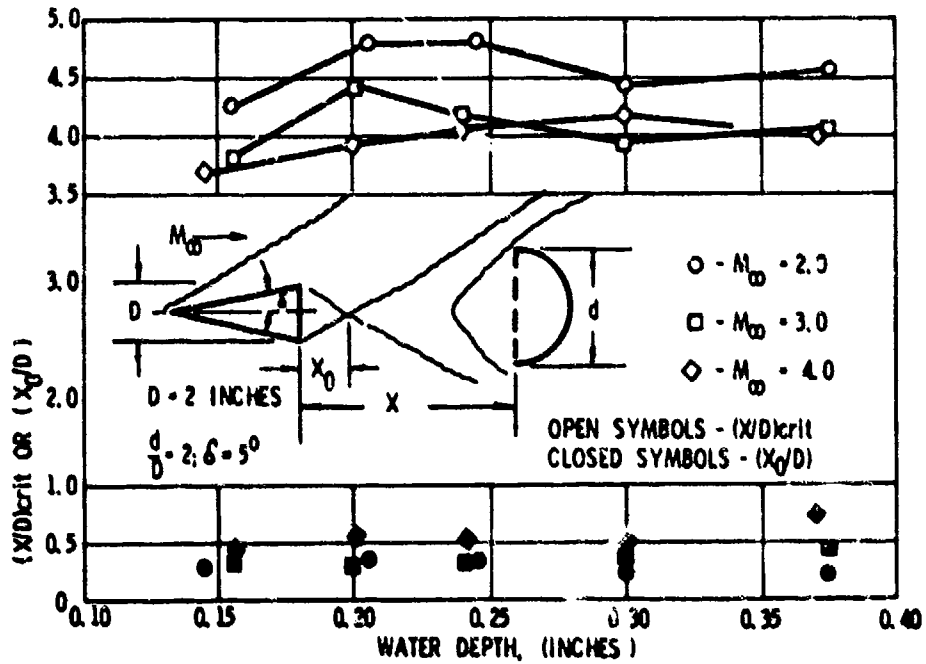


Figure 17. Variation of Critical Trailing Distance and Wake Trailing Hydraulic Jumps Convergence Point Location with Water Depth

Based on both the experimental results and the theoretical considerations, a water depth of 0.190 inches was chosen to be used for all subsequent tests.

The experimental results from the above and other preliminary tests show that flow characteristics are influenced by model geometry. Figure 16 shows that the nondimensional ratio X_0/D was different for different size wedges at most Froude numbers and water depths tested. However, the hydraulic jump angles were almost the same for both size wedges; Table III. Figure 18 shows a large variation in hydraulic jump detachment or standoff distance with circular cylinder diameter. Based on Campbell's theory for predicting the detached shock location (Reference 50) it was expected that the data should group around the curve shown in Figure 18. According to Campbell, the shock standoff distance for any body is uniquely dependent on the inverse square of the density ratio across a normal shock. If this theory holds with application of the gas-hydraulic analogy, then the hydraulic jump standoff distance would be a function of the inverse square of the depth ratio across a normal hydraulic jump. The standoff distance data is plotted in Figure 19 as a function of this variable as determined from Equation (7). There appears to be a general grouping of the data about the straight line drawn in the figure. However, there is appreciable scatter and no one diameter is closest to the line at all Froude numbers (depth ratios).

In view of the above considerations, the model forebody chosen for the majority of the Flow Field Interference Studies and Influencing Parameter Investigations, Sections IV, 2 and 3, was the 5 degree 2 inch sharp wedge. This model produced bow hydraulic jump angles that agreed well with shallow water theory and the wake convergent point location was fairly constant with Froude number. As the photographs show in Figure 20, although the capillary ripples were more pronounced ahead of the bow wave of the 5 degree wedge, there was less cresting and flow turbulence behind this wave at the higher Froude numbers compared to that behind the bow wave of the 15 degree wedge.

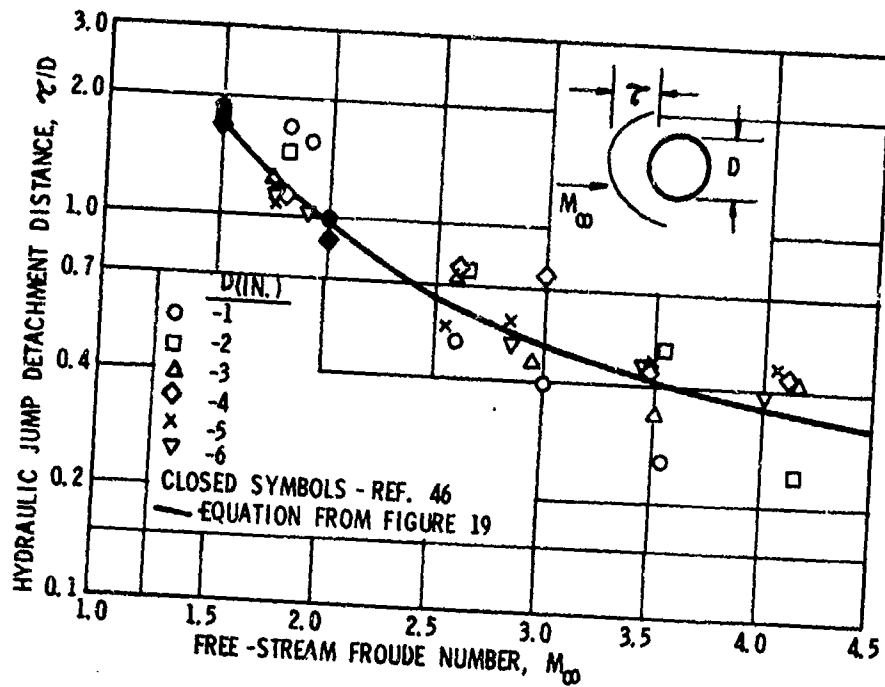


Figure 18. Variation of Hydraulic Jump Detachment Distance with Free-Stream Froude Number for Various Cylinder Diameters

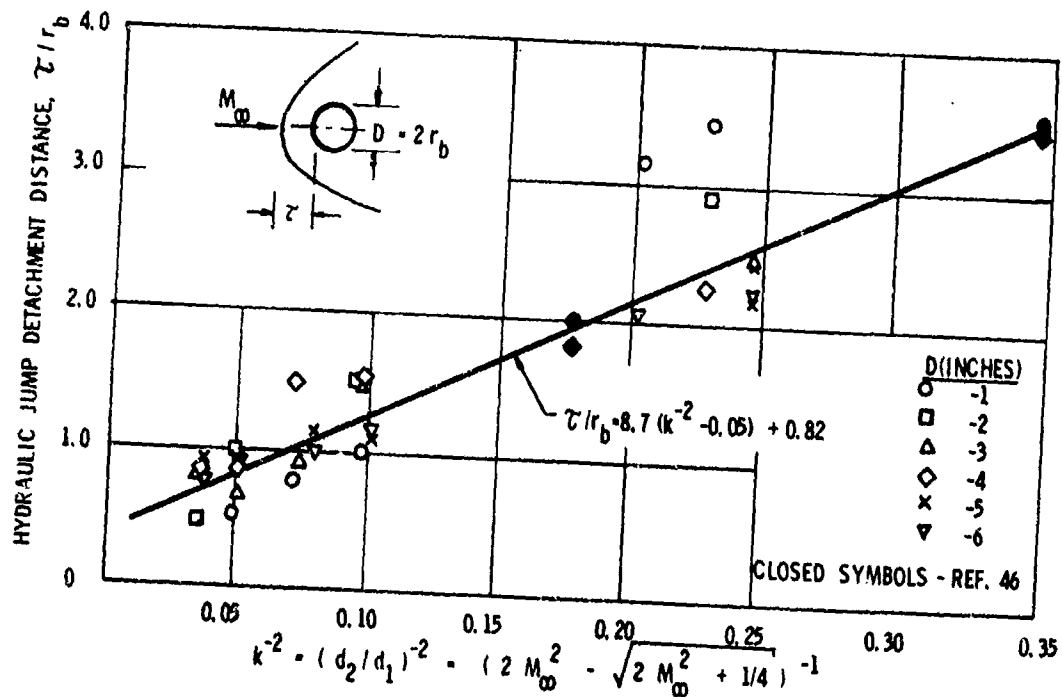
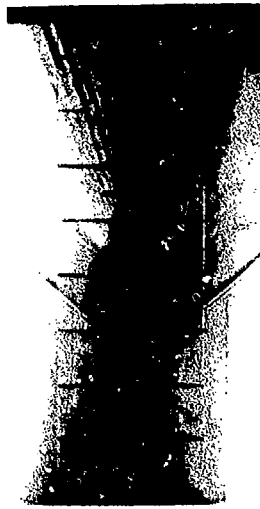


Figure 19. Variation of Hydraulic Jump Detachment Distance with the Inverse Square of the Depth Ratio Across a Normal Hydraulic Jump for Various Cylinder Diameters



$\delta = 5^\circ; D = 2$

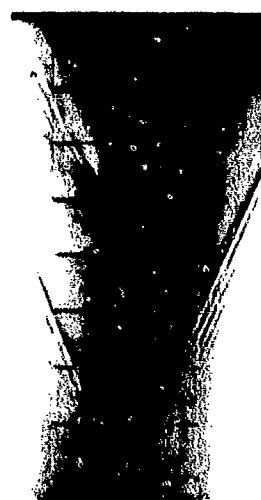


$\delta = 15^\circ; D = 2$

a. - Free-Stream Froude Number = 2



$\delta = 15^\circ; D = 4$



$\delta = 5^\circ; D = 2$

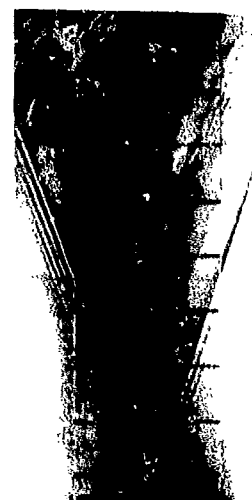


$\delta = 15^\circ; D = 2$

b. - Free-Stream Froude Number = 3



$\delta = 15^\circ; D = 4$



$\delta = 5^\circ; D = 2$



$\delta = 15^\circ; D = 2$

c. - Free-Stream Froude Number = 4



$\delta = 15^\circ; D = 4$

Figure 20. Comparison of the Shallow Water Flow Fields About Three Wedge Models

With the simulated parachute in the wake of the 5 degree 2 inch sharp wedge, water "cresting over" and turbulence behind the parachute bow wave occurred at Froude numbers of 3 and above. Water wave heights and hence wave photographic definitions decreased with decreasing Froude number. The wake neck region lost almost all of its definition at Froude number 2 and below. For these reasons, the Froude number selected for most of the subsequent tests was 2.5.

2. FLOW FIELD INTERFERENCE STUDIES

a. Shock Impingement

It was postulated in Section II, 2, c, Model Supports, that a non-reflected oblique shock wave, which may originate at the intersection of a support strut leading edge and the wind tunnel wall boundary layer, could alter the forebody wake and affect its modification by a trailing decelerator. This possibility was investigated during these shallow water tests.

A sharp wedge, either 5 or 15 degree deflection angle, was placed ahead of and to the side of the 5 degree 2 inch wedge forebody and a trailing 4 inch diameter simulated parachute, as shown in Figure 21. Using the two wedges and testing at Froude numbers of 2, 3, and 4, oblique hydraulic jumps of various strengths were generated. The wedges were positioned to allow for jump impingement at any desired location from the nose of the forebody to the base of the parachute.

Figure 22 presents shadowgraphs from selected tests showing the effect on flow field patterns due to impingement of the oblique hydraulic jumps. Jump impingement on the leading body did not produce significant wake flow changes; however, the wake appeared to move off the centerline for most tests. At times the jump would separate the leading body boundary layer and move forward to the nose. Jump impingement in the near wake and parachute bow wave regions produced significant changes in the wake flow patterns. The wake and parachute bow hydraulic jump moved off the centerline and the parachute bow wave detachment distance

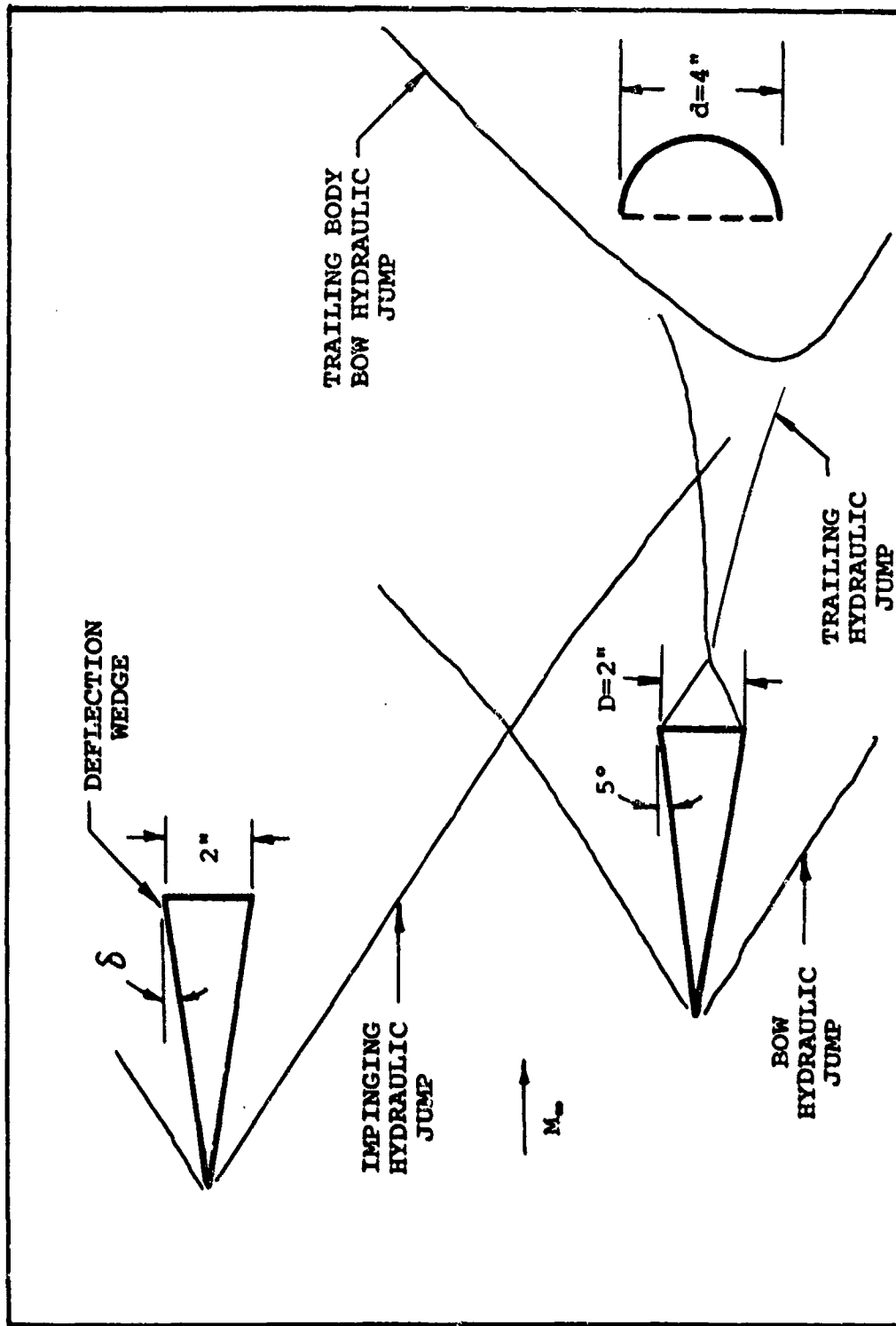


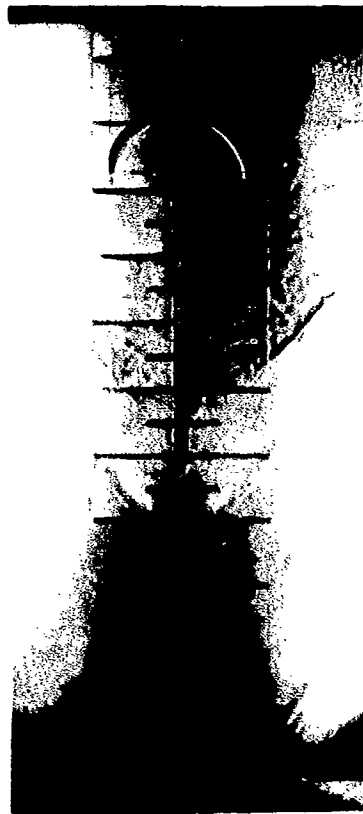
Figure 21. Shock Impingement Interference Study Test Arrangement and Flow Field Patterns



b. - Hydraulic Jump in Near Wake Region



d. - Hydraulic Jump on Simulated Parachute
Bow Hydraulic Jump



a. - No Impinging Hydraulic Jump



c. - Hydraulic Jump on Wedge

Figure 22. Shadowgraphs from Selected Tests Showing the Effect of Impingement of Oblique Hydraulic Jumps on the Flow Field About a Sharp Wedge and a Trailing Simulated Parachute at $M_\infty = 3.0$

increased slightly. Figure 23 shows that the critical trailing distance increased with the presence and the strength of the impinging hydraulic jump at a given Froude number.

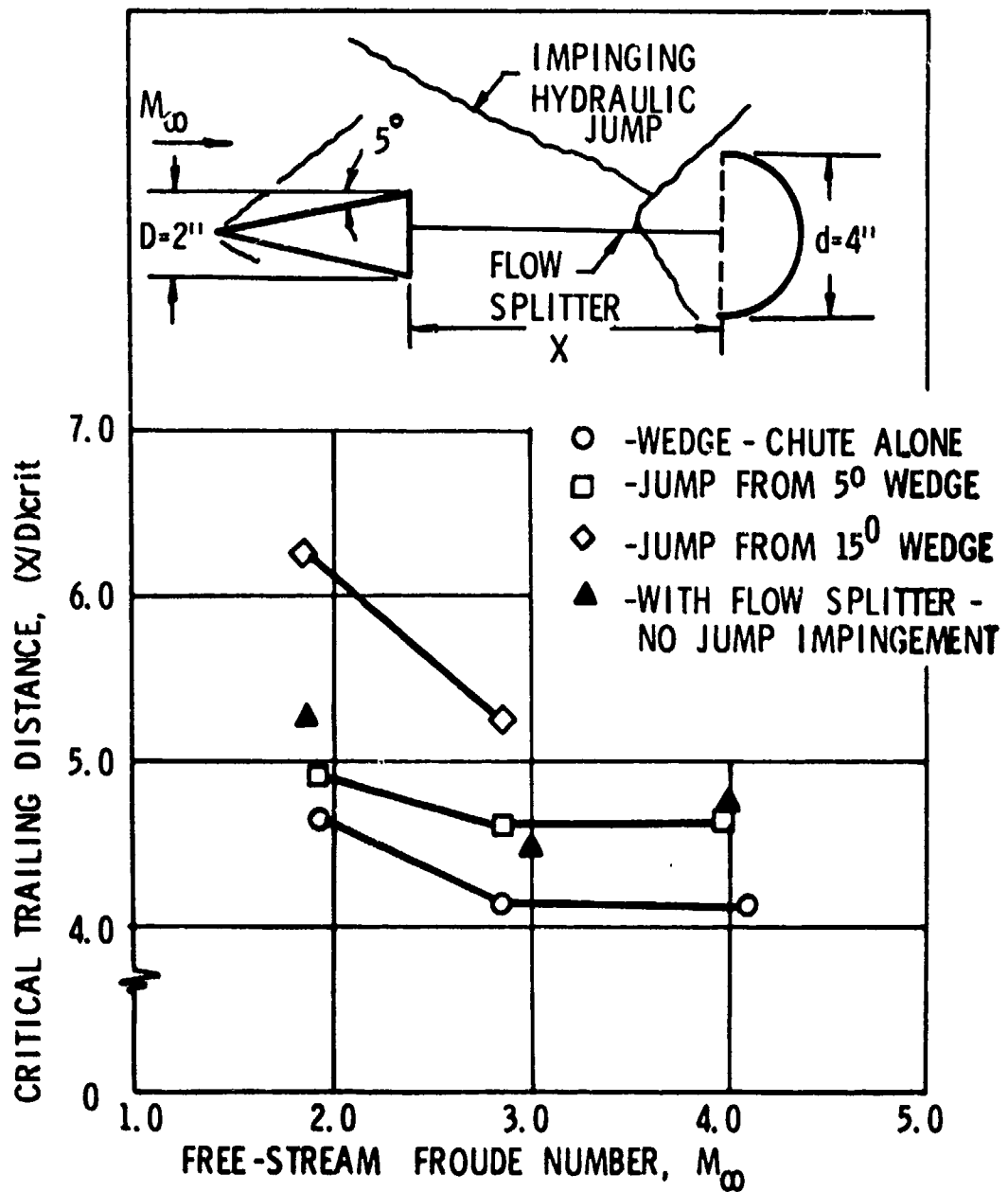


Figure 23. Variation of Critical Trailing Distance With Free-Stream Froude Number for Various Strength Impinging Hydraulic Jumps and for a Flow Splitter

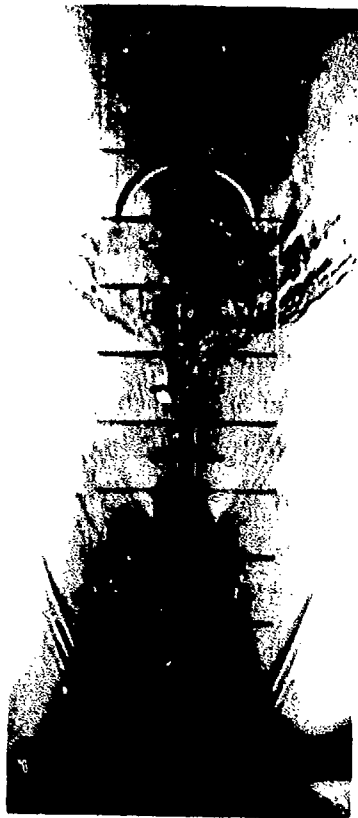
b. Flow Splitter

Figure 23 also includes data points showing the increase in $(X/D)_{crit}$ due to the addition of a flow splitter. The splitter was a 1/16 inch acrylic plastic sheet 2 inches high placed between the 5 degree 2 inch wedge forebody and the trailing 4 inch diameter simulated parachute. It divided the wake flow at the centerline from the forebody base downstream to the parachute inlet. This splitter was to simulate the riser suspension line system discussed in Section II, 2, c, Body Connectors, which was suspected to influence wake modification. As can be seen in Figure 24, $(X/D)_{crit}$ was increased due to the increase in parachute bow wave detachment distance that takes place when the bow wave interacts with and separates the boundary layer on the flow splitter.

c. Disturbing Body

In Section II, 2, c it was noted that the confluence point of the suspension lines of a parachute type decelerator results in a concentrated mass that can be considered as a disturbing body between the parachute and the forebody base. This disturbing body was simulated on the water table by circular cylindrical rods, 1/4 and 3/8 inches in diameter. They were inserted into the wake region between a 5 degree 2 inch wedge and a trailing 4 inch diameter simulated parachute.

With the parachute at large trailing distances, the insertion of the rods anywhere in the wake region caused little change in the flow pattern. When the rods were placed at short downstream positions from the wake convergence point, bow hydraulic jumps were generated that quickly coalesced with the trailing hydraulic jumps. Only when the parachute bow hydraulic jump was located just downstream of the wake convergence point and the rods were inserted at the centerline location of the bow hydraulic jump was there a significant flow field alteration. Insertion of the rods at this location caused the parachute bow hydraulic jump to move upstream and appreciably modify the forebody wake.

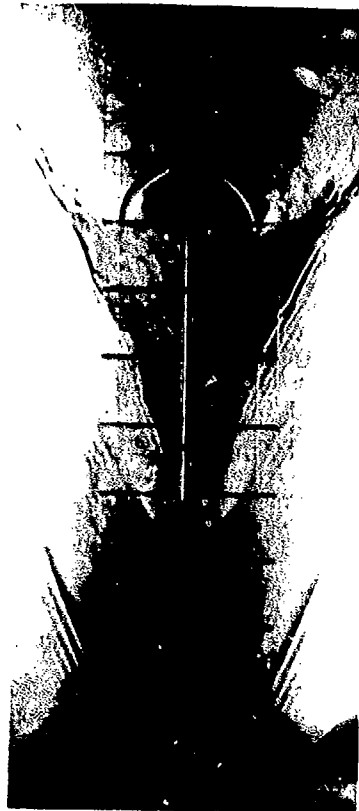


$X/D = 4.5$

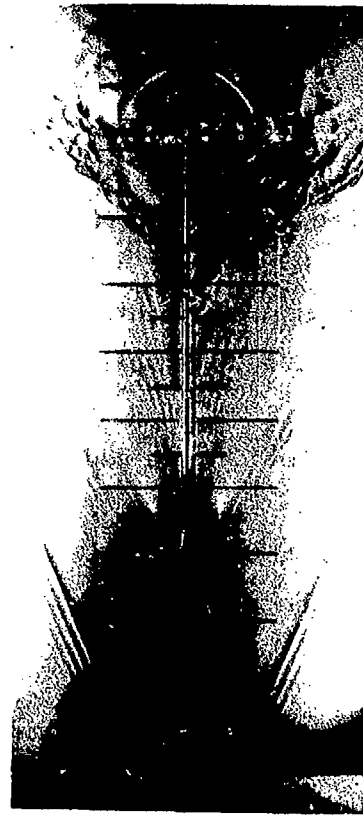


$X/D = 6.0$

a. - Wedge-Simulated Parachute Without Flow Splitter



$X/D = 4.5$



$X/D = 6.0$

b. - Wedge-Simulated Parachute With Flow Splitter

Figure 24. Shadowgraphs From Selected Tests Showing the Effect of Flow Splitters on the Flow Field About a Sharp Wedge and a Trailing Simulated Parachute at $M_\infty = 3.0$

d. Base Bleed

In Section II, 2, c, it was also concluded that base bleed could increase the critical trailing distance. This was also found to be the case during the water table investigations. Figure 25 presents the results obtained. The location of the wake convergence point moved downstream as the amount of base bleed increased. With a 4 inch diameter

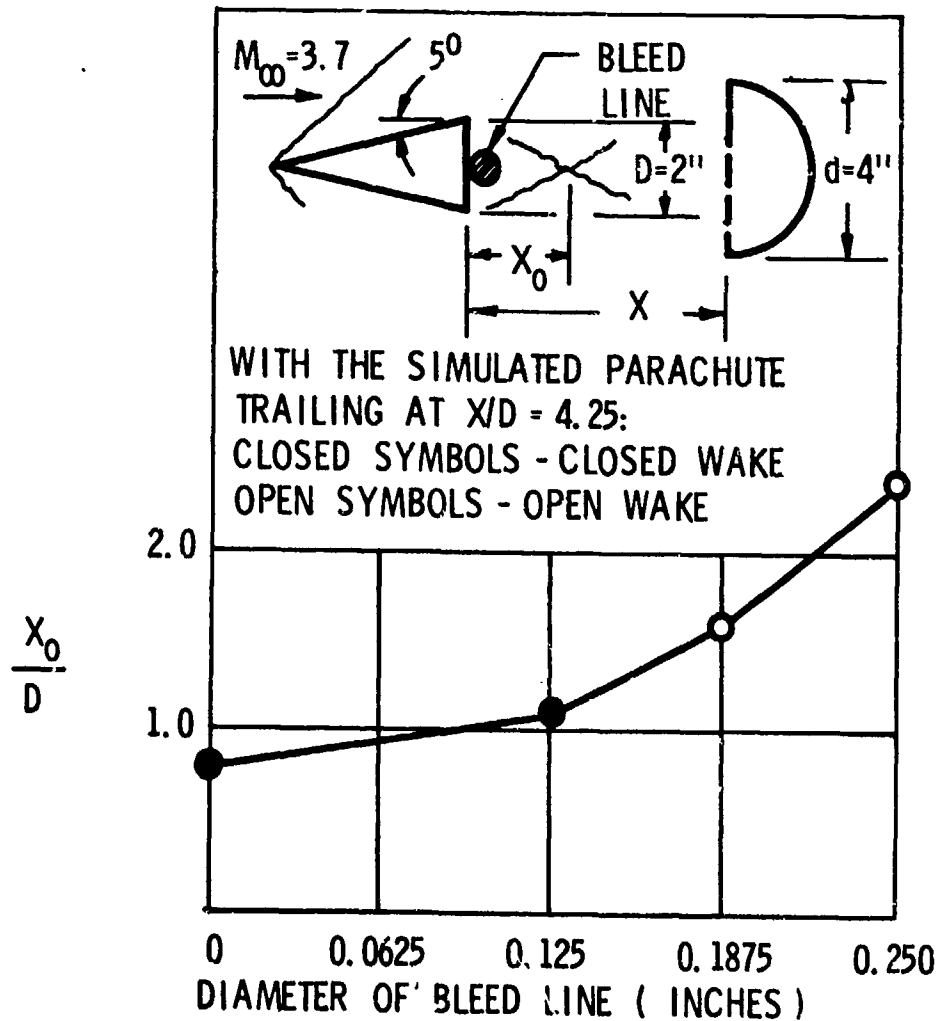


Figure 25. Variation of Wake Trailing Hydraulic Jumps Convergence Point Location With Bleed Line Diameter

simulated parachute trailing the 5 degree 2 inch wedge at 4.25 calibers, the wake was closed for bleed line diameters of 0.125 inch and below. The wake was highly modified for bleed line diameters of 0.1875 inch and above.

Bleed was provided by injecting water 1/2 inch from the water surface through vinyl plastic extruded tubing which was taped to the base of the forebody. This arrangement allowed the water to flow directly downward as it exited the tubing. A head of approximately one foot of water provided a smooth flow of water without splashing for all line diameters.

3. INFLUENCING PARAMETER INVESTIGATIONS

a. Froude Number and Trailing Body Size

A number of shallow water tow tests were performed with the 5 degree 2 inch wedge and trailing simulated parachutes to investigate the effects of Froude number and parachute size on critical trailing distance. The results from these tests are tabulated in Table V and presented in Figures 26 and 27.

Figure 26 shows that critical trailing distance was insensitive to Froude number for Froude numbers from 3 to 5, regardless of trailing body size. For Froude numbers below 3, $(X/D)_{crit}$ increased slightly with decreasing Froude number. The critical trailing distance increased significantly with increasing diameter of the simulated parachute.

The relationship between $(X/D)_{crit}$ and trailing body size is indicated in Figure 27. The critical trailing distance increased rapidly with increasing d/D for small parachute diameters. As d/D became large, $(X/D)_{crit}$ appeared to level off; this was most apparent at the higher Froude numbers.

TABLE V
TEST RESULTS - FROUDE NUMBER AND TRAILING
BODY SIZE INVESTIGATIONS

Nominal Froude Number	a		$(\frac{x}{D})_{crit}$	Nominal Froude Number	a		$(\frac{x}{D})_{crit}$	
	d/D	Froude Number			d/D	Froude Number		
1.5	1.0	1.40	3.38	3.0	1.5	3.03	3.19	
	1.5	1.43	5.31		2.0	3.00	3.88	
	2.0	1.40	5.78		2.5	3.13	4.63	
	2.0	1.27	5.38		3.0	3.08	5.13	
	2.5	1.43	6.75		3.0	2.98	5.38	
	3.0	1.43	---		4.0	3.10	6.13	
	4.0	---	---		4.0	2.98	6.13	
2.0	1.0	1.95	2.75	3.5	2.0	3.58	3.88	
	1.5	1.98	3.38		4.0	1.0	4.10	2.13
	2.0	2.05	4.25			1.5	4.30	3.13
	2.0	2.05	4.42			2.0	4.00	3.88
	2.5	2.05	5.13			2.5	4.15	4.56
	3.0	1.95	5.88			3.0	3.95	5.38
	4.0	2.00	7.13			4.0	4.03	6.56
2.5	1.0	2.50	2.63	4.5		2.0	4.65	3.88
	1.0	2.45	2.38		5.0	1.0	5.00	6.38
	1.5	2.55	3.38			1.5	5.00	3.25
	2.0	2.55	4.13			2.0	4.98	4.06
	2.0	2.43	4.13			2.5	4.95	4.88
	2.5	2.55	4.88			2.5	4.95	4.88
	3.0	2.50	5.44			3.0	4.95	5.38
	4.0	2.50	6.38			4.0	4.88	6.38
3.0	1.0	3.10	2.13	4.0		4.80	6.45	
	1.0	3.10	2.19					
	1.5	3.03	3.38					

^a Forebody for all tests was 5 degree 2 inch sharp wedge.
Trailing body for all tests was simulated parachute.

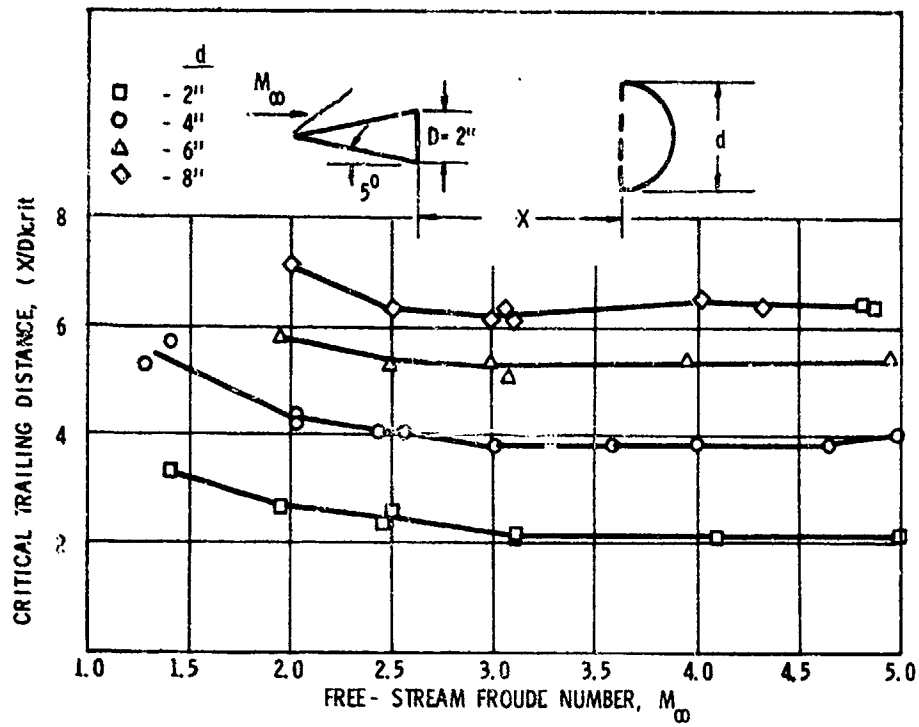


Figure 26. Variation of Critical Trailing Distance With Free-Stream Froude Number for Various Size Simulated Parachutes Trailing a Sharp Wedge

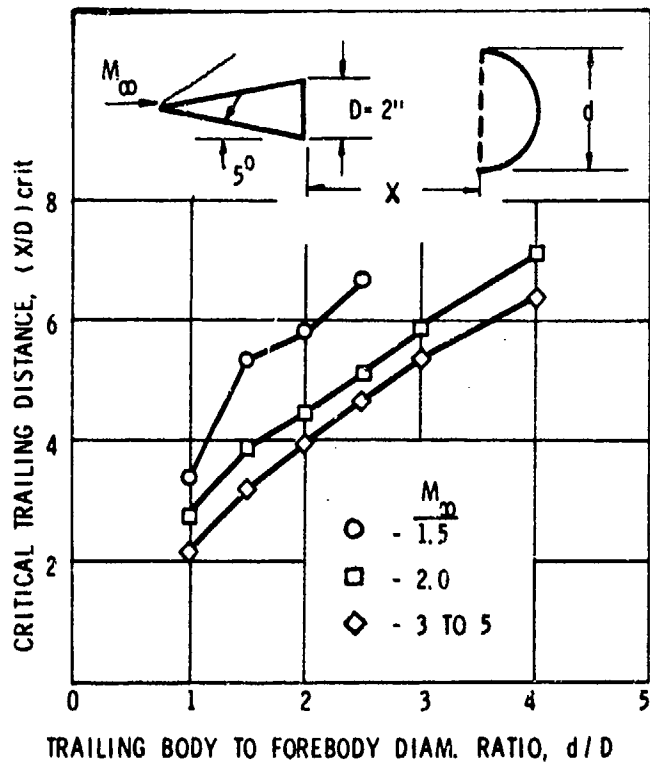


Figure 27. Variation of Critical Trailing Distance With Simulated Parachute Size for Various Free-Stream Froude Numbers

b. Trailing Body Size and Shape

Various sizes of wedges, plates, cylinders, and balloon type models were tested in free-stream and in the wake of the 5 degree 2 inch wedge forebody at a Froude number of 2.5 to investigate the effects of trailing body size and shape on critical trailing distance. The results from these tests, along with the data from the tests using the simulated parachute as the trailing body, are tabulated in Table VI and presented in Figure 28.

Figure 28 shows the same general relationship between $(X/D)_{crit}$ and d/D as was pointed out in the previous section. That is, $(X/D)_{crit}$ increased rapidly with increasing d/D for small values of d/D and leveled off as d/D became large. However, the type or shape of the trailing body also significantly affected the critical trailing distance. For example, the greater the wedge deflection angle, the greater the critical trailing distance. This would indicate that $(X/D)_{crit}$ increased with trailing body bluntness. One measure of body bluntness can be obtained from the magnitude of the body's shock standoff distance when immersed in a supersonic free-stream. Generally, the greater the shock standoff distance, the blunter the body. That this was the case for the shallow water tow models can be seen in Table VI. The blunter the wedge, the greater the hydraulic jump standoff distance, τ . In addition, the trailing bodies that produced the largest critical trailing distances, for a given trailing body size, exhibited the largest nondimensional jump standoff distance, τ/d .

An attempt was made to find an explicit relationship involving critical trailing distance, hydraulic jump standoff distance (τ/d) and trailing body size (d/D) for these particular tests. The difference between $(X/D)_{crit}$ and the product of τ/d and d/D was labeled Φ , and plotted as a function of the width ratio d/D as shown in Figure 29. Values for the expression Φ were found to group around the curve shown in Figure 29 regardless of trailing body type. Functions, representing various fits of the data, were expressed in terms of a number of power

TABLE VI
TEST RESULTS - TRAILING BODY SIZE AND SHAPE INVESTIGATIONS

Trailing Body	d/D ^a	r/d	(X̄/D) ^{crit}	(X̄/D) ^{crit}	Trailing Body	d/D ^a	r/d	(X̄/D) ^{crit}	(X̄/D) ^{crit}	
30° Wedge	1.0	0.05	1.13	1.21	Circular Cylinder	2.5	0.72	4.10	4.22	
	1.5	0	1.70	1.64		3.0	0.69	4.80	4.78	
	2.0	0.01	2.00	2.09		4.0	0.60	5.53	5.50	
	2.5	0.01	2.58	2.45		60° Wedge	1.0	1.20	2.38	2.36
	3.0	0.01	2.60	2.74			1.5	0.90	3.00	2.99
	4.0	0.03	3.00	3.20			2.0	0.90	3.60	3.87
1.0	0.30	1.55	1.46	2.5	0.80		4.50	4.42		
Balloon Type	1.5	0.35	2.15	2.17	3.0	0.75	4.90	4.96		
	2.0	0.40	2.50	2.87	4.0	0.74	5.75	6.06		
	2.5	0.33	3.00	3.23	Simulated Parachute	1.0	1.25	2.38	2.41	
	3.0	0.25	3.35	3.46		1.5	1.33	3.38	3.64	
	4.0	0.23	4.00	4.02		2.0	1.19	4.13	4.46	
	1.0	0.60	2.00	1.76		2.5	1.02	4.88	4.97	
1.5	0.60	2.50	2.54	3.0		0.96	5.44	5.59		
2.0	0.60	3.13	3.27	4.0		0.90	6.38	6.70		
45° Wedge	2.5	0.50	3.70	3.67	Plate	0.5	1.80	1.63	1.51	
	3.0	0.45	4.12	4.06		1.0	1.50	2.65	2.66	
	4.0	0.42	4.88	4.78		1.5	1.20	3.65	3.44	
	0.5	0.70	1.13	0.96		2.0	1.15	4.50	4.37	
Circular Cylinder	1.0	0.90	2.13	2.06	2.5	1.05	5.38	5.05		
	1.5	0.85	2.75	2.92	3.0	1.05	6.00	5.83		
	2.0	0.80	3.50	3.67	4.0	0.93	7.10	6.82		

^a Forebody for all tests was 5 degree 2 inch sharp wedge.
(X̄/D)^{crit} - Values calculated using Equation 14.

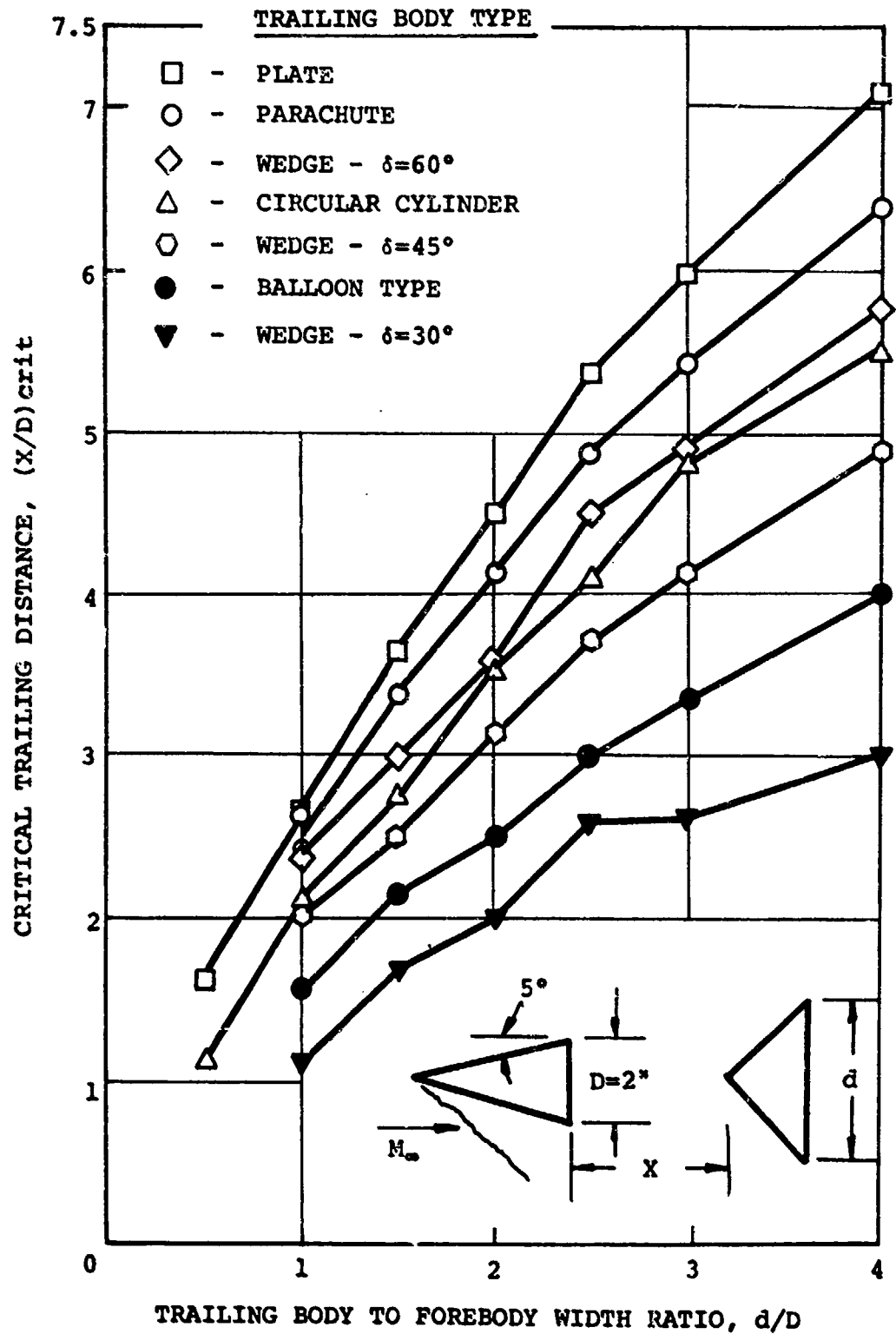


Figure 28. Variation of Critical Trailing Distance With Trailing Body Size for Various Types of Trailing Bodies

series. A second degree polynomial gave a reasonable approximation. The critical trailing distance was then expressed as:

$$(X/D)^*_{crit} = \frac{\pi}{d} \frac{d}{D} + 1.285 \frac{d}{D} - 0.1275 \left(\frac{d}{D}\right)^2 \quad (14)$$

Values for the critical trailing distance using Equation 14 are tabulated in Table VI and plotted in Figure 30 as a function of the experimental $(X/D)_{crit}$ values to show the degree of agreement between the two. The empirical relationship provides an excellent approximation of the critical trailing distance for the forebody and trailing bodies tested at a nominal Froude number of 2.5

c. Forebody Shape

A 4 inch simulated parachute was tested in the wake of a number of forebodies at a free-stream Froude number of 2.5 to investigate the effect of forebody shape on critical trailing distance. The results from these tests are tabulated in Table VII.

It is noted that $(X/D)_{crit}$ ranged from 3.59 to 4.53, a change of only 1 caliber for all forebodies tested. Changing the shape of the forebody, then, did not significantly change the critical trailing distance. It does appear that $(X/D)_{crit}$ decreased as the nose of the 15 degree sharp wedge became more blunt. When the bases of the 15, 30, and 60 degree sharp wedges were extended rearward, by the addition of 4 inch long plates, the critical trailing distances increased for all wedge deflection angles.

Also measured were the distances from the forebody base to the wake convergence points; X_0 values. These values were nondimensionalized and included in Table VII. When these values were subtracted from the $(X/D)_{crit}$ values, the effect of forebody shape became a little more apparent. Figure 31 presents plots of $(X/D)_{crit} - X_0/D$ as a function of wedge deflection angle for sharp and blunt wedges with and without afterbodies

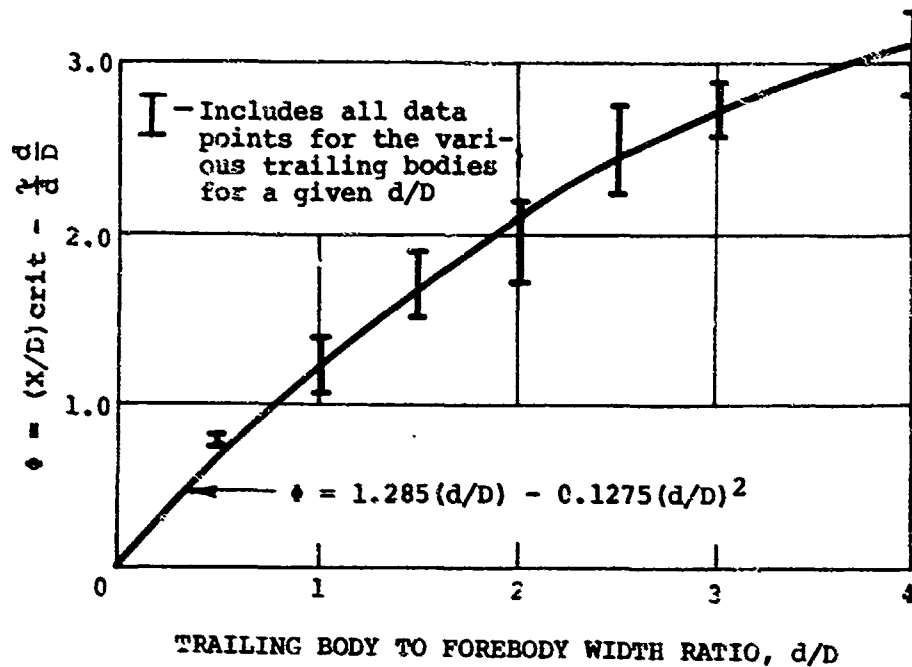


Figure 29. Graphical Aid for the Development of an Explicit Relationship Involving Critical Trailing Distance, Hydraulic Jump Standoff Distance, and Trailing Body Size

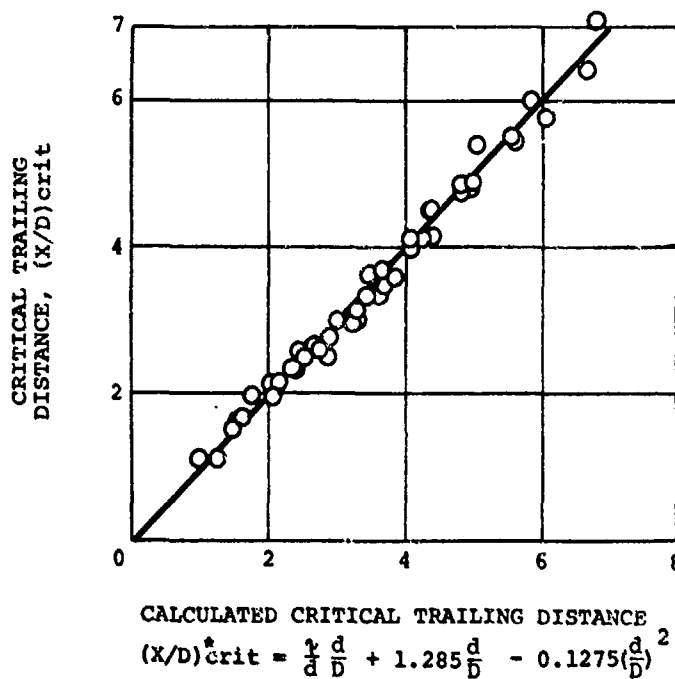


Figure 30. Comparison Between Calculated and Experimental Critical Trailing Distances

TABLE VII

TEST RESULTS - FOREBODY SHAPE INVESTIGATIONS

Forebody Classification ^a	Design Variables	$\frac{X_0}{D}$	$(\frac{X}{D})_{crit}$	$(\frac{X}{D})_{crit} - \frac{X_0}{D}$
Sharp Wedge	$\delta = 60$	0.87	3.90	3.03
" "	$\delta = 45$	0.79	3.80	3.01
" "	$\delta = 30$	0.51	3.59	3.08
" "	$\delta = 15$	0.58	4.14	3.56
" "	$\delta = 10$	0.64	4.20	3.56
" "	$\delta = 7.5$	0.59	4.08	3.49
" "	$\delta = 5$	0.40	4.13	3.73
Blunted Wedge	$R = 1/8$	0.60	3.97	3.37
" "	$R = 3/8$	0.67	4.05	3.38
" "	$R = 3/4$	0.80	3.88	3.08
Half Cylinder	---	0.50	3.81	3.31
Wedge-Plate	$\delta=15; L=4$	0.55	4.53	3.98
" "	$\delta=30; L=4$	0.60	4.19	3.59
" "	$\delta=60; L=4$	0.50	4.30	3.80
Blunted Wedge-Plate	$R=1/8; L=4$	0.60	4.35	3.75
" "	$R=3/8; L=4$	0.50	4.41	3.91
" "	$R=3/4; L=4$	0.50	4.33	3.83
Half Cylinder-Plate	$L=4$	0.55	4.32	3.77
Wedge-Plate-Flare	$\delta=10; L=4; \delta=0$	0.52	4.33	3.81
" " (1)	$\delta=10; L=4; \delta=5$	0.79	4.43	3.64
" " (2)	$\delta=10; L=4; \delta=15$	0.70	4.17	3.47
" " (3)	$\delta=10; L=4; \delta=25$	1.14	4.01	2.87
Circular Cylinder	---	0	3.94	3.94
Apollo	---	0	3.75	3.75
Mercury - Gemini	---	0.15	4.10	3.95
Skirted Blunt Body	---	0.82	3.96	3.14
Ogive-Plate	$R = 2$	0.82	4.24	3.42
" "	$R = 8$	0.90	4.34	3.44
Plate	$L = 1$	0.85	4.46	3.61
" "	$L = 4$	0.52	4.28	3.76
" "	$L = 8$	0.60	4.34	3.74

^aForebody base width, D, was 2 inches and the trailing body was the 4 inch simulated parachute for all tests except when flare was used. (Refer to TABLE I)

- (1) Trailing body was 5 inch simulated parachute.
- (2) Trailing body was 6 inch simulated parachute.
- (3) Trailing body was 8 inch simulated parachute.

(plates). For simplicity, the difference $(X/D)_{crit} - X_0/D$ will be called the modified critical trailing distance.

From the figure, it can be seen that sharp wedges with deflection angles of 30 degrees and greater produced shorter modified critical trailing distances than wedges with angles of 15 degrees and less. When the 15 degree sharp wedge was blunted, the modified critical trailing distance decreased. For all these wedges and for a half cylinder, when a 4 inch plate was added to the base, the modified critical trailing distance increased. From Figure 32 it is seen that the modified critical trailing distance decreased with increasing flare angle for a sharp wedge-plate-flare forebody.

These results show that the modified critical trailing distance was slightly increased as forebody bluntness was decreased. This was true for forebody bluntness decreases due to:

1. increasing the forebody length
2. decreasing base flare angle
3. decreasing nose radius
4. decreasing wedge deflection angle

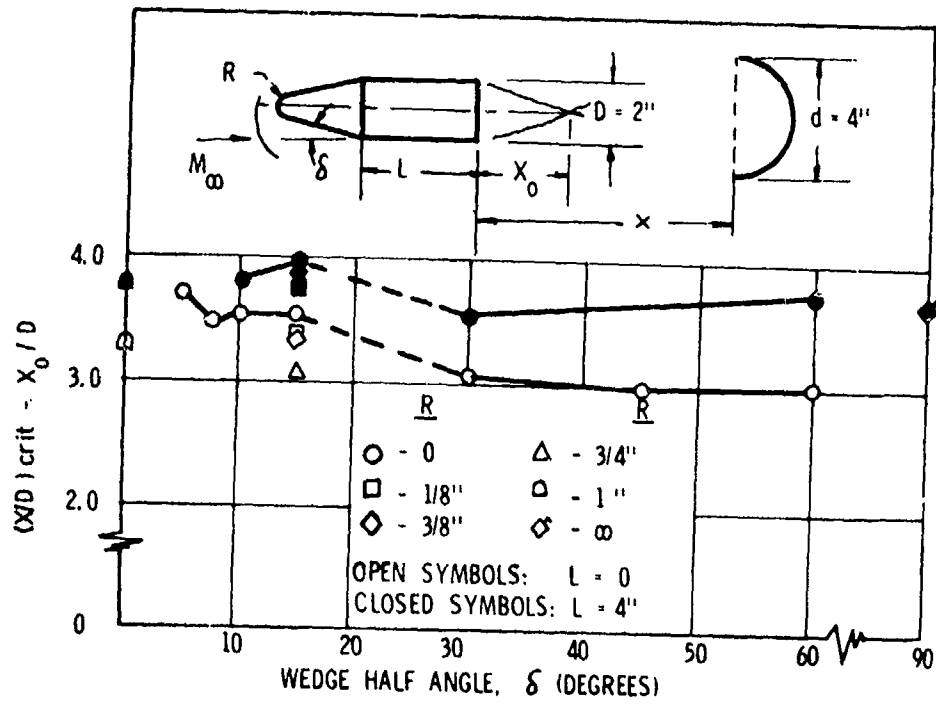


Figure 31. Variation of Modified Critical Trailing Distance With Wedge Half Angle for Various Shape Wedges at $M_\infty = 2.5$

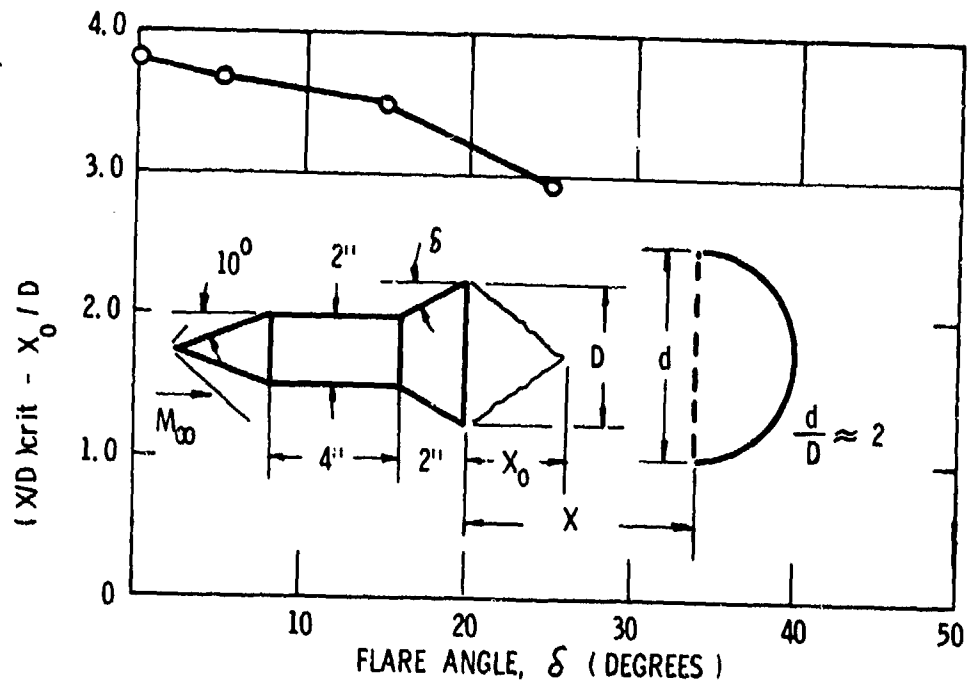


Figure 32. Variation of Modified Critical Trailing Distance With Forebody Flare Angle at $M_\infty = 2.5$

SECTION V

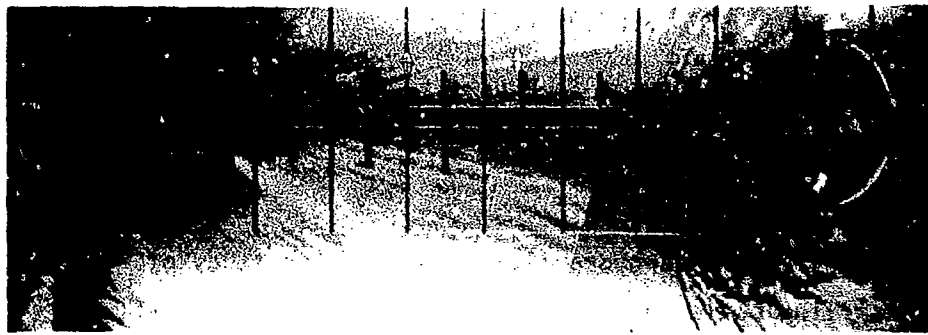
MECHANISM FOR WAKE MODIFICATION

1. SHALLOW WATER FLOW

The applicability of the gas-hydraulic analogy to the study of wake modification by trailing bodies has been established through comparison of water table and wind tunnel test results. Flow field patterns and relationships between critical trailing distances and influencing parameters, similar to those observed in compressible gas flow, were found during the tests on the shallow water tow table. A detailed study of the shallow water tests, then, should aid in obtaining a description of the mechanisms governing wake modification for two and three-dimensional bodies immersed in supersonic compressible gas flow.

The processes involved with the modification of forebody wakes by trailing bodies towed through shallow water can best be observed using shadowgraphs obtained from a series of tests at shorter and shorter trailing distances. Figure 33 presents shadowgraphs from such a series. All tests were performed at a free-stream Froude number of 2.5 with a 5 degree 2 inch wedge forebody and a 4 inch diameter simulated parachute trailing body. The flow patterns and processes involved are typical of those observed for the other Froude numbers and forebody-trailing body combinations tested. Figure 34 presents sketches of the water flow patterns for closed, modified and open wakes; and the nomenclature introduced in these sketches will be used in the description of the process of wake modification.

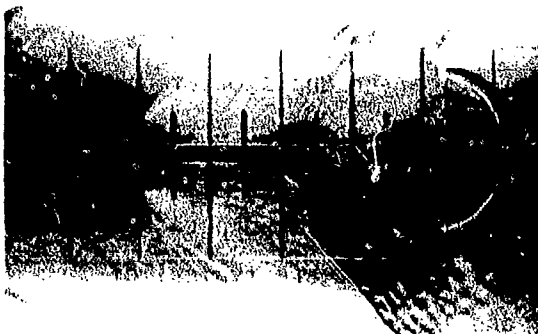
The top photograph of Figure 33 is assembled from two shadowgraphs taken in free-stream. The forebody and trailing body were tested separately and the images joined in relative position for comparison purposes.



Assembled
Images Of
Separate
Free-Stream
Tests



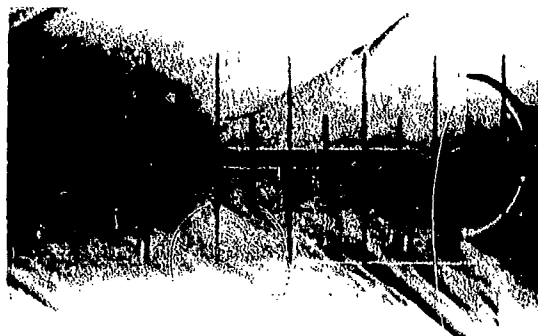
$X/D = 8.0$



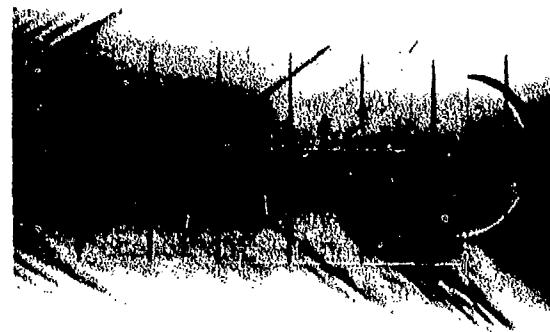
$X/D = 4.3$



$X/D = 4.2$

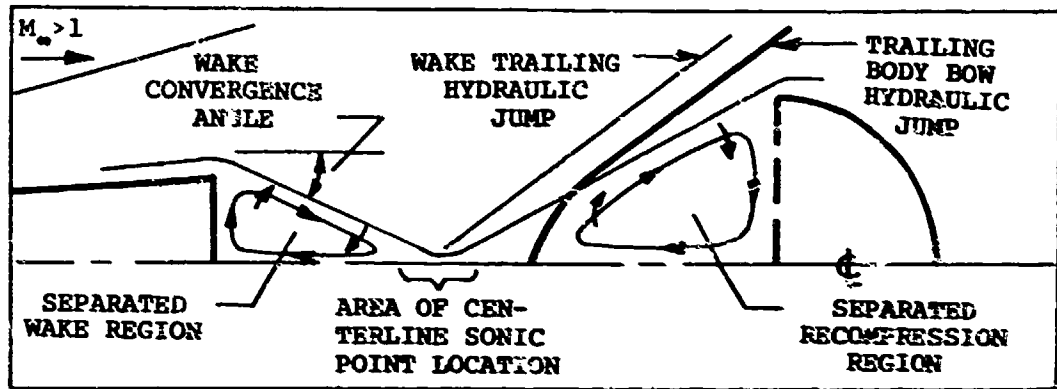


$X/D = 4.0$

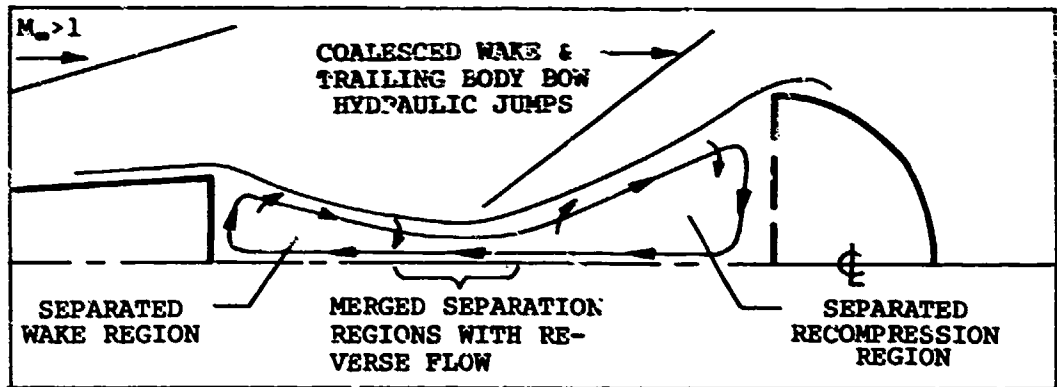


$X/D = 3.0$

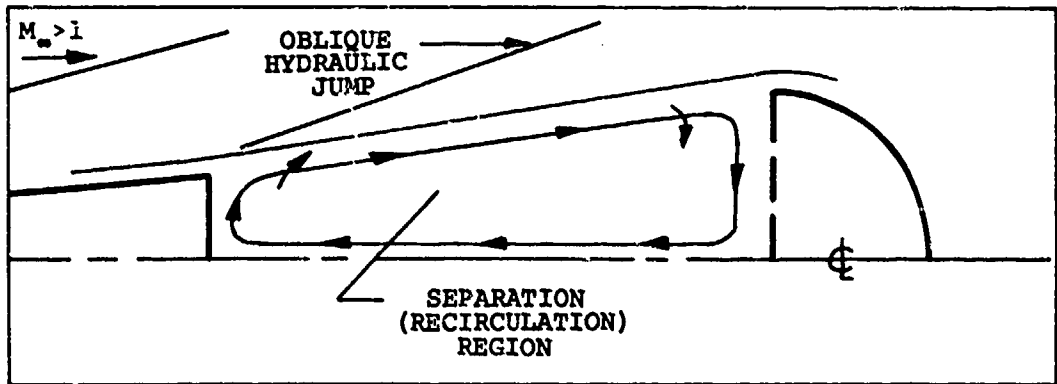
Figure 33. Shadowgraphs From Selected Tests Showing Two-Body Flow Field Patterns for Various Trailing Distances



a. Closed Wake



b. Modified Wake



c. Open Wake

Figure 34. Sketches of Two-Body Flow Field Patterns for Closed, Modified, and Open Wakes

The flow field about the forebody and trailing body at a large trailing distance shows a strong resemblance to those patterns found in free-stream. In both cases, an attached bow hydraulic jump formed ahead of the leading body, the water depth decreased as it turned around the base and converged toward the wake centerline, and a trailing hydraulic jump formed downstream of the wake convergence point. A detached bow hydraulic jump formed ahead of the trailing body in both free-stream and in the wake at $X/D = 8.0$. At an X/D of 4.3 the flow characteristics were essentially the same, except that large portions of the wake hydraulic jump and the trailing body bow hydraulic jump had coalesced at locations away from the wake centerline. Although no measurements were made, it was readily apparent that the water depth behind the bow hydraulic jump of the trailing body was greater than the water depth in the forebody base flow region. At an X/D of 4.2 there was only one oblique hydraulic jump in the wake and it was not closed across the centerline. At this trailing distance, water flowed upstream from the region immediately ahead of the trailing body to the forebody base flow region. In addition, the wake convergence angle was less than that at the larger trailing distances. At an X/D of 4.0 the wake convergence angle was almost zero, the water depth in the separated flow regions between the two bodies was greater than the base flow region depth at the larger trailing distance, and the trailing hydraulic jump originated near the forebody base. At a trailing distance of 3.0 calibers the wake convergence angle was negative (the wake diverged), an oblique hydraulic jump formed ahead of the divergence, and only one separated flow region was distinguishable in the area between the two bodies.

Flow differences as described above for shorter and shorter trailing distances can be said to represent changes that would occur during the modification of a closed wake into an open wake. Of course, the shadowgraphs could be studied in reverse order; that is, as trailing distance increases. This would show that; (1) the single separation region between the two bodies divides into a separated wake region (base flow region) and a separated recompression (depth increasing) region, (2) the flow over the base of the forebody changes from a compression into an expansion and converges toward the wake centerline, and (3) the oblique

hydraulic jump off the divergence moves downstream and separates into a wake trailing hydraulic jump and a closed trailing body bow hydraulic jump that blocks flow into the base flow region from the separated recompression region ahead of the trailing body. These flow changes, then, would represent the process for the reconstruction of a closed wake from an open wake.

Returning to the case of decreasing trailing distance, wake modification was shown to begin at that trailing distance where the bow hydraulic jump of the trailing body was located near the wake convergence point. In this position, the bow hydraulic jump coalesced with the wake trailing hydraulic jump and opened across the wake centerline (no jump in water depth). Water flowed upstream into the base flow region raising its depth and decreasing the wake convergence angle.

Application of the gas-hydraulic analogy to the above process implies that wake modification in compressible gas flow would begin at that trailing distance where the bow shock of the trailing body becomes located near the sonic point in the wake. At that point, supersonic wake centerline velocities would be eliminated, allowing gas flow into the base region from the higher pressure region ahead of the trailing body. This would raise the pressure level in the base flow region and decrease the wake convergence angle.

2. COMPRESSIBLE GAS FLOW

That the above is an accurate description of the process for wake modification for two and three-dimensional bodies in compressible gas flow is supported in the literature. Charwat et al (Reference 51) postulated that modification of the wake of a wedge by a trailing circular cylinder was similar to flow field modifications in a rectangular cutout in the boundary of a flat plate. The separated wake region of the backward facing step in the cutout is modified by the separated recompression region ahead of the forward facing step of the cutout. He presented experimental evidence that showed that wake modification in the cutout began at that separation distance where the point of convergence

of the separated wake region coincided with the point of separation of the the recompression region. At this critical separation distance the wake trailing shock and the shock ahead of the separated recompression region became one recompression shock wave in the cutout. Using schlieren photographs and pressure measurements, Charwat showed that not only were the separated wake regions similar for the backward facing step and the wedge, but that the flow behind the bow shock of the cylinder contained a vortical structure characteristic of the separated recompression region ahead of the forward facing step in the cutout.

That Charwat's postulation is a reasonable explanation of the process of wake modification for three-dimensional bodies is supported by the analytical calculations performed by Karpov (Reference 37). Karpov took mixing flow theories, of the type given by Crocco and Lees in Reference 21 which are used for analyses of separated wake and recompression regions, and applied them to the study of the flow field between two closely coupled axisymmetric bodies. By analytically separating the two bodies, Karpov determined the distance between the bodies required to reconstruct a supersonic wake from a modified one and showed excellent agreement with critical trailing distance as determined by experiments.

Basically, Karpov's method establishes the equilibrium position of the wake convergence angle for a given separation distance. This is done through a mass flux balance between the flow that enters the separation (recirculation) region at the place where the flow converges on the trailing body and the flow that leaves the separation region over the entire length of the separation region. As trailing distance is allowed to increase, the mass flux into the separation region is insufficient to compensate for the mass flux out and the wake convergence angle must be increased to compensate. In his calculations, this process is allowed to continue until the flow converges on the centerline and a wake trailing shock wave forms. The trailing distance where this occurs is, then, the critical trailing distance.

3. RELATIONSHIPS BETWEEN CRITICAL TRAILING DISTANCE AND THE INFLUENCING PARAMETERS

Wake modification has been shown to be governed by the process of the joining of two separated flow regions; the downstream region being at a higher pressure level than the upstream region. Wake reconstruction has been shown to be governed by the process of the dividing of a single separated flow region into two separated flow regions of different pressure levels; the two regions being isolated when the flow becomes supersonic on the centerline. Wake modification is effected by the convergence of two separated bodies and wake reconstruction is effected by the separation of two closely coupled bodies. The separation distance of the two bodies where modification or reconstruction occurs is the critical trailing distance. The observed trends and relationships between the critical trailing distance and the influencing parameters are in agreement with those implied by the above descriptions for the mechanisms for wake modification and reconstruction.

Critical trailing distance was shown to be dependent upon direction of trailing body traverse, if any. Upstream traverses (wake modifications) gave shorter critical trailing distances than downstream traverses (wake reconstructions). As Karpov pointed out in Reference 37, this is to be expected based on the differences between the governing mechanisms. That is, for wake reconstruction his calculations established a critical trailing distance when the condition of balance of the discharges was provided and a wake trailing shock and a "head wave in front of the second body" formed. From this point, wake modification would not begin until the second body is moved upstream and its head wave approaches so close to the wake trailing shock that the pressure in the base flow region increases.

Based upon the mechanism describing wake reconstruction, $(X/D)_{crit}$ would be larger for smaller initial wake convergence angles. The shallow water tow tests showed that $(X/D)_{crit}$ increased and wake convergence angle decreased with increasing base bleed. Wake convergence angle is related to forebody base pressure by the Prandtl-Meyer expansion over the

forebody base. Charwat, in Reference 51, presented a compilation of data that showed first an increase, then decrease and finally a leveling off of base pressure as the Reynolds number of the approach flow increased. $(X/D)_{crit}$ was shown to have this same relationship with Reynolds number.

Based upon the mechanism describing wake modification, $(X/D)_{crit}$ would be larger for larger trailing body bow shock wave detachment distances. That is, for two bodies located at the same trailing distance, the one with the greater shock detachment distance, τ , would have the greater critical trailing distance. The shallow water tow tests showed that both $(X/D)_{crit}$ and τ increased with increasing trailing body size and bluntness and with the presence of a flow splitter, disturbing body or an impinging oblique hydraulic jump. Roberts (Reference 12) indicated an increase in $(X/D)_{crit}$ with decreasing trailing body porosity and Heinrich (Reference 52) showed that τ also increased with decreasing porosity of rigid ribbon parachute models.

SECTION VI

CONCLUSIONS AND RECOMMENDATIONS

1. CONCLUSIONS

As a result of this analytical and experimental investigation, the mechanism for the process of modification of conventional supersonic wakes by trailing aerodynamic decelerators has been established and the parameters that influence wake modification have been identified.

Wake modification begins when the bow shock wave of the trailing decelerator becomes located at the wake sonic point. At this critical trailing distance, supersonic wake centerline velocities are eliminated and gas flows upstream into the forebody base region from the higher pressure region ahead of the decelerator. The critical trailing distance, was shown to increase with; (1) increasing base bleed, (2) increasing trailing body size and bluntness, (3) decreasing trailing body porosity, (4) decreasing forebody bluntness and (5) the addition of forebody supports and forebody-decelerator connectors. Critical trailing distance first increases, then decreases and finally levels off as Reynolds number increases over three orders of magnitude. No definite relationship between Mach number and critical trailing distance has been established.

Testing on the shallow water tow table, with application of the gas-hydraulic analogy, proved to be a simple and reliable method for the qualitative study of the flow fields between leading and trailing bodies. Details of the process of wake modification by trailing decelerators were readily observable on the water table. Flow field patterns and relationships between critical trailing distances and influencing parameters, similar to those obtained from wind tunnel tests, were found during tests on the shallow water tow table.

Results from the shallow water tow tests were used to establish the following relationship between the nondimensional variables of critical

trailing distance, hydraulic jump standoff distance (τ/d) and trailing body size (d/D):

$$(X/D)^*_{crit} = \frac{\tau}{d} \frac{d}{D} + 1.285 \frac{d}{D} - 0.1275 \left(\frac{d}{D}\right)^2 \quad (14)$$

Based on the demonstrated applicability of the shallow water tow table to the study of wake modification, it is postulated that a similar relationship exists for wake modification in compressible gas flow.

The literature search and supplementary wind tunnel tests showed that forebody wakes can be modified by trailing decelerators at trailing distances as large as 12 calibers and that decelerator performance is greatly influenced by the degree of wake modification. The results from this investigation combined with those in the References can be used to give a reasonable approximation of the degree of wake modification, if any, for a particular forebody-decelerator combination.

2. RECOMMENDATIONS

Analyses of the type presented by Karpov in Reference 37 should be expanded to aid in the determination of surface pressures on the front face of decelerators operating in modified wakes. Decelerators that operate satisfactorily in modified wakes include the flexible portion of the Supersonic Guide Surface parachute (Reference 2) and parachutes employing the principle of supersonic aerodynamic reefing (Reference 53). Since base bleed has been shown to influence wake modification, it can be used as a means to effect aerodynamic reefing of trailing decelerators.

Now that the process of wake modification by trailing decelerators has been described, the influencing parameters identified, and general trends and relationships between the critical trailing distance and the influencing parameters established, additional investigations should be conducted to obtain explicit quantitative relationships. Further, the

analytical methods for the description of the flow fields about forebody-decelerator combinations, such as those presented in References 5 and 6, should be expanded to include modified wake flow field analyses of the type presented by Karpov.

REFERENCES

1. Charters, A. C.; and Turetsky, R. A.: Determination of Base Pressure from Free-Flight Data, Ballistic Research Laboratories Report No. 653. (ATI 26679), March 1948.
2. Heinrich, H. G.: Aerodynamic Characteristics of the Supersonic Guide Surface and the Spiked Ribbon Parachutes, AFFDL-TR-65-104, (AD 478 533), December 1965.
3. Sieling, W. R.; Prziembel, C. E. G.; and Page, R. H.: Axisymmetric Turbulent Near-Wake Studies at Mach 4: Blunt and Hemispherical Bases, AF-OSR-68-2465 (AD 681 165), November 1968.
4. Donaldson, I. S.; "On the Separation of a Supersonic Flow at a Sharp Corner", AIAA Journal, Vol. 5, No. 6, June 1967, pp 1086-1088.
5. Brunner, T. W.; and Nerem, R. M.: Initial Results on the Theoretical Prediction of Drag for a Trailing Decelerator at Supersonic Speeds, AIAA Paper No. 70-1177 presented at the AIAA Aerodynamic Deceleration Systems Conference, Dayton, Ohio September 1970.
6. Noreen, R. A.; Rust, L. W.; and Rao, P. P.: Analysis of the Supersonic Flow About a Forebody-Decelerator Combination, AFFDL-TR-71-35, Vols I and II, (AD 893254L and AD 901908L), March 1972.
7. Coats, J. D.: Static and Dynamic Testing of Conical Trailing Decelerators for the Pershing Re-Entry Vehicle, AEDC-TN-60-188, (AD 245 015L), October 1960.
8. Charczenko, N.; and McShera, J. T.: Aerodynamic Characteristics of Towed Cones Used as Decelerators at Mach Numbers From 1.57 to 4.65, NASA-TN-D-994, December 1961.
9. Charczenko, N.: Aerodynamic Characteristics of Towed Spheres, Conical Rings, and Cones Used as Decelerators at Mach Numbers From 1.57 to 4.65, NASA-TN-D-1789, April 1963.
10. Heinrich, H. G.; and Hess, R. S.: Drag Characteristics of Plates, Cones, Spheres and Hemispheres in the Wake of a Forebody at Transonic and Supersonic Speeds, RTD-TDR-63-4242, (AD 457 056), December 1964.
11. Alexander, W. C.: Investigation to Determine the Feasibility of Using Inflatable Balloon Type Drag Devices for Recovery Applications in the Transonic, Supersonic, and Hypersonic Flight Regime, Part II, Mach 4 to Mach 10 Feasibility Investigation, ASD-TDR-62-702, Part II, (AD 295 489), December 1962.
12. Roberts, B.G.: An Experimental Study of the Drag of Rigid Models Representing Two Parachute Designs at M = 1.40 and 2.19, Royal Aircraft Establishment Technical Note No. AERO-2734, (AD 256 987), December 1960.

13. Sims, L. W.: Analytical and Experimental Investigation of Supersonic Parachute Phenomena, ASD-TDR-62-844, (AD 334 868), February 1963.
14. Bell, D. R.: Pressure Measurements on the Rigid Model of a Balloon Decelerator in the Wake of a Simulated Missile Payload at Mach Numbers 1.5 to 6.0, AEDC-TDR-64-65, (AD 435 861), April 1964.
15. Deitering, J. S.; and Hilliard, E. E.: Wind Tunnel Investigation of Flexible Aerodynamic Decelerator Characteristics at Mach Numbers 1.5 to 6, AEDC-TR-65-110, (AD 464 786), June 1965.
16. Sims, L. W.: The Effects of Design Parameters and Local Flow Fields on the Performance of Hyperflo Supersonic Parachutes and High Dynamic Pressure Parachute Concepts, AFFDL-TR-65-150, Vol. 1, (AD 476 520), October 1965.
17. Slattery, R. E.; Clay, W. G.; and Stevens, R. R.: "Interactions Between Hypersonic Wake and a Following Hypersonic Projectile", AIAA Journal, Vol. 1, No. 4, April 1963, pp 974-975.
18. Dayman, B., Jr.; and Kurtz, D. W.: "Forebody Effects on Drogue Drag in Supersonic Flow", Journal of Spacecraft and Rockets, Vol. 5, No. 11, November 1968, pp 1335 - 1340.
19. Kavanau, L. L.: "Results of Some Base Pressure Experiments at Intermediate Reynolds Numbers With $M = 2.84$ ", Journal of the Aeronautical Sciences, Vol. 21, No. 4, April 1954, pp 257 - 260 and 274.
20. Van Hise, V.: Investigation of Variation in Base Pressure Over the Reynolds Number Range in Which Wake Transition Occurs For Two-Dimensional Bodies at Mach Numbers From 1.95 to 2.92. NASA-TN-D-167, November 1959.
21. Crocco, L.; and Lees, L.: "A Mixing Theory For The Interaction Between Dissipative Flows and Nearly Isentropic Streams", Journal of the Aeronautical Sciences, Vol. 19, No. 10, October 1952, pp 649-676.
22. Kavanau, L. L.: "Base Pressure Studies in Rarefied Supersonic Flows", Journal of the Aeronautical Sciences, Vol. 23, No. 3, March 1956, pp 193 - 207 and 230.
23. Whitfield, J. D.: Critical Discussion of Experiments on Support Interference at Supersonic Speeds, AEDC-TN-58-30, (AD 201 108), August 1958.
24. Whitfield, J. D.; and Potter, J. L.: On Base Pressures at High Reynolds Numbers and Hypersonic Mach Numbers, AEDC-TN-60-61, (AD 234 477), March 1960.
25. Miller, C. G. III: An Experimental Investigation of Support Interference on a Blunt Body of Revolution at a Mach Number of Approximately 20, NASA-TN-D-2742, April 1965.

26. Schueler, C. J.: An Investigation of Support Interference on AGARD Calibration Model B, AEDC-TN-60-35, (AD 233 041), February 1960.
27. Myers, A. W.; and Hahn, J. S.: Drag and Performance Characteristics of Flexible Aerodynamic Decelerators in the Wake of Basic and Modified Arapaho "C" Test Vehicle Configurations at Mach Numbers from 2 to 5, AEDC-TR-67-75, (AD 813 808), May 1967.
28. Bauer, A. B.: "Near Wake Injection Experiments", AIAA Journal Vol. 6, No. 8, August 1968, pp 1597 - 1598.
29. Cortright, E. M.; and Schroeder, A. H.: Preliminary Investigation of Effectiveness of Base Bleed in Reducing Drag of Blunt-Base Bodies in Supersonic Stream, NACA-RM-E51A26, March 1951.
30. Cassanto, J. M.; and Hoyt, T. L.: "Flight Results Showing the Effect of Mass Addition on Base Pressure", AIAA Journal, Vol. 8, No. 9, September 1970, pp 1705 - 1707.
31. Nerem, R. M.: "Pressure and Heat Transfer on High-Speed Aerodynamic Decelerators of the BALLUTE Type", Proceedings of the AIAA Aerodynamic Deceleration Systems Conference, Houston, Texas, September 1966, pp 135 - 143.
32. Henke, D. W.: Establishment of an Unsymmetrical Wake Test Capability for Aerodynamic Decelerators - Volume III. Experimental Wake Survey and Body Surface Pressure Data, AFFDL-TR-67-192 - Vol. III, (AD 675 182), August 1968.
33. Nerem, R. M.: Theoretical and Experimental Studies of Supersonic Turbulent Wakes and Parachute Performance, Proceedings of the AIAA Aerodynamic Deceleration Systems Conference documented in FTC-TR-69-11, (AD 854 169), April 1969, pp 243 - 254.
34. Ward, L. K.; and Myers, A. W.: Free-Flight Testing of Aerodynamic Decelerators in a Supersonic Wind Tunnel, AEDC-TR-67-93, (AD 815 090), June 1967.
35. Klann, J. L.; and Huff, R. G.: Experimental Investigation of Interference Effects of Lateral-Support Struts on Afterbody Pressures at Mach 1.9, NACA-RM-E56C16, May 1956.
36. Mirande, J.: "Mesure de la Resistance d'un Corps de Revolution, a $M = 2, 4$, au Moyen de la Suspension Magnetique O.N.E.R.A.", La Recherche Aeronautique, No. 59, Mai-Juin 1959, pp 24 and 25.
37. Karpov, Yu. L.; Semenkevich, Yu. P.; and Cherkez, A. Ya.: "On Calculating the Separated Flow Between Two Bodies", AN SSSR. Izvestiya. Mekhanika zhidkosti i gaza. NNo. 3, 1968, pp 88 - 94.
38. Isaachsen, I.: "Innere Vorgange in stromenden Flussigkeiten and Gasen", Z.V.D.I., Bd. 55, 1911, S. 428 - 431.

39. Preiswerk, E.: Application of the Methods of Gas Dynamics to Water Flows With Free Surface, Parts I and II, NACA-TM Translations - 934 and 935 (ATI 43689 and ATI 43837), March 1940.
40. Bruman, J. R.: Application of the Water-Channel - Compressible Gas Analogy, North American Aviation Report NA-47-87, (ATI 4824), March 1947.
41. Ippen, A. T.; Harleman, D. R. F. et al: Studies on the Validity of the Hydraulic Analogy to Supersonic Flow; Parts I through V, Air Force Technical Reports AF-TR-5985, Parts I Through IV, (ATI 77510 (I & II)), (ATI 110 693 (III)), (ATI 160 258 (IV)), and (AD 21103 (V)), 1950 to 1952.
42. Ames Research Staff: Equations, Tables, and Charts for Compressible Flow, NACA-TR-1135, 1953.
43. Babish, C. A. III: Equations, Tables, and Charts for Flow of Shallow Water With a Free Surface, Air Force Flight Dynamics Laboratory Technical Memorandum AFFDL-TM-69-2-FDFR, September 1969.
44. Anon.: Research and Development - AF Technical Facility Capability Key, Air Force Systems Command Pamphlet AFSCP 80-3, September 1967, p 298.
45. Heinrich, H. G.; and Ibrahim, S. K.: Application of the Water Surface Wave Analogy in Visualizing the Wave Pattern of a Number of Primary and Secondary Body Combinations in Supersonic Flow, Air Force Wright Air Development Center, Report-WADC-TR-59-457, (AD 231 291), September 1959.
46. Lau, R. A.: Wake Analysis for Supersonic Decelerator Applications, Vol. I - Theoretical Analysis and Correlation of Wind-Tunnel and Shallow-Water Channel Results, NASA-CR-1543, March 1970 and Volume II - Application of Gas-Hydraulic Analogy to Shallow-Water Tow Channel Results, NASA-CE-1544, March 1970.
47. Lamb, H.: Hydrodynamics 6th Ed., Dover Publications, New York, 1945.
48. Laitone, E. V.: "A Study of Transonic Gas Dynamics by the Hydraulic Analogy", Journal of the Aeronautical Sciences, Vol. 19, No. 4, April 1952, pp 265 - 272.
49. Gupta, O. P.: "An Analytical Method for Evaluating the Optimum Depth in Hydraulic Analogy Experiments", AIAA Journal, Vol 3, No. 10, October 1965, pp 1953 - 1954.
50. Campbell, J. F.: Supersonic Aerodynamic Characteristics and Shock Standoff Distances for Large-Angle Cones With and Without Cylindrical Afterbodies, NASA-TN-D-5334, August 1969.

51. Charwat, A. F.; Roos, J. N.; Dewey, F. C.; and Hitz, J. A.: "An Investigation of Separated Flows - Part I: The Pressure Field", *Journal of the Aerospace Sciences*, Vol. 28, No. 6, June 1961, pp 457 - 470.
52. Heinrich, H. G.; Rose, R. E.; and Kovacevic, N. D.: Flow Characteristics of Rigid Ribbon Parachute Canopies in Supersonic Flow AFFDL-TR-65-103, (AD 112 499), December 1965.
53. Babish, C. A. III: "Drag Level Staging Through Modification of Supersonic Wake Fields by Trailing Aerodynamic Decelerators", *Proceedings of the AIAA Aerodynamic Deceleration Systems Conference*, Houston, Texas, September, 1966, pp 55 - 63.